3.4 Research on one-side weather resistance test

3.4.1 Flexural strength

The flexural strength of marble D cut perpendicular (PE) to the rift in initial stage and after 100 and 200 cycles in the climate chamber is presented in Figure 88. A and B presented in the figure are testing directions along the surface plane. Corresponding values for marble E cut parallel to the rift (PA) are presented in Figure 89. After 200 cycles the flexural strength of marble D has decreased 34-65 % depending on the testing direction. Respectively the values for marble type E have diminished
6-12%. The measurement results are shown in detail in Appendix 1.

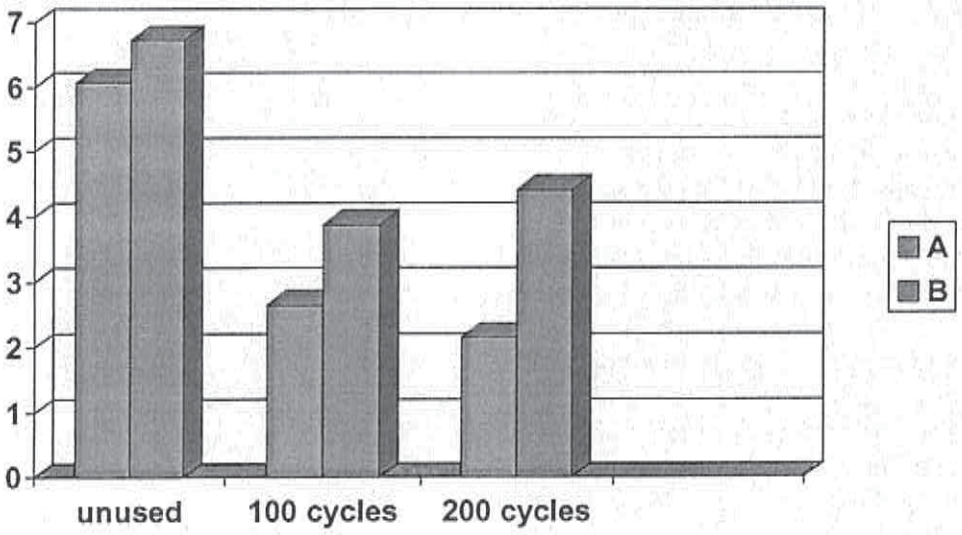

Figure 88. Flexural strength of marble D (PE) (MPa).

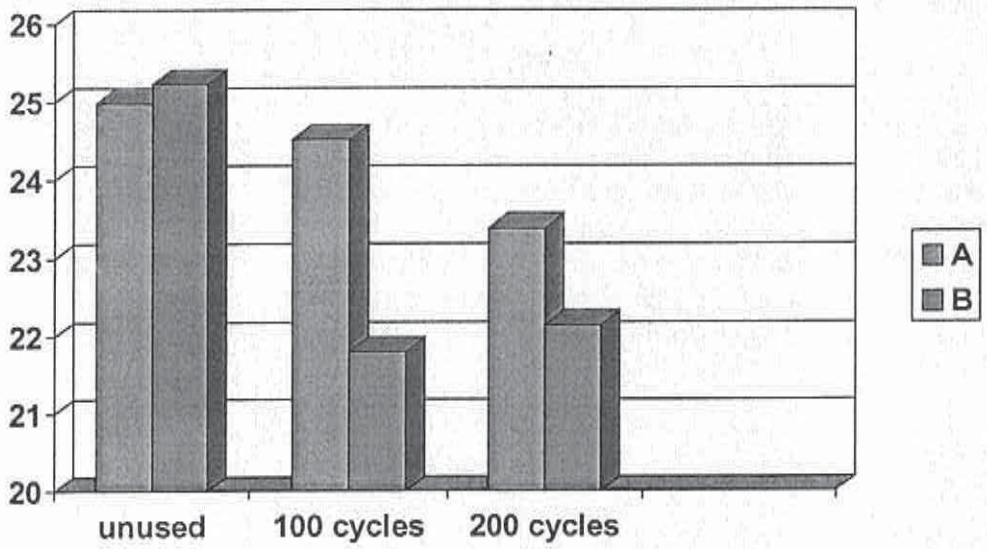

Figure 89. Flexural strength of marble E (PA) (MPa).

3.4.2 Water absorption, apparent porosity, bulk density

The water absorption and apparent porosity of marble type D (PE) at initial stage and after 100 and 200 cycles in the climate chamber is presented in Figures 90 and 91. A notable increase of the values could be measured after 100 cycles, but during the additional 100 cycles the values remained practically unchanged. The measurement results are shown in detail in Appendix 1.

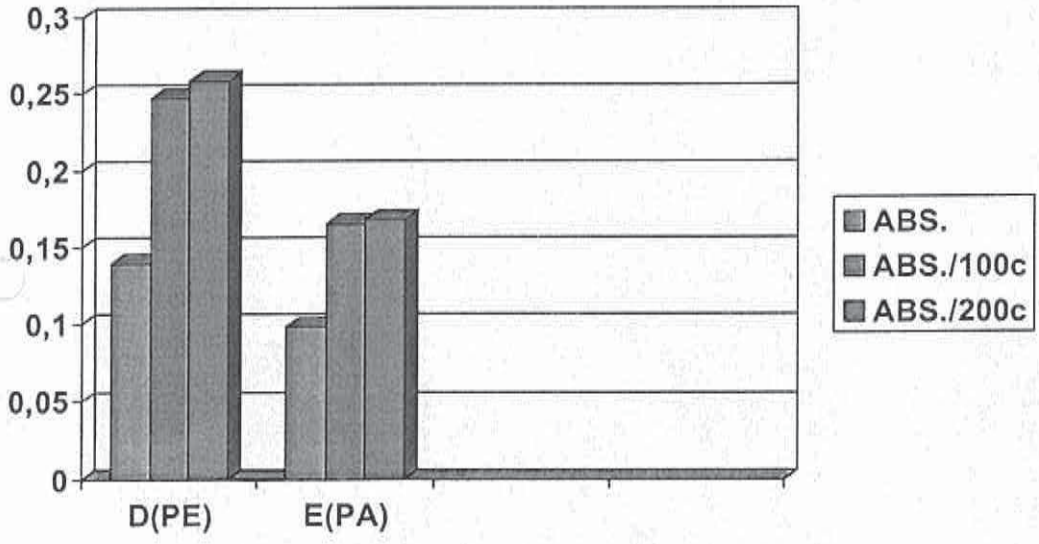

Figure 90. Water absorption of the marbles D and E (w-%).

3.4 Research on one-side weather resistance test

3.4.1 Flexural strength

The flexural strength of marble D cut perpendicular (PE) to the rift in initial stage and after 100 and 200 cycles in the climate chamber is presented in Figure 88. A and B presented in the figure are testing directions along the surface plane. Corresponding values for marble E cut parallel to the rift (PA) are presented in Figure 89. After 200 cycles the flexural strength of marble D has decreased 34-65 % depending on the testing direction. Respectively the values for marble type E have diminished 6-12%. The measurement results are shown in detail in Appendix 1.

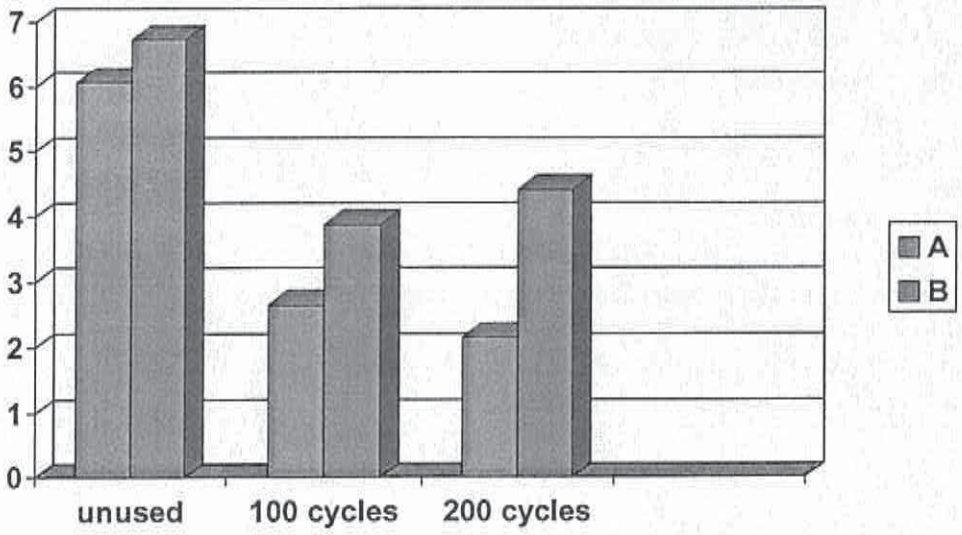

Figure 88. Flexural strength of marble D (PE) (MPa).

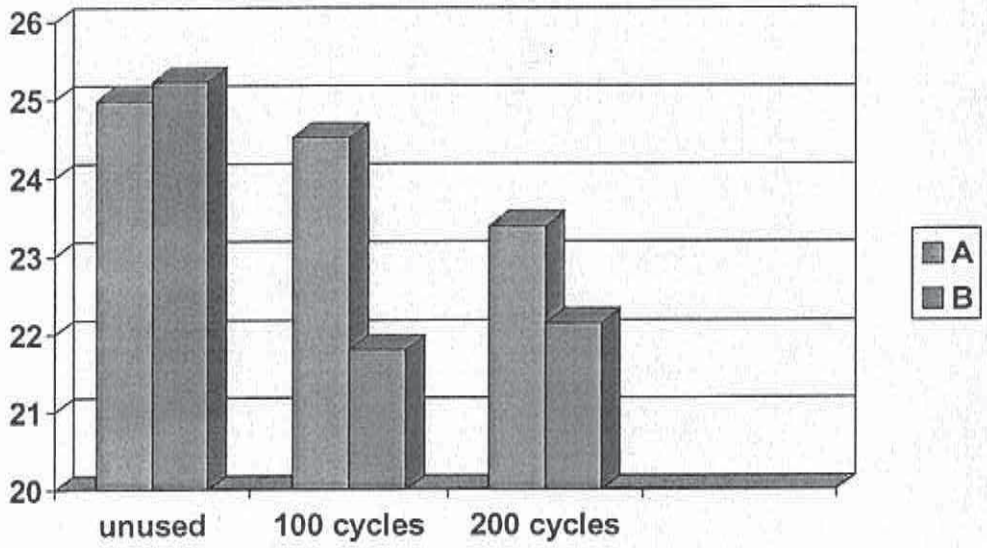

Figure 89. Flexural strength of marble E (PA) (MPa).

3.4.2 Water absorption, apparent porosity, bulk density

The water absorption and apparent porosity of marble type D (PE) at initial stage and after 100 and 200 cycles in the climate chamber is presented in Figures 90 and 91. A notable increase of the values could be measured after 100 cycles, but during the additional 100 cycles the values remained practically unchanged. The measurement results are shown in detail in Appendix 1.

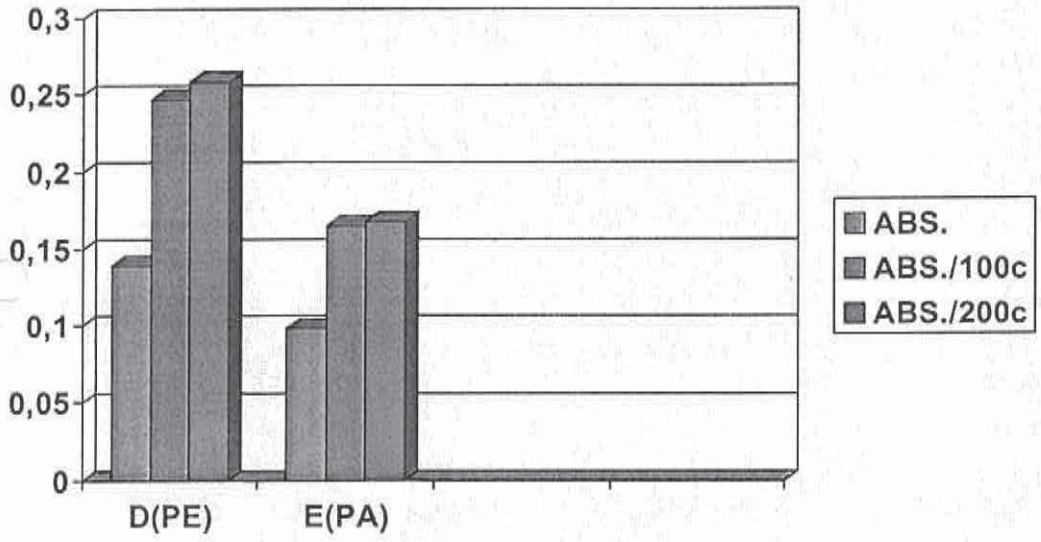

Figure 90. Water absorption of the marbles D and E (w-%).

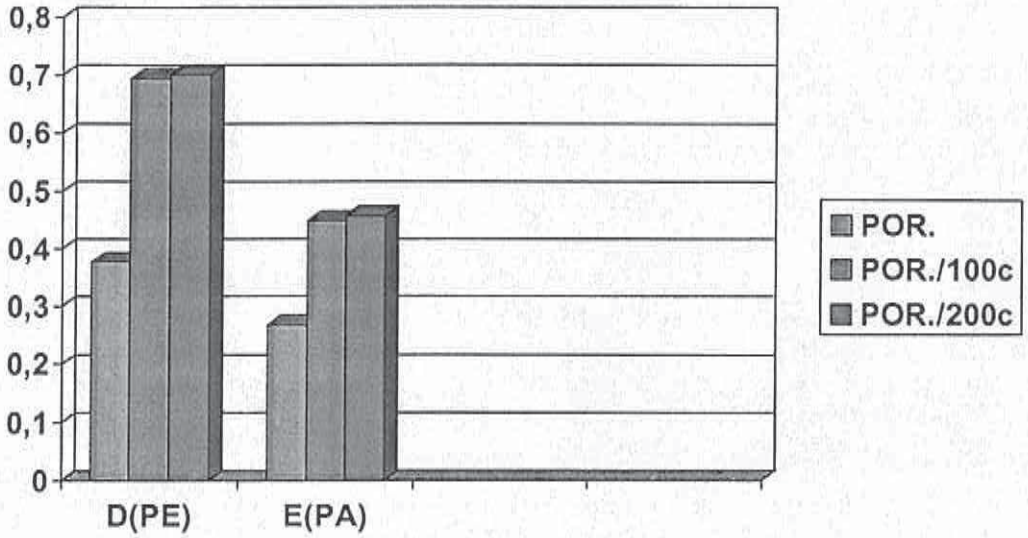

Figure 91. Apparent porosity of the marbles D and E (vol-%).

The relative changes of the water absorption, ΔW, and apparent porosity, Δp_o, of the marbles that have taken place during the weather resistance tests are presented in Table 18. The basis of the comparison is in all cases the value of the unused marble.

Table 18. The relative changes of water absorption and apparent porosity of marbles D and E in the weather resistance test.

marble type	ΔW		Δp_o	
	100 cycles %	200 cycles %	100 cycles %	200 cycles %
D(PE)	+78	+86	+84	+86
E(PA)	+68	+71	+68	+71

3.4.3 Mineral composition

3.4.3.1 X-ray diffraction

According to the X-ray diffraction diagram marble D (PE) consisted almost entirely of calcite, i.e. calcium carbonate, $CaCO_3$. Quartz, α-SiO_2, and dolomite, $CaMg(CO_3)_2$, were also observed. The contents of these accessory minerals were, however, low, at most only a couple of weight percents. The diffraction diagram of marble D(PE) is shown in Appendix 1.

According to the X-ray diffraction diagram marble E(PA) consisted almost entirely of calcite, i.e. calcium carbonate, $CaCO_3$. Marble contained also a substantial amount, probably about 5 w-%, of dolomite, $CaMg(CO_3)_2$. Quartz, α-SiO_2, was also observed, but its content was low. The diffraction diagram of marble E(PA) is shown in Appendix 1.

3.4.3.2 Thermal analysis

The thermal behaviour of the marbles was practically identical. The thermal curves contained only one phenomenon, the disintegration reaction of calcite in the temperature region of 700°C-950°C. In the curves of the marble E(PA) there was, however, a small effect, "a shoulder", at about 750°C. This probably refers to dolomite whose disintegration reaction includes two separate steps, first of which is comprised of the dissociation of magnesite and the second of the dissociation of calcite.

The weight losses of the marbles at 1000°C, Δm_T, and the temperatures of the maximum rate of the weight change, T_{max}, taken as the temperatures of the peaks of the DTG-curves are shown in Table 19. The thermal curves of the marbles are shown in Appendix 1.

Table 19. The weight loss and the temperature of the DTG-peak of the marbles in thermal analysis.

marble	Δm_T w-%	T_{max} °C
D(PE)	44.2	922
E(PA)	45.1	917

3.4.4 Microstructure

3.4.4.1 Thin section study

Photographs of the microstructure of marble D(PE), unused and after 100 cycles in the climate chamber, are shown in Figures 92 and 93. Following observations were made:

- fine-grained, fairly even grained, nor oriented, massive
- average grain size 200-300 µm
- nearly pure carbonate rock, contains very little quartz
- some alteration of the grains
- signs of granular decohesion after 100 cycles in the climate chamber

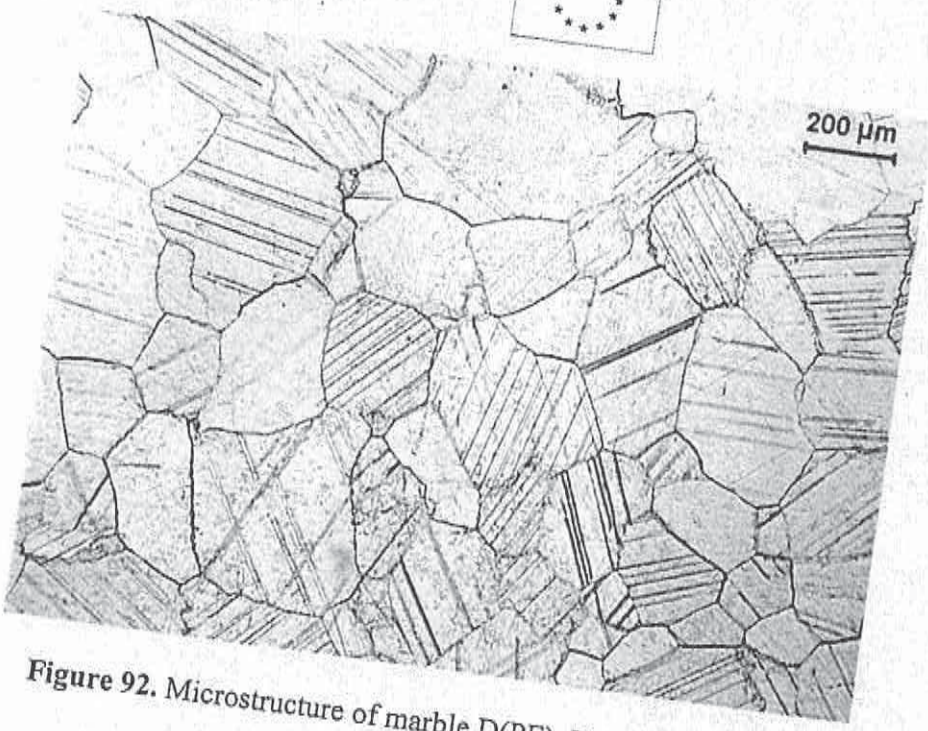

Figure 92. Microstructure of marble D(PE). Unused. Plane-polarized light.

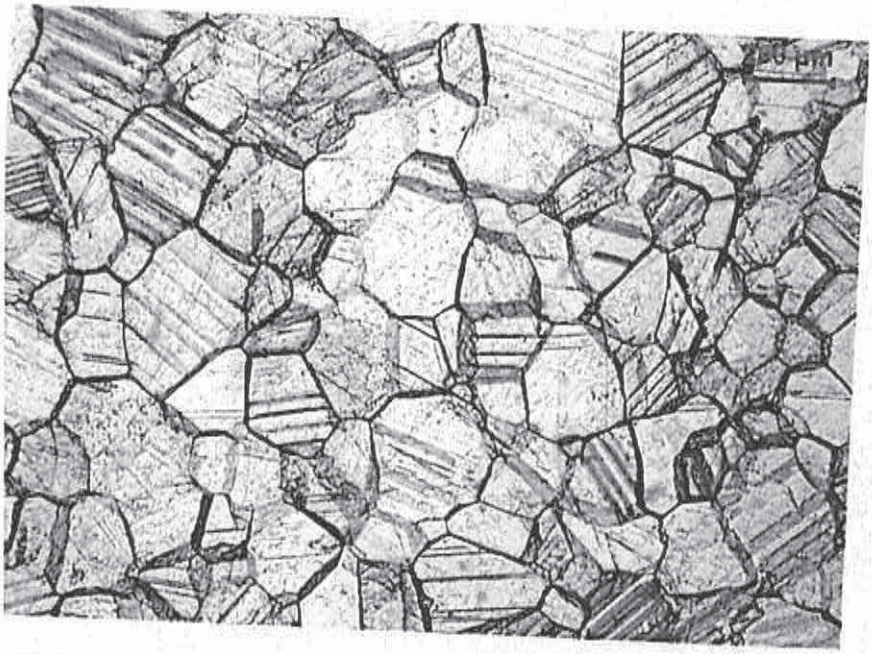

Figure 93. Microstructure of marble D(PF) 100 cycles in th

Photographs of the microstructure of marble E(PA), unused and after 100 cycles in the climate chamber, are shown in Figures 94 and 95. Following observations were made:

- fine-grained, not oriented
- grain size varies from microcrystalline up to 0.5 mm
- nearly pure carbonate rock, contains some quartz and opaque minerals
- some alteration of the grains
- no changes observable after 100 cycles in the climate chamber

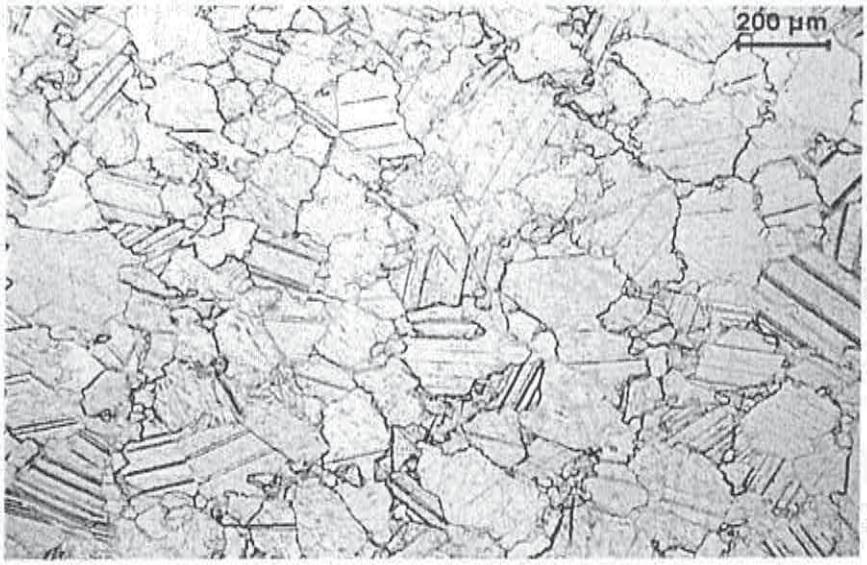

Figure 94. Microstructure of marble E(PA). Unused. Plane-polarised light.

Figure 95. Microstructure of marble E(PA). 100 cycles in the climate chamber. Plane-polarised light.

3.4.4.2 SEM-study

BSE- and SE-images of marble D (PE) both unused and after 100 cycles in the climate chamber show that grain boundaries can clearly be distinguished. Strains caused by 100 cycles in the climate chamber seemed to effect the structure of the marble in such a way that the grain boundaries could be distinguished even more easily.

BSE- and SE-images of marble E(PA)Show that grain boundaries can only partly and even then very vaguely be distinguished. No changes could be seen in the structure of the marble after 100 cycles in the climate chamber.

SEM-pictures of fractured surfaces of marble D(PE) after 100 cycles in the climate chamber, are shown in Figures 96-97. The individual grains can easily be distinguished from each other. Clear cracks can also be noticed between the grains. These cracks become considerably wider when the marble is exposed to the freeze/thaw strains in the climate chamber. The maximum crack width after cycling in the climate chamber can be around 6-7 µm. The homoblastic structure of the marble can be clearly seen.

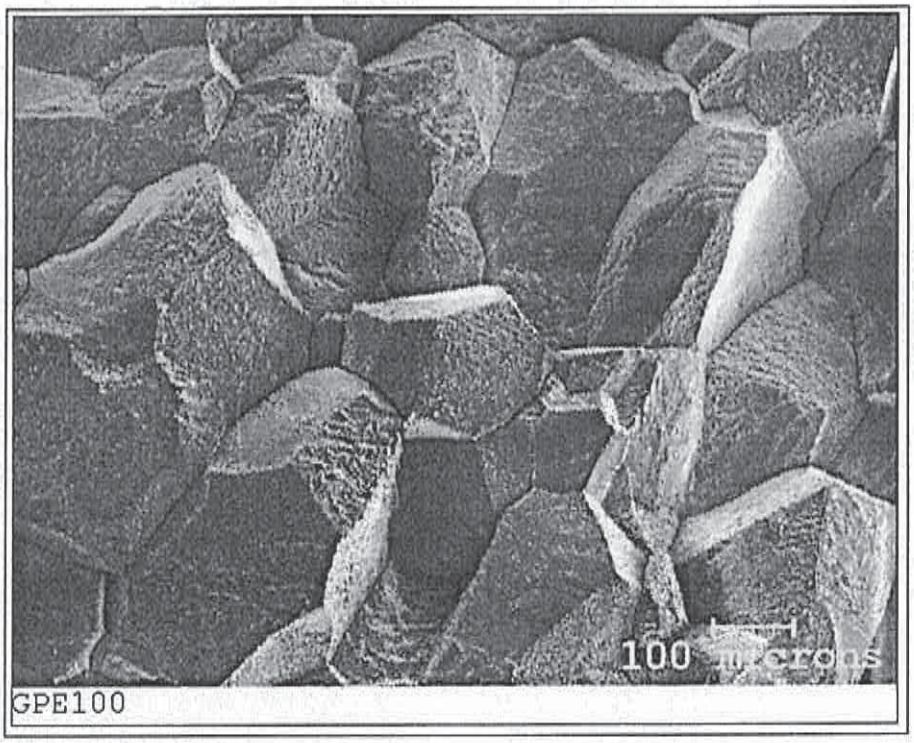

Figure 96. Marble D(PE), 100 cycles in the climate chamber. SE-image of fractured surface, 100x.

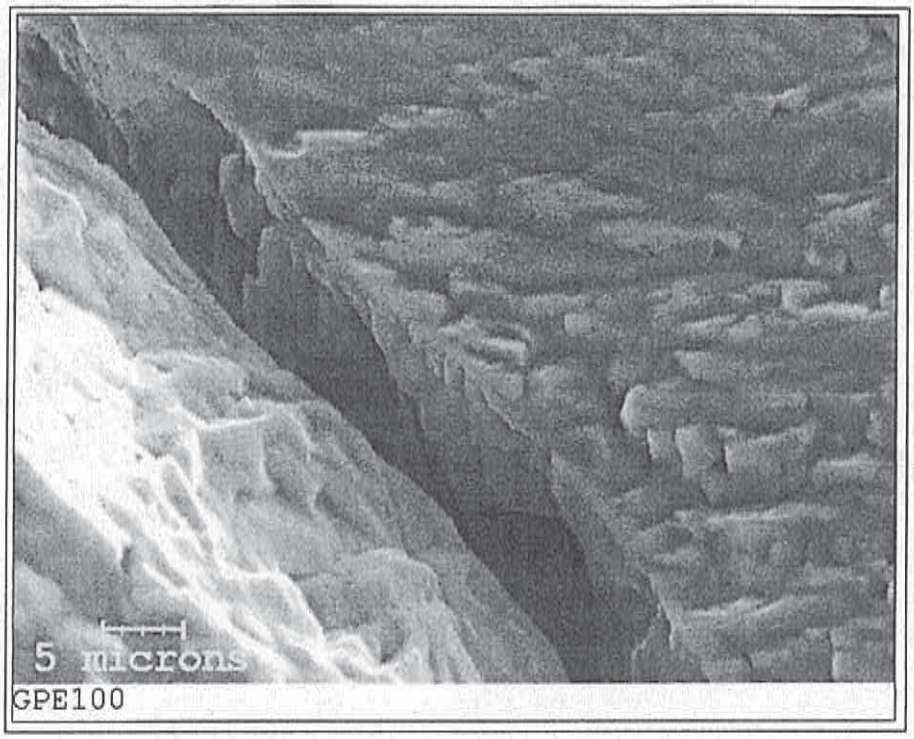

Figure 97. Marble D(PE), 100 cycles in the climate chamber. SE-image of fractured surface, 2500x.

SEM-picture of fractured surface of marble E (PA) after 200 cycles in the climate chamber, is shown in Figure 98. The grain boundaries can be seen only in some places. Thus, it is impossible to distinguish the grains from each other. Some very narrow cracks can be noticed between some of the grains. Some more of these cracks exist and they become a little wider when the marble is exposed to the freeze/thaw strains in the climate chamber. The maximum crack width after cycling in the climate chamber is 0.2-0.3 μm. The xenoblastic structure of the marble can clearly be seen.

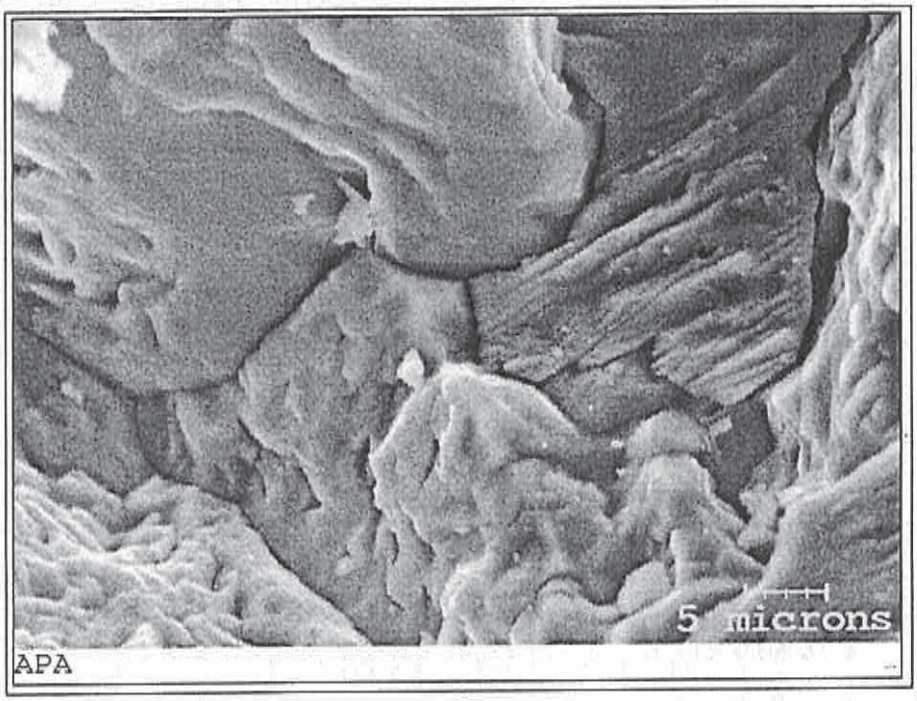

Figure 98. Marble E(PA), unused. SE-image of fractured surface, 2500x.

3.4.5 Colour measurement, gloss

During the weather resistance tests the colour of the marble panels was measured 4 (100 cycles) or 5 times (200 cycles). The number of cycles of the measurements were as follows:

code	100 cycles number of cycle	200 cycles number of cycle
1	0	0
2	26	53
3	53	93
4	103	150
5		200

According to the colour measurements the whiteness of the marbles seemed to increase, though the changes were not very notable or even unambiguous at all points. Instead, there was a clear tendency for the co-ordinate a to move towards more negative and for the co-ordinate b to move towards more positive values. This means that the marbles became more yellow and more green. This could refer to fouling of the marble surfaces, possibly due to impurities from the water spraying system of the climate chamber. The results from the colour measurements of the marbles are shown in Figures 99-101. The detailed results are presented in Appendix 3.

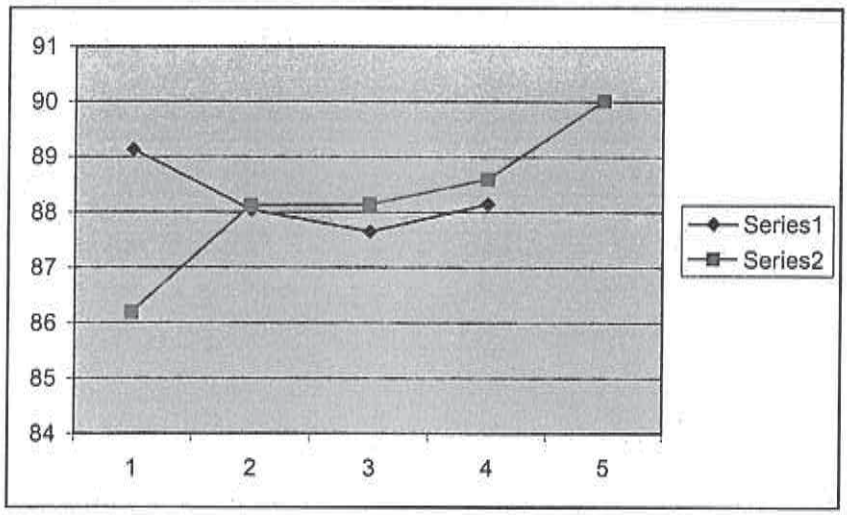

Figure 99. CIELAB colour co-ordinate L of marble E(PA). Series 1 = weather resistance test with 100 cycles, series 2 = weather resistance with 200 cycles.

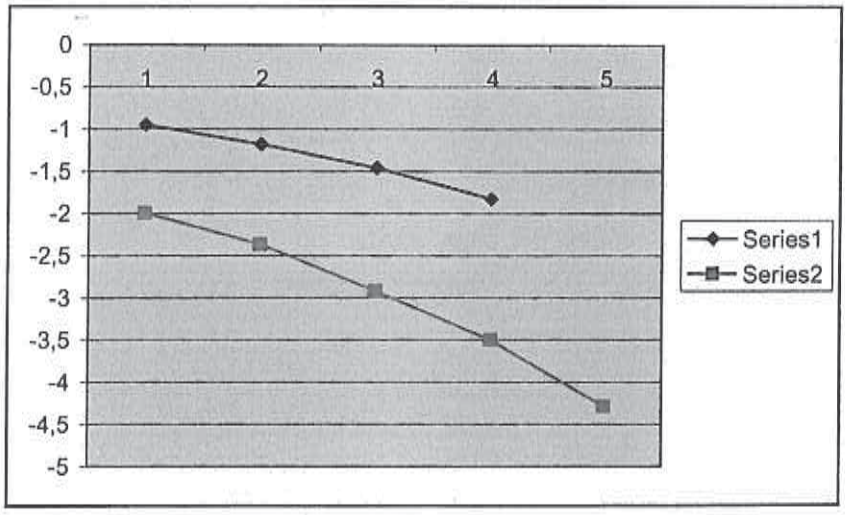

Figure 100. CIELAB colour co-ordinate a of marble E(PA). Series 1 = weather resistance test with 100 cycles, series 2 = weather resistance with 200 cycles.

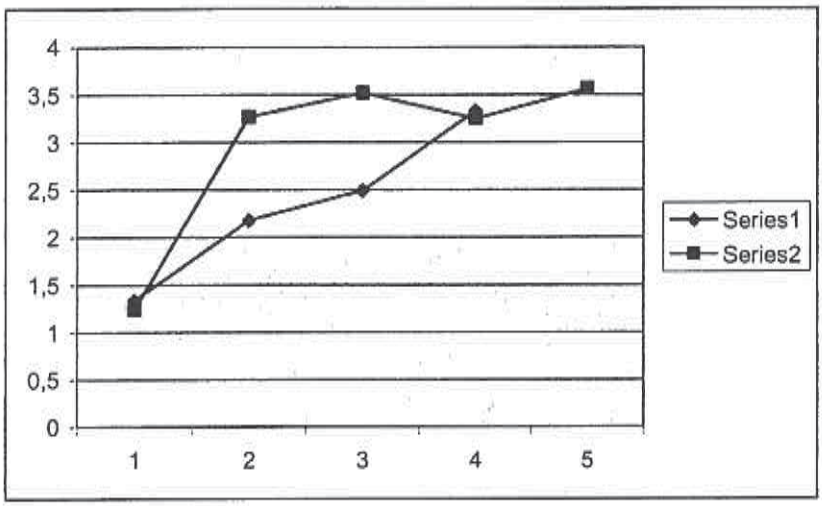

Figure 101. CIELAB colour co-ordinate b of marble E(PA). Series 1 = weather resistance test with 100 cycles, series 2 = weather resistance with 200 cycles.

No change in the values of gloss could be observed in any of the marble specimens. The surfaces of the marble panels used in the weather resistance test were not polished.

3.4.6 Warping

In the weather resistance tests all the panels showed convex bowing, i.e. they bowed towards the inside of the climate chamber. The degree of bowing was, however, hardly noticeable. The measured displacements, δ, and the corresponding radii of curvature, r, are presented in Table 20.

Table 20. Bowing of the marble panels in the weather resistance tests presented as displacements (δ) and radii of curvature (r).

marble	test mm	δ m	r
D(PE)	100	0.12	250
200	0.07	430	
E(PA)	100	0.08	380
200	0.12	250	

3.4.7 Discussion

3.4.7.1 Strength properties

The flexural strengths of the marble types chosen for the study differed considerably from each other. Marble E was very strong with an initial flexural strength of around 25 MPa. On the other hand marble D was weak with an initial flexural strength of 6-7 MPa. Marble D seemed to be somewhat (10%) weaker in testing direction A than in direction B, which could refer to some kind of schistosity in stone structure. In this respect, the strength results of marble E were more even.

The strength of marble D decreased noticeably on the test wall, which most probably is a sign of the effect of some sort of a deterioration mechanism. The loss of strength in testing direction B was 35-40%, but it was even more pronounced, 55-65%, in direction B, where the marble already originally was weaker. On the other hand, marble E showed far better durability. The loss of strength observed in marble E was about 5% in testing direction A and a bit over 10% in testing direction B.

The results in the subproject "Test wall" were parallel to those discussed here. Thus, the loss of strength can be considered to be a real phenomenon, and it can't be explained to be due to sampling or random variation of strength. The strength losses detected in the weather chamber seemed, however, to be a little higher than those observed in the test wall after 1 or 1.5 years. According to the results of the subproject "Environmental condition" this is most probably a consequence of the fact that the strain level due to thermal variations and freeze/thaw cycles has been somewhat higher in the weather chamber than on the test wall. In the measurements made at Finlandia Hall around 80 freeze/thaw cycles were observed during the period of 1.5 years of the test wall study. In this respect only the test with 100 cycles would correspond roughly to 2 years and the test with 200 cycles to 4 years on the test wall. It must be noted, however, that the 1.5 years period of the test wall specimens included only one winter. On the other hand, the daily thermal variation of temperature in marble was clearly greater in the weather resistance tests than in reality.

The fact that the strengths were of the same order of magnitude after 100 and 200 cycles in the weather chamber was also a very noteworthy feature in the results. This would indicate that the loss of strength in the weather chamber happened already during the very first cycles, and after that the deterioration process proceeded slowly. Also in this respect the results were parallel to those of the test wall specimens.

3.4.7.2 Water absorption properties

Both marble types were very dense. The water absorption of marble D was 0.14 w-% (apparent porosity 0.38 vol-%) and that of marble E only 0.10 w-

% (apparent porosity 0.27 vol-%). The bulk density of both types was between 2713-2715 kg/m^3.

The water absorption and apparent porosity of both marble types increased considerably in the weather chamber. The relative increase in marble D was around 85%. The increase observed in the specimens taken from the test wall was practically the same. The relative increase in marble E was about 70%, which was considerably more than observed in the test wall specimens (9-13%). This can be due to the higher level of strains subjected to marbles in the weather chamber compared to the 18-month period on the test wall as discussed above in chapter 5.1. It is interesting, however, that the high increase in water absorption properties of marble E, which refers to crack formation in the structure, is not very extensively reflected in its strength properties. This could refer to the existence of other features in the microstructure of marble E that can compensate the weakening effect of cracking. It can be considered, however, that heavy cracking of marble forms a risk factor for durability properties in the long run.

The increase in the values of the water absorption properties between specimens subjected to 100 and 200 cycles in the weather chamber was small. Thus, the results in this respect are in line with those from the strength determinations.

The fact that porosity of marbles increases when subjected to thermal strains refers to a deterioration mechanism that causes cracks to marble structure. These cracks can either go straight through the individual grains or, more probably, along the grain boundaries. Emergence of cracks to marble structure would also explain the loss of strength observed. It seems, however, that at least a certain amount of cracks appears almost immediately when marble is subjected to strains but then the process slows down and the degree of cracking stays more or less at the same level. Also, it is obvious that the various marble types show very different tendencies for cracking. Likewise, the effect of cracking on mechanical properties seems to be different in different types of marbles..

3.4.7.3 Composition and microstructure

According to X-ray diffraction and thermal analysis both marble types chosen for the study composed almost completely of calcite. In addition, both of them contained small amounts of quartz and some dolomite. In marble E the content of dolomite was substantial, probably about 5%.

According to the definition by prof. Royer-Carfagni from University of Parma marble structures can be classified along the axis of xenoblastic-homoblastic. Xenoblastic marble structure is characterized by interlacing of irregular grains that are closely fitted to each other along their wavy contours. On the other hand, homoblastic marble structure is characterized by regular-shaped grains with straight or gently curving boundaries.

Thin section study of the marble types revealed that the structure of marble D was clearly homoblastic and that of marble E clearly xenoblastic.

The average grain size of the marble types was around 0.2 mm. Marble D was fairly even-grained, but in marble E the variation of grain sizes was more pronounced, probably because of its xenoblastic nature. Especially this was shown as very fine-grained (cryptocrystalline) lenses among the groundmass.

The composition and the microstructure of the marbles were similar to those of the corresponding marbles used in the subproject "Test wall". This confirms that the marble slabs used in the various projects were of the same quality, thus, probably also of the same origin.

No changes could be observed in the microstucture of marbles after the weather resistance tests with thin section study. It is presumable, however, that this only indicates that the method is not suitable for monitoring the deterioration process taking place in marble. Instead, thin sections can be used for characterizing the type of microstructure of various marbles.

SEM-study of polished marble sections didn't give any new information on the structure or on the change of structure of marbles. As thin sections polished sections can be used to reveal the structure type of marbles, but the method is not sensitive enough to monitor the changes taking place in the microstructure due to environmental or thermal strains.

The various structural types of marbles could be identified also in the SEM-study of fractured surface specimens of marbles. The individual grains could be distinguished very easily in marble D (homoblastic). On the other hand the structure of marble E was massive with only a few individual grains or parts of grains to be distinguished from the even-grey background (xenoblastic).

SEM-study of fractured specimens revealed cracks already in the unused marbles. These were especially prominent in marble D, but some, although narrow, cracks could be found in the specimen of unused marble E, too. All the cracks found were located between the grains, i.e. they went along the grain boundaries. The presence of cracks along with the interlocking tendency of grains in marble structure seem to explain at least part of the differencies observed in the strength properties of unused marbles.

Cracking was remarkably more serious in the specimens of marbles that had been in the weather chamber. The amount of cracks was considerably higher and the cracks were wider than in the unused specimens. Especially marble D was badly deteriorated; according to the mere microstructural features marble E was in relatively good condition. The maximum crack width ob-

served was even 6-7 µm in marble D, 0.2-0.3 µm in marble E. However, in general the cracks were narrower in both marble types.

Crack formation on the test wall is a clear sign of deterioration occurring in marble. The fact that the cracks go along the grain boundaries, not straight through the grains, indicates to a mechanism that tends to separate the grains from each other. Thus, cracking can be a consequence of thermal variations taking place in marble slabs as the thermal expansion behaviour of calcite crystals of which the grains of marbles are composed is anisotropic, i.e. the expansion coefficient is higher in the direction of one crystallographic axis than in the other perpendicular to the first one. Another possible explanation can be the freeze/thaw effect which tends to widen the cracks already existing in marble structure and also in this way to create new. Naturally, both of the mentioned mechanisms can act simultaneously.

3.4.7.4 Colour measurements, warping

According to the colour measurements both marble types were very white with the L value of CIELAB co-ordinates varying between 86 and 89. Both marbles had a slight greenish hue with the value of co-ordinate a varying between -1 and -2.5. They had also a slight yellowish hue with the value of the co-ordinate b varying between +1 and +2.

The whiteness of the marbles increased when the slabs were subjected to thermal strains in the weather chamber. Presumably this is a sign of the deterioration process taking place in marble. It is common knowledge in the manufacturing of marble products that their whiteness can be increased by thermal treatment. As it is obvious that variation of temperature causes granular decohesion in marble, it seems plausible to suppose that it is just this deterioration that is reflected also in the colour of marble as increased whiteness. Also in this respect the behaviour of the marble slabs was similar to that of the slabs on the test wall.

A minor but clear tendency for the co-ordinate a to move towards more negative and for the co-ordinate b to move towards more positive values was observed in all the marble types. This means that they are turning more green and more yellow. This could refer to fouling of marble surfaces, possibly by the effect of impurities from the pipelines. Mostly for this reason the colour change of the marbles after the tests was clear.

Bowing of the marble slabs in the weather resistance tests was hardly noticeable. In real conditions at Finlandia Hall bowing of the marbles used in the tests was much more prominent. Thus, even if it is possible to achieve similar changes of marble properties in one-sided weather resistance test as in real conditions, the test, at least in the form used in the project, fails to produce the factor/factors that cause the slab to bow.

3.4.8 Conclusions

According to the studies made the deterioration of marble structure taking place when subjected to thermal strains is caused by granular decohesion, which forms cracks along the grain boundaries. Granular decohesion seems to be a consequence of the anisotropic thermal expansion behaviour of calcite crystals. For this reason marble grains that are composed of calcite crystals break away from each other when thermal variations affect the material.. The strain caused by freezing and thawing may have an accelerating effect on the deterioration process after it has started and enough cracks have been formed.

The marble structure, however, influences its resistance against environmental strains. Homoblastic marble structure seems to be very apt to granular decohesion, which means that its durability e.g. in facades is poor. On the other hand, xenoblastic marble structure is much more resistant. However, it seems that thermal variations can generate heavy cracking also to xenoblastic marbles, although their strength properties are not affected to the same extent. Thus, no final conclusions about the durability of xenoblastic marbles in the long run can be made according to the results of this project.

The results achieved show that the damaging of marble structure takes place very soon after it has been subjected to thermal strains, probably already during the very first cycles of thermal variation. After that the deterioration process slows down, and the properties of marble will stay more or less stable. Thus, in order to predict the behaviour of marble for any longer periods of time a longer period of time for monitoring the marble properties would also be required. A reliable view e.g. of the rate of strength decrease as an indication of the progress of the deterioration process can be acquired only in that way.

According to the results it is possible to simulate the changes in the marble properties caused by real environmental conditions with the one-sided weather resistance test. E.g. the loss of strength, the increase in porosity and the microstructural alterations occurring in marble when tested in the weather chamber were very similar to those observed to take place in marble on the test wall. Thus, the test can be used to predict the behaviour of marbles as facade material and to classify various types of marbles according to their suitability for the purpose. However, the test is slow and expensive to perform. Also, the inability to produce bowing in the test slabs is a serious disadvantage.

3.5 Evaluation of marble samples from other buildings

3.5.1 Presentation of the objects

Marble samples from three different buildings were studied. Some background information dealing with these cases are presented as follows:

case 1
- private owned building situated in Helsinki
- part of the facades coated with marble, supporting structure from concrete elements, ventilation slot between marble and concrete, metal fixings
- built in 1965-1966
- severe deterioration: very notable warping and considerable loss of strength
- marble panels taken off in 1999
- white marble from Carrara, exact type or origin unknown

case 2
- private owned building situated in Helsinki
- facades coated with marble, supporting structure from concrete elements, ventilation slot between marble and concrete, metal fixings
- built in two parts: older part is approximately 25 years and younger part approximately 15 years old
- severe deterioration: some warping and considerable loss of strength
- older part in much better condition
- white marble from Carrara, exact type or origin unknown

case 3
- public building situated in Oulu
- facades coated with marble, supporting structure from concrete elements, ventilation slot between marble and concrete, metal fixings
- built in 1979
- no warping, no loss of strength, breaking around the fixings
- panels taken off in 2000
- white, heavily structured marble from finnish Lapland

In addition, the microstructure of a sample taken from the northern tower wall of Finlandia Hall was studied. The cylindrical sample, ∅ 30 mm, was taken in November 2000 by drilling through a 30 mm thick panel. The panels on that wall had been installed during summer-autumn 1998.

3.5.2 Mineral composition

The marble from the building representing case 1 was practically pure calcite, i.e. calcium carbonate. It contained only a few percents of quartz, feldspar and possibly mica as impurities. The weight loss of the marble in thermal analysis was 44.0 w-%.

The marbles from the building representing case 2 were practically pure calcite, i.e. calcium carbonate. The marble from the older part contained only a few percents of quartz, the marble from the younger part a few percents of quartz and feldspar as impurities. The weight loss of the older marble in thermal analysis was 44.3 w-% and that of the younger 44.2 w-%.

The main component of marble from the building representing case 3 was dolomite, i.e. calcium magnesium carbonate. Thus, it was not question about marble. It contained also a notable amount of quartz and feldspar plus some mica and calcite as impurities. The weight loss of the dolomite in thermal analysis was 43.3 w-%.

3.5.3 Thin section study

A photograph of the microstructure of the marble from case 1 is shown in Figure 102. Following observations were made:

- fine-grained ground mass, slightly oriented, average grain size 0.1-0.2 mm
- in places more coarse-grained veinlets with a thickness of about 1 mm, veinlets show the same orientation as the ground mass
- grain boundaries clear, often straight, grains easily distinguished
- nearly pure carbonate rock, only a little quartz and opaque minerals, possibly feldspar

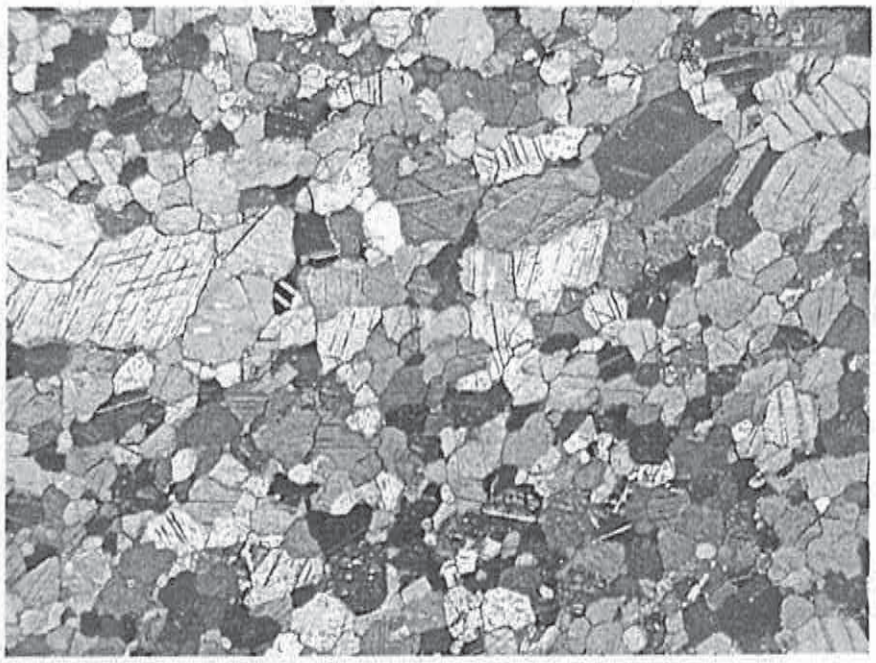

Figure 102. Microstructure of marble from case 1. Cross-polarized light.

Photographs of the microstructure of the older marble from case 2 is shown in Figure 103. Following observations were made:

- ground mass fine-grained, even-grained, not oriented
- grain boundaries easily distinguished
- a few very fine-grained cryptocrystalline lenses, max. length about 10 mm, inside the ground mass
- no heavy cracking
- outer surface dirty and uneven

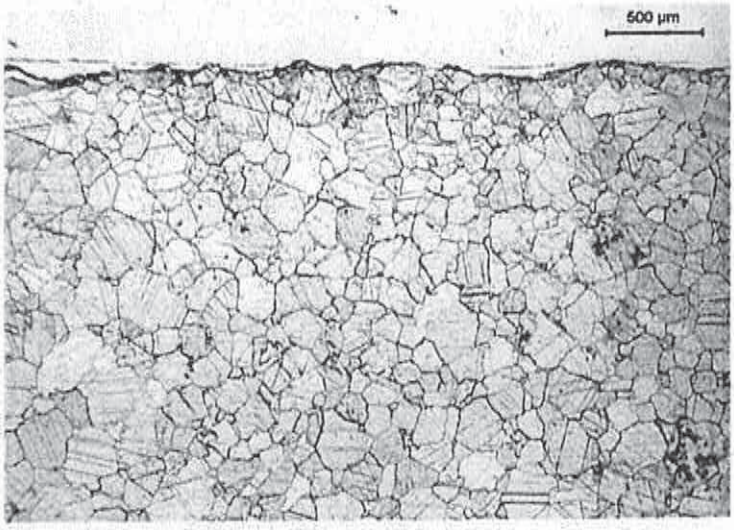

Figure 103. Microstructure of older marble from case 2. Plane-polarized light.

Photographs of the microstructure of the younger marble from case 2 are shown in Figure 104. Following observations were made:

- ground mass fine-grained, fairly even-grained, not oriented
- grain boundaries easily distinguished
- a few very fine-grained cryptocrystalline lenses, max. length about 2-3 mm, inside the ground mass
- cracks between the grains extending to a depth of about 2-3 mm from the outer surface and to a depth of about 1-2 mm from the inner surface, some cracks cut the surface
- outer surface dirty

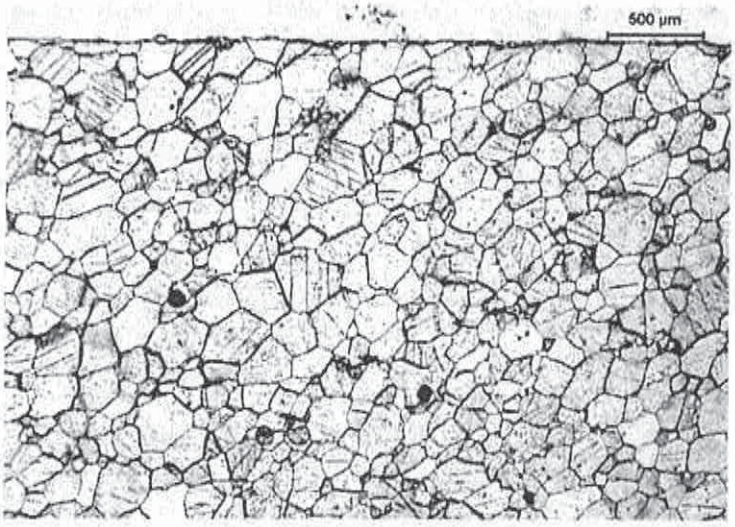

Figure 104. Microstructure of younger marble from case 2. Plane-polarized light.

A photograph of the microstructure of the dolomite from case 3 is shown in 8re 94. Following observations were made:

- ground mass very fine-grained, microcrystalline, dense
- clearly oriented, layered
- in places more coarse-grained veinlets with a thickness of about 1 mm, mostly oriented parallel to layering, a few also cross the layering
- some separate fine- to medium-grained quartz grains in rows, parallel to layering
- mainly carbonate rock, moderate content of quartz, other minerals include feldspar (probably plagioclase), mica (probably muscovite) and opaque minerals
- in places mica forms veinlets, partly with opaque minerals

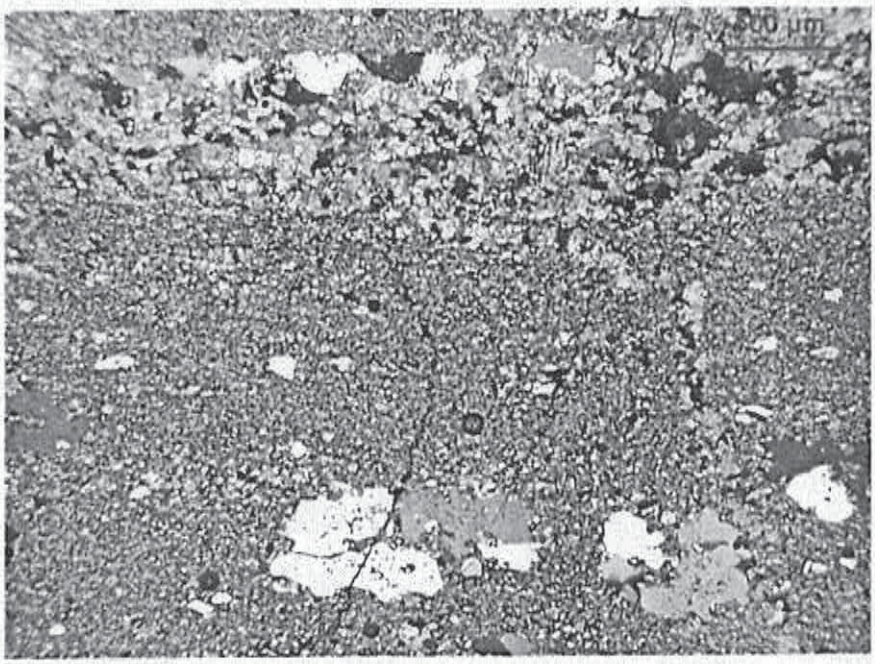

Figure 105. Microstructure of dolomite from case 3. Cross-polarized light.

A photograph of the microstructure of the marble from Finlandia Hall is shown in Figure 106. Following observations were made:

- fine-grained, fairly even-grained, slightly oriented
- average grain size 0.2-0.3 mm
- grain boundaries clear, straight, grains easily distinguished
- nearly pure carbonate rock, a little quartz and opaque minerals

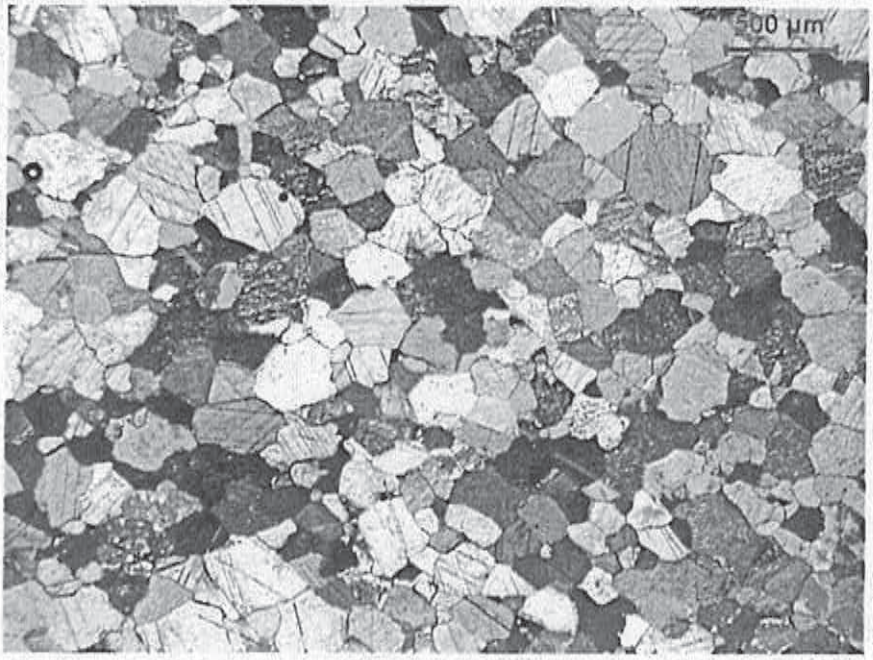

Figure 106. Microstructure of marble from Finlandia Hall. Cross-polarized light.

3.5.4 SEM-study

SEM-pictures of fractured surfaces of marble from case 1 is shown in Figure 107. The individual grains can at least for the most part be distinguished from each other. Cracks can be noticed practically between all the grains. The maximum crack width is around 2 µm. The average grain size of the marble is about 200 µm.

Figure 107. Marble from case 1. SE-image of fractured surface, 100x.

SEM-pictures of fractured surfaces of marble from case 2 are shown in Figures 108 and 109. The individual grains can at least for the most part be distinguished from each other in the marble of the older part. In the marble of the younger part the grains are almost detached from each other. Wide cracks can be noticed between all the grains. The average grain size of the older marble is about 200 µm, that of the younger marble around 200-300 µm.

Rakennuttaja
Byggherre

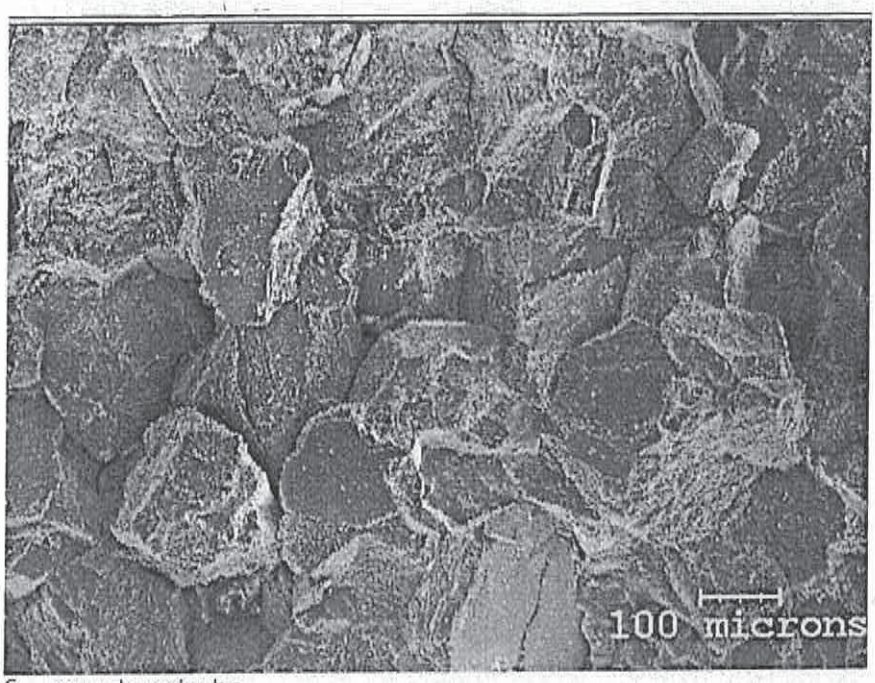

6, murtopinta

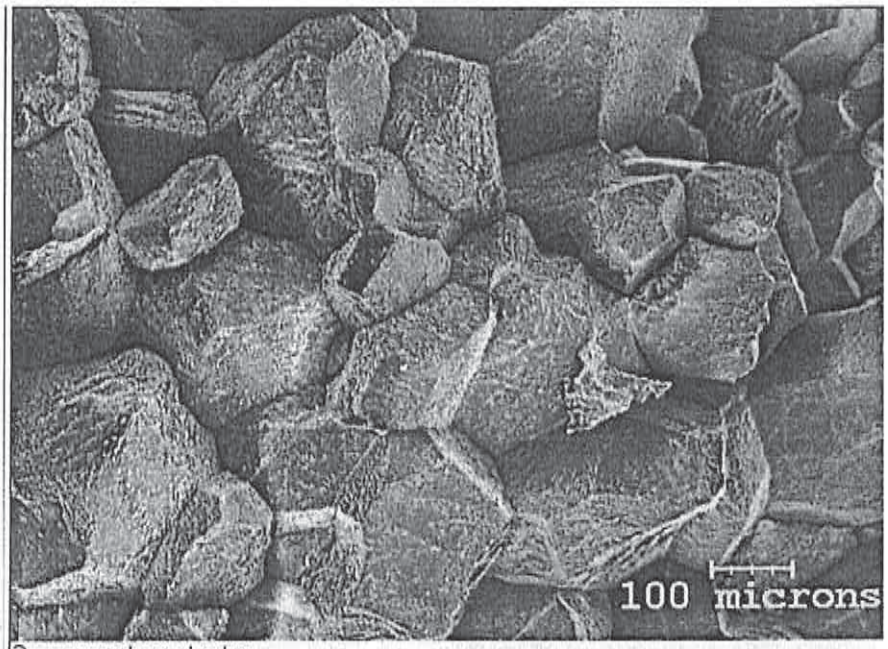

igure 109. Marble from case 2, younger part. SE-image of fractured s
ıc 00x.

SEM-pictures of fractured surfaces of dolomite from case 3 is shown in Figure 110. The individual grains can easily be distinguished from each other. The microstructure is intact; only a few very narrow cracks can be noticed between some of the grains. The average grain size of the dolomite is about 20-30 µm.

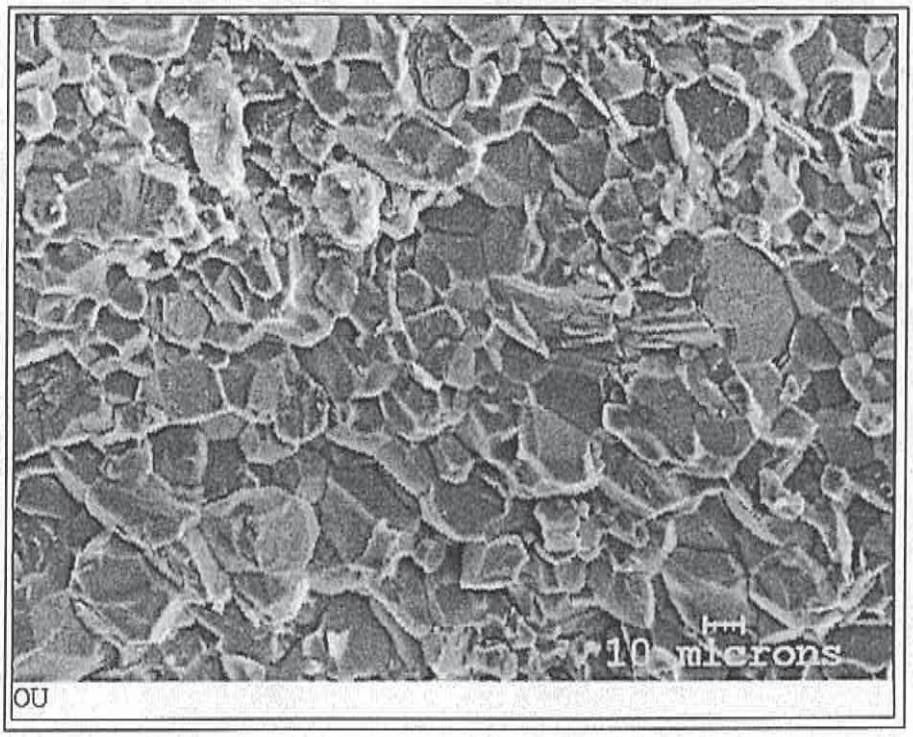

Figure 110. Dolomite from case 3. SE-image of fractured surface, 500x.

SEM-pictures of fractured surfaces of marble from Finlandia Hall is shown in Figure 111. The individual grains can at least partly be distinguished from each other. Cracks can be noticed between some of the grains. The maximum crack width is around 0.8-0.9 µm. The average grain size of the marble is about 200 µm.

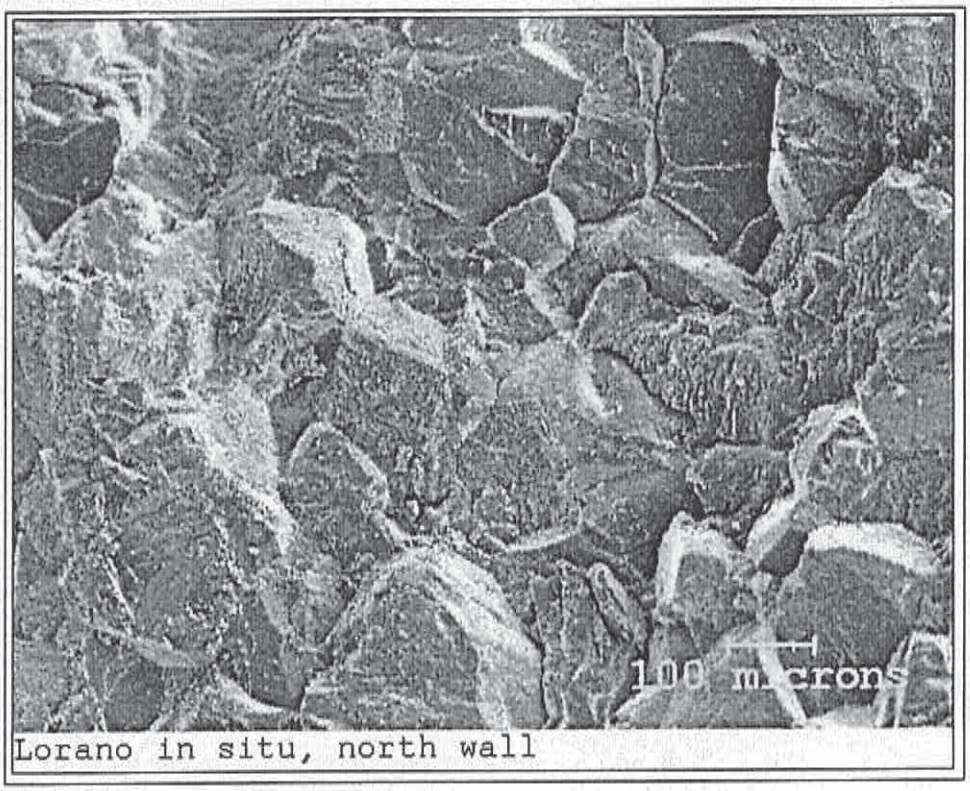

Figure 111. Marble from Finlandia Hall, north wall. SE-image of fractured surface, 100x.

In connection with the SEM-study also the chemical composition of the marble from the northern wall of Finlandia Hall was surveyed by using an energy dispersive PGT Imix spectrometer (EDS). The analysis was made from the fractured surface very close to the outer surface of the panel. The composition observed was practically that of the unused marble, only a little chlorine was detected.

3.6 EFFECT OF THERMAL CYCLING ON MARBLE PROPERTIES

3.6.1 Thermal microfracturing of marble

Stone facades are exposed to thermal loads created by periodic temperature changes. Diurnal temperature changes can be remarkable in Nordic climates like for example in Finland. Temperature increase creates thermal expansion of marble. Because marble is composed of thermally anisotropic minerals as calcite, temperature changes result in the development of thermal stresses within the material. Thermal stresses often combine to produce tensile strains, which can exceed the strength of the material leading to fracturing, which serves to relieve the internal stresses. Fractures due to thermal stresses extend over relatively small areas and are therefore referred to as microfractures (Sage 1988, Winkler 1997).

In addition to the extent of temperature changes, the development of thermal microfractures in marble is related to the presence of structural discontinuities within the material, to the physical properties, thermal properties and spatial orientation of minerals present. Structural discontinuities exist as intra-, inter-, and/or transgranular fractures (Krantz 1983). These are sites of weakness and serve as stress concentrators and potential locations for thermal microfracture initiation and propagation.

Physical properties of minerals and their contacts determine the strength, which thermal stress has to exceed before the initiation of microfracturing. Thermal stresses depend on thermal and physical properties like thermal expansitivity and modulus of elasticity. Also high thermal gradients created by rapid temperature changes and low thermal diffusivity induce thermal stresses. Spatial orientation of calcite crystals in marble affects the developing thermal stresses. When heated to 100°C calcite contracts 0.042% perpendicular to its crystallographic c-axis and expands 0.189% parallel to its c-axis. Unfavorable crystallographic orientations of contiguous grains can lead to high stress concentrations and fracturing of grain boundaries. According to Royer-Carfagni (1999) thermal fracturing tends to favor decohesion of grain boundaries rather than cleavage fractures of single crystals.

Thermal microfracturing may increase the porosity and result in strength reduction of marble. Sage (1988) has reported a 70-170 % increase in water absorption and 49-64 % reduction in flexural strength of medium grained marbles subjected to heating from 24 to 66°C. Microfractures generated at the surface of marble structures provide an additional pore network of flow channels, which permit the migration of aggressive solutions beneath the surface. The result is the accelerated deterioration of marble.

Diurnal atmospheric heating-cooling cycles of rock are believed to be sufficient to dilate marble in a matter of a few years (Winkler 1997). According

to Sage (1988) the first heating cycle causes the largest thermal strain and porosity increase in a medium-grained crystalline marble. Repeated heating cycles to the same temperature cause only minor changes in thermal strain. Widhalm et al. (1996) reported the increasing water absorption capacity with growing number of heating-cooling cycles in Carrara-marble.

3.6.2 Marble samples and sample preparation

The materials of this study consist of three different types of Carrara Bianco -marble with the codes A, D and E. Sample A was tested in two directions:

- parallel to the rift (APA)
- perpendicular to the rift (APE)

The sample preparation included sawing of the specimens with diamond saw, coding of the samples, temperature cycling of the one part of the specimens, and the preparation of thin sections of the fluorescence resin impregnated specimens. At the Laboratory of Engineering Geology and Geophysics the specimens were washed and dried in room temperature before the measurements of the physical properties.

To be able to study structural and mineralogical properties of the marble types and structural changes caused by temperature cycling, six thin sections of every marble sample were prepared, representing untreated, temperature cycled, and mechanically tested specimens.

A half of each sample (12 specimens) was temperature cycled in dry conditions. One temperature cycle lasting about 8 hours consisted of altering the temperature from -20°C to +60°C. In the study specimens were decided to be exposed to about 500 cycles. Detailed report of the thermal cycling and the mechanical tests is given in Appendixes 5 and 6.

3.6.3 Physical properties

3.6.3.1 Density, porosity and water absorption

Grain density gives the average density of the solid rock material and the closed pores. The value of grain density is mainly dependent on the mineralogy. Because of this it was used to indicate the mineralogical homogeneity of the samples and the possible mineralogical changes caused by temperature cycling.

Bulk density gives the average density of the solid rock material and the open and closed pores. Bulk density is the normal index property measured from building stones. The mineralogy and porosity affect the value of the bulk density.

Porosity i.e. effective porosity, gives the pore volume percentage in which water can be absorbed from the specimen surface. The value of porosity depends on the amount of the open interconnected pores. Porosity was used to indicate the volume of initial cracking and possible thermal cracking caused by temperature cycling.

Water absorption gives the weight percentage of rock material in which water can be absorbed. The value of the water absorption is affected with the porosity and the grain density of rock material.

Coefficient of capillary water absorption gives the speed of water absorption into capillary pores of rock material from the horizontal surface upwards. The amount, aperture, and interconnectivity of the open pores affect the coefficient. The coefficient was used to characterize the initial crack network and the possible thermal cracking caused by temperature cycling. The physical index properties determined in this study are summarized in Table 21.

Table 21. The physical properties, their symbols and units used in the study.

Physical Property	Symbol	Unit
Grain density	ρ_g	kgm^{-3}
Bulk density	ρ_b	kgm^{-3}
Porosity	n_e	vol-%
Water absorption	W_m	w-%
Coefficient of capillary water absorption	C	$gm^{-2}s^{-0.5}$

The physical properties were determined using the water immersion procedure, which was modified particularly for this study and deviated from the standard test procedures for building stones. Normal tap water was used in the study. The used procedure based on the measurement of dry mass weighted in air (m_d), water saturated mass weighted in air (m_s), and water saturated mass weighted in water (m_{sub}). In addition the temperature of water was measured to determine water density (ρ_w). In the measurement of the coefficient of capillary water absorption also the partially saturated mass (m_i) after immersion time t_i was measured seven times during the 72 hours immersion. The physical properties were calculated using the following formulas:

$$\rho_g = \frac{m_d \rho_w}{m_d - m_{sub}} \quad (2)$$

$$\rho_b = \frac{m_d \rho_w}{m_s - m_{sub}} \quad (3)$$

$$n_e = \frac{(m_s - m_d)}{(m_s - m_{sub})} \times 100\ \% \quad (4)$$

$$W_m = \frac{(m_s - m_d)}{m_d} \times 100\ \% \quad (5)$$

$$C = \frac{m_i - m_d}{A\sqrt{t_i}} \quad (6)$$

ρ_g = Grain density (kgm^{-3}),
ρ_b = Bulk density (kgm^{-3}),
n_e = The effective porosity (%),
W_m = Water absorption (w-%),
C = Capillary water absorption coefficient ($gm^2s^{-0.5}$),
= The mass of the dried specimen weighted in air (kg),
m_s = The mass of the saturated specimen weighted in air (kg),
m_{sub} = The mass of the saturated specimen weighted in water (kg),
m_i = The mass of the specimen after immersion time t_i weighted in air (kg),
t_i = The immersion time corresponding to the capillary absorption time phase (s),
A = The area of the specimen base (m^2), and
ρ_w = Density of water (kgm^{-3}).

The average values with standard deviation of the physical properties of the untreated and temperature cycled marble samples are presented in the Tables 22 and 23. Untreated E deviates from other marble samples by much smaller porosity and coefficient of capillary water absorption. The same phenomenon is evident in temperature cycled samples, but the differences between the marble types are diminished by temperature cycling.

Table 22. Average values and standard deviations of the physical properties of the untreated marble samples (N=24).

Marble Type / Standard Deviation (Sd)	Grain Density (kgm^{-3})	Bulk Density (kgm^{-3})	Porosity (vol-%)	Water Absorption (w-%)	Capillary water absorption coefficient ($gm^{-2}s^{-0.5}$)
E	2721	2717	0.16	0.06	0.12
Sd	1.49	1.37	0.01	0.00	0.02
D	2720	2710	0.37	0.14	1.28
Sd	1.79	2.07	0.02	0.01	0.15
APA	2717	2708	0.34	0.13	0.87
Sd	1.18	1.24	0.01	0.00	0.05
APE	2718	2708	0.36	0.13	0.94
Sd	0.39	0.60	0.01	0.01	0.14

Table 23. Average values and standard deviations of the physical properties of the temperature cycled marble samples (N=12).

Marble Type / Standard Deviation (Sd)	Grain Density (kgm^{-3})	Bulk Density (kgm^{-3})	Porosity (vol-%)	Water Absorption (w-%)	Capillary water absorption coefficient ($gm^{-2}s^{-0.5}$)
E	2721	2709	0.43	0.16	1.11
Sd	1.32	1.36	0.02	0.01	0.10
D	2721	2704	0.61	0.23	2.96
Sd	1.73	1.36	0.05	0.02	0.50
APA	2717	2702	0.55	0.20	2.28
Sd	1.24	1.31	0.01	0.00	0.17
APE	2717	2702	0.57	0.21	2.43
Sd	0.46	0.98	0.04	0.01	0.35

Scatter diagrams were used to indicate the relation between two physical properties. Porosity-capillary water absorption coefficient -chart in Figure 112 shows a clear logarithmic positive correlation between the open pore volume and the speed of capillary water absorption of the untreated samples. Increasing porosity seems to accelerate the capillary water absorption in other marble types than E, which seems to have very modest pore network.

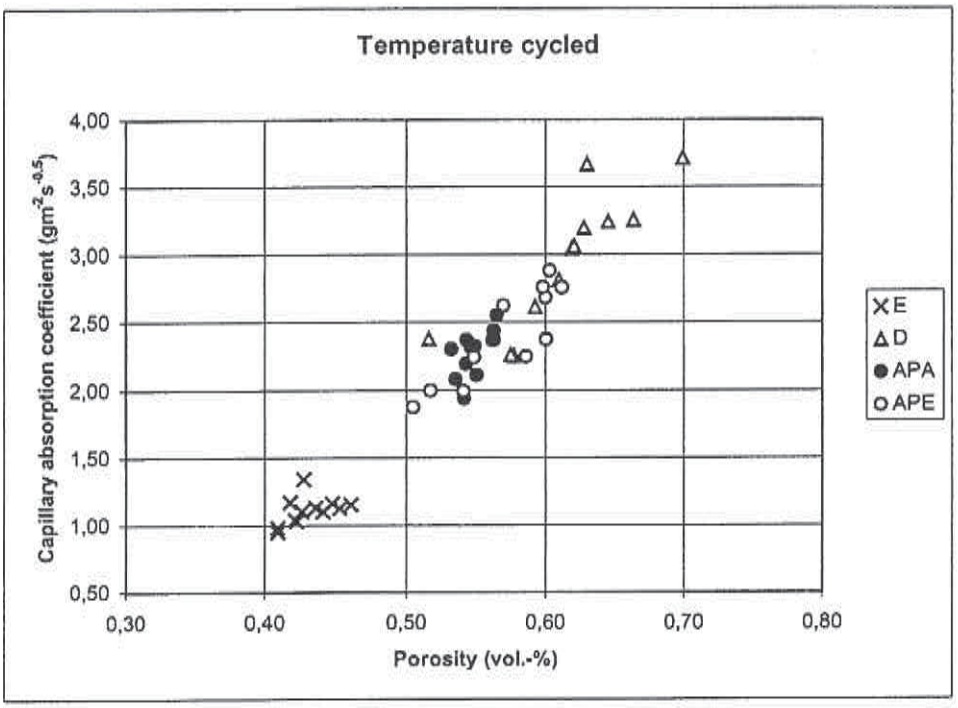

Figure 112. The porosity-capillary water absorption coefficient-relationship of the Temperature cycled marble samples E, D, PA and APE (N=12)..

3.6.3.2 Capillary water absorption

Figure 113 shows the average capillary water absorption curves of the untreated marble samples. Marble D has the highest speed and amount of capillary water absorption. Both Eand APE samples have very similar behaviour despite of the different orientation of the specimens. Also the capillary absorption phase (the first linear part) and the diffusion phase (the latter linear part) are clearly distinguishable (see Hammecker et al. 1993). On the other hand E shows much slower capillary absorption and the two absorption phases are not easily distinguishable.

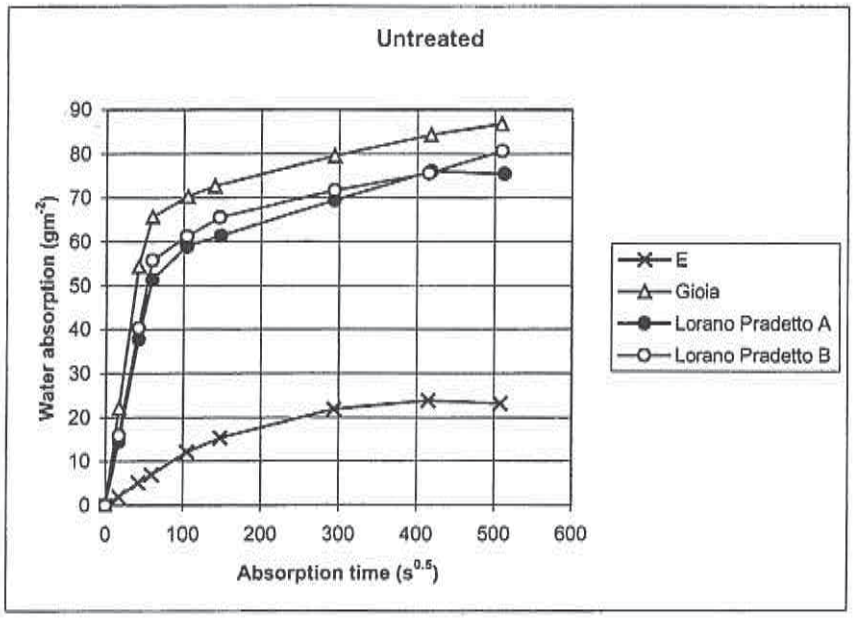

Figure 113. The average capillary water absorption curves of the untreated marble samples of E,D, Eand APE (N=24).

Figure 114 shows the average capillary water absorption curves of the temperature cycled marble samples. Marble D has the highest speed and amount of capillary water absorption. After temperature cycling both E and APE samples have very similar behaviour despite of the different orientation of the specimens. Also the capillary absorption phase and the diffusion phase are clearly distinguishable. Marble E shows slower capillary absorption but now the two absorption phases are readily distinguishable. All marble types have similar diffusion properties (slope of the latter linear part) after cycling.

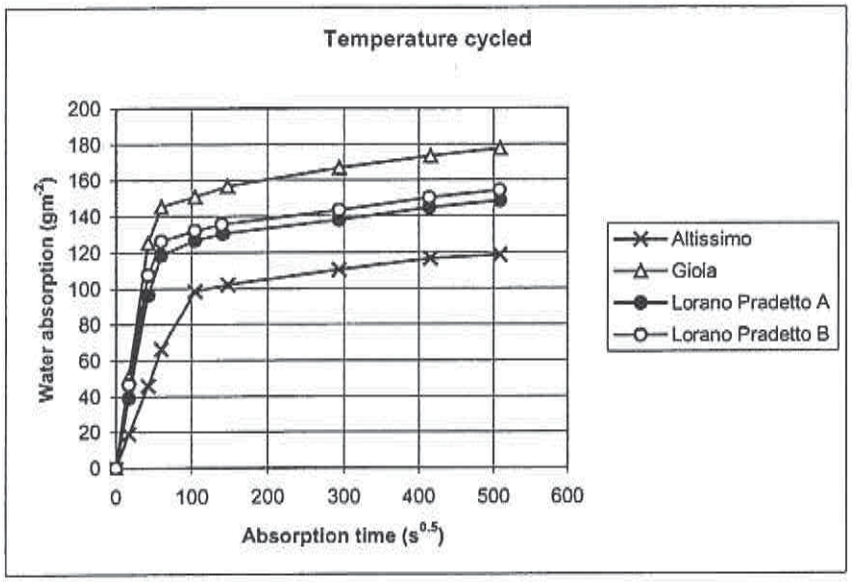

Figure 114. The average capillary water absorption curves of the temperature cycled marble samples of E,D, E and APE (N=12).

3.6.3.3 The effect of temperature cycling on the physical properties

The summary of the changes of the physical properties of the marble samples due to temperature cycling is presented in Table 24. Temperature cycling causes no measurable changes in grain densities of the samples, but a slight reduction (from 0.2 to 0.3 %) in bulk density is noticeable due to porosity increase.

Temperature cycling has a strong effect both on porosity and capillary water absorption coefficient. Marble D and both A samples have been subjected to very similar porosity increase (from 58 to 65 %), but in E an increase of 169 % has occurred. Similar behaviour can be seen in water absorption values. D and both A-samples have been subjected to an increase of 54 to 64 %, but in E the remarkable increase of 167 % has occurred. Sage (1988) reported 70 to 170 % increase in water absorption in heating of marble to + 66°C, which gives a very good reliability to the results obtained in this study.

Of all the determined physical properties, the temperature cycling has the most remarkable effect on the coefficient of capillary water absorption. In D E and APE the increase of this coefficient varies between 131 and 162 %, while E is subjected to an increase of 825 % due to temperature cycling. The behaviour of E and APE samples with different structural orientation is very similar in temperature cycling.

Table 24. The changes (untreated -> cycled) of the physical properties of the marble samples due to temperature cycling.

Marble Type / Change %	Grain Density (kgm^{-3})	Bulk Density (kgm^{-3})	Porosity (vol-%)	Water Absorption (w-%)	Capillary water absorption coefficient ($gm^{-2}s^{-0.5}$)
E (change %)	2721 -> 2721 (0 %)	2717 ->2709 (-0.3 %)	0.16->0.43 (+169 %)	0.06->0.16 (+167 %)	0.12->1.11 (+825 %)
D (change %)	2720 -> 2721 (0 %)	2710->2704 (-0.2 %)	0.37->0.61 (+65 %)	0.14->0.23 (+64 %)	1.28->2.96 (+131 %)
E (change %)	2717 -> 2717 (0 %)	2708->2702 (-0.2 %)	0.34->0.55 (+62 %)	0.13->0.20 (+54 %)	0.87->2.28 (+162 %)
APE (change %)	2718 -> 2717 (0 %)	2708->2702 (-0.2 %)	0.36->0.57 (+58 %)	0.13->0.21 (+62 %)	0.94->2.43 (+159 %)

Detailed data with curves of the changes in the determined physical properties caused by temperature cycling in all marble samples is presented in Appendix 5.

3.6.4 Microstructural properties

3.6.4.1 General aspects

Structural index properties determined from the marble samples included
- mineralogical composition,
- structure of rock and
- average grain size.

These properties were determined from thin sections TS-1 and TS-2 with a polarizing microscope. Resin filled fractures were determined from all types of thin sections. Fracture quality was determined by calculating the amount of resin filled fractures across the reference line belonging to following fracture categories: intragranular, intergranular, and transgranular.

Thin sections TS-1 and TS-2 were compared to reveal the structural changes caused by temperature cycling only. Thin sections TS-3 and TS-4 were compared to reveal the differences in structure of rupture created by bending strength test of the untreated and temperature cycled specimens. Thin sections TS-5 and TS-6 were compared to indicate the differences in the structure of rupture created by uniaxial compressive strength test of the untreated and temperature cycled specimens.

3.6.4.2 Mineralogy

Marble structures are classified from xenoblastic to homoblastic varieties. Xenoblastic structure is characterized by interlacing of irregular crystals closely fitted along their wavy contours. Homoblastic structure in marble is characterized by regular-shaped grains with straight or gently curving boundaries (Royer-Carfagni 1999).

All marble types show similar average grain size from 0.17 to 0.21 mm and standard deviation from 0.03 to 0.05 mm. D is the most coarse-grained type. E represent the xenoblastic end-member and D the homoblastic end-member, while A samples show intermediate structure. Xenoblastic structure causes uneven grain-size in E. Increased porosity and the coefficient of capillary water absorption coefficient seem to be related more to homoblastic than xenoblastic structure. All the marble types are composed of carbonate minerals with a small fraction of opaque minerals. Table 25 shows the mineralogy, grain size, and structure of the marble types.

Table 25. Mineralogy, grain size, and structure of the marble types (stdev = standard deviation, N= number of calculated grains).

Marble type	Grain size, average (mm)	Grain size stdev (mm)	N	Structure	Main minerals	Accessory minerals
E	0.18	0.05	222	Xenoblastic	Carbonates	Opaques
D	0.21	0.03	176	Homoblastic	Carbonates	Opaques
APA	0.17	0.03	215	Homoblastic/ Xenoblastic	Carbonates	Opaques
APE	0.19	0.04	199	Homoblastic/ Xenoblastic	Carbonates	Opaques

3.6.4.3 Microcracking

A. Temperature cycling

The crack densities were measured in three thin sections. Absent or very localized resin filling made reliable and comparable measurements of crack densities impossible in five thin sections. Microcrack densities of the untreated (TS-1) and temperature cycled (TS-2) thin sections based on the observation of resin filled cracks are presented in Appendix 5.

B. Bending strength test

The rupture in bending occurs frequently along the grain boundaries both in untreated and temperature cycled specimens. Cracks parallel to rupture are present especially in some temperature cycled specimens. E and D also show a decohesion zone near the rupture in untreated specimens. Cleavage

cracks are seldom associated with the rupture in bending. The quality of the rupture in the marble specimens after bending strength test based on the observation of resin filled cracks is presented in Appendix 5.

C. Compressive strength test

The cracking created by compression is located frequently along the grain boundaries both in untreated and temperature cycled specimens. Transgranular cracks exist mainly in temperature cycled specimens and intragranular cracks in untreated but also in temperature cycled specimens, especially in E. The quality of microcracks in the marble specimens after uniaxial compressive strength test based on the observation of resin filled cracks is presented in Appendix 5.

3.6.4.4 The effect of temperature cycling on the structural properties

Mineralogical changes are not expected to be caused by temperature cycling from -20°C to + 60°C. Mineralogical studies show no changes and this result is also supported by grain density measurements. The changes caused by temperature cycling are related to pore structure of marble i.e. thermal microfracturing. Increase of crack density of especially intergranular but also intragranular cracks was directly observed in the thin sections of D - marble, but this is evident also in the other marble types. This is also indicated by the clear increase of the values of porosity and coefficient of capillary water absorption. Thermal microfracturing mainly results in the decohesion of grain boundaries, but also in the opening of the cleavage cracks in some cases.

According to thin section studies, temperature cycling affects the location, where the bending rupture occurs in marble. Rupture occurs basically along grain boundaries in untreated and temperature cycled specimens, but transgranular cracks parallel to bending rupture may be created easier in temperature cycled than untreated specimens.

According to thin section studies, temperature cycling does not affect the cracking created by uniaxial compression. The only effect that can be claimed is that the transgranular cracking may be more frequent in temperature cycled than in untreated specimens.

3.6.5 Elastic stress-strain behaviour

3.6.5.1 Interpretation methods

For all compression test samples the elastic parameters, Young's modulus *(E)* and Poisson's ratio *(ν)*, are defined. The definition is basically done as secant value from the range of -0.01% radial strain *(ε_r)* to half of peak strength *(σ_p)* (Figure 115). The range is changed only if axial or radial

stress-strain behaviour is clearly non-linear within this range. The definition of the determination limits is presented in Hakala (1996). (Appendix 6.)

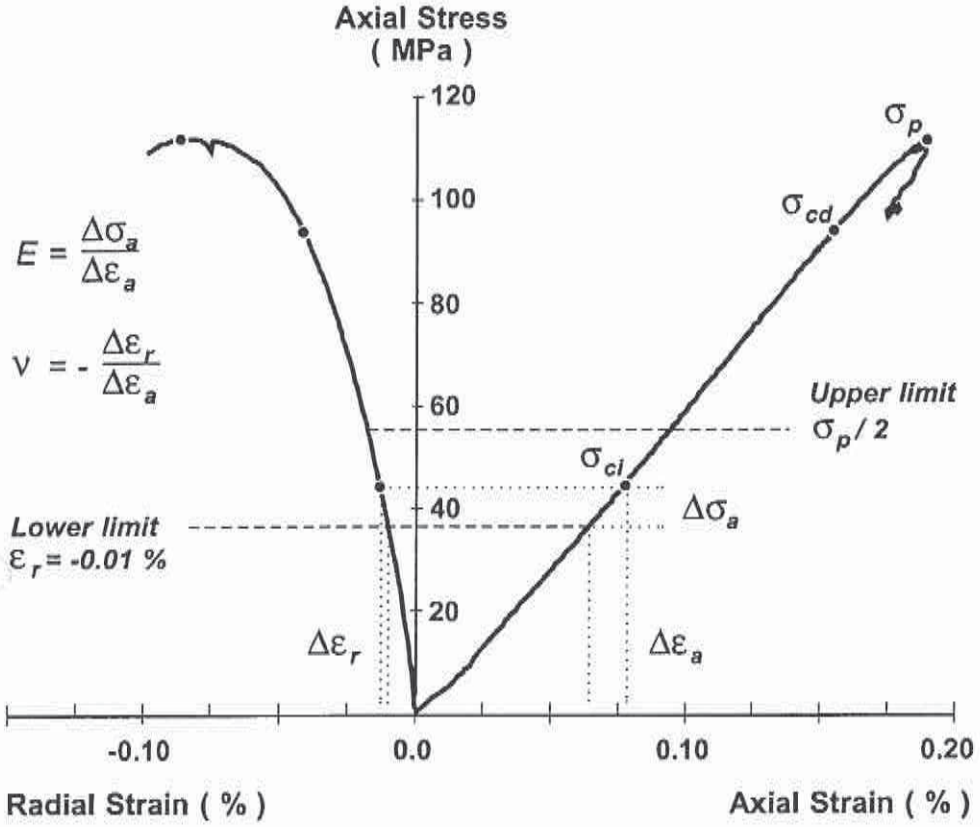

Figure 115. Determination of elastic parameters in compression.

3.6.5.2 Characteristics of uni- and triaxial stress-strain behaviour

On the test sample scale all the marbles are very homogenous and non orientated massive rock. The deviation of observed stress-strain and strength bahaviour is therefore relatively small (Figures 116-118).

Based on the test result marble E is the strongest of the studied marble types. Peak strength, crack damage and crack initiation values are noticeably higher than the rest of the marble types have. On the other hand, there doesn't seem to be big differences in the critical strain values between the E marble and the rest of the marble types. Therefore, it can be said that the E is more brittle compared to the other marbles.

Between the cycled and reference samples, there is clear difference in critical strain values, especially in uniaxial tests. The axial stress-strain behaviour of cycled samples is nonlinear at the beginning of the test. This is due to the micro cracks (damage) developed during the thermal cycling process.

In triaxial test the differences between reference and cycled samples are smaller than in uniaxial tests.

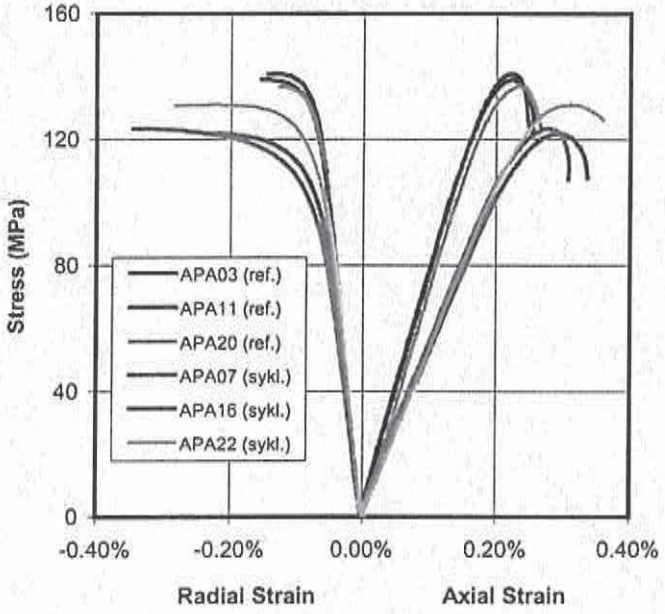

Figure 116. Uniaxial stress-strain behaviour of marble E.

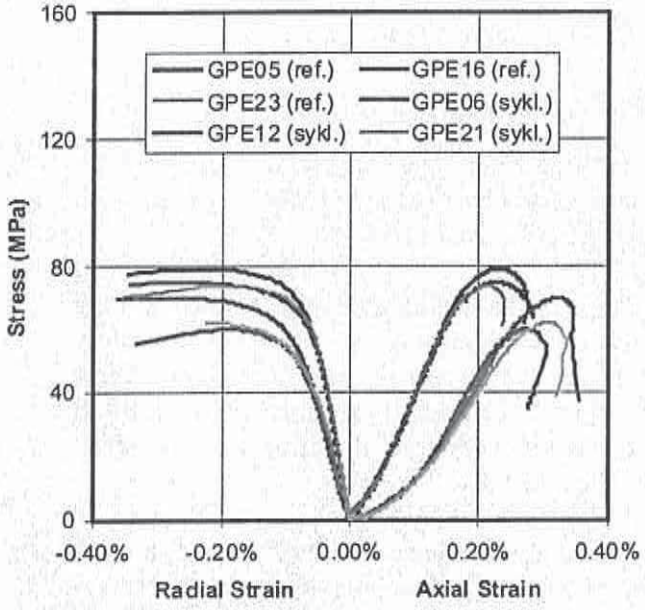

Figure 117. Uniaxial stress-strain behaviour of marble D.

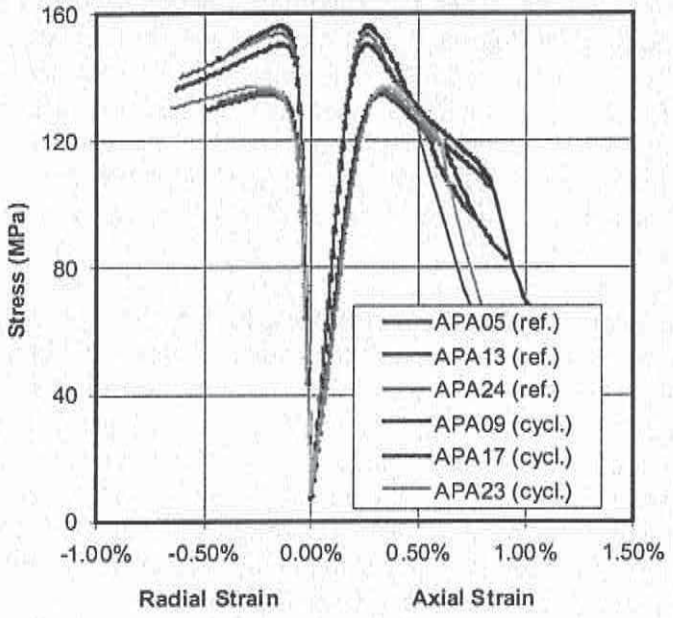

Figure 118. Triaxial stress-strain behaviour of marble E.

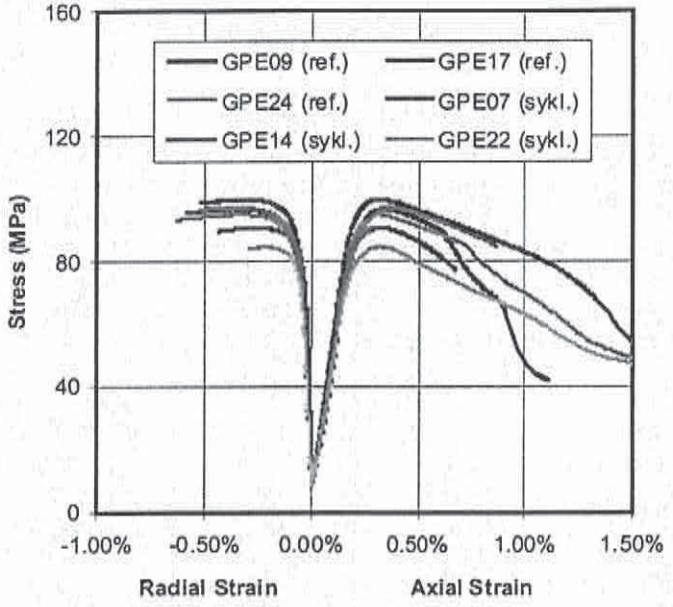

Figure 119. Triaxial stress-strain behaviour of marble D.

3.6.5.3 Young's modulus

The uniaxial Young's modulus of the studied marble samples were between 73 GPa and 26 GPa. The corresponding triaxial values were between 81 GPa and 34 GPa. Marble E was clearly most rigid of the tested marble types. The Young's modulus of reference E samples were about 70 - 80 GPa. The corresponding value for APA, APE and D marble types were about 45 - 55 GPa. The maximum standard deviation of one uniaxial test group were 3.1 GPa, which was about 13% of the average value. The maximum standard deviation of one triaxial test group was 4.2 GPa being 11% of the average value.

The thermal cycling has clear influence to the Young's modulus of the tested marble types. In every case the cycled Young's modulus were lower than the corresponding reference values. The biggest difference was in the results of APE samples. The average Young's modulus of cycled samples were only about 45% of the reference values. The corresponding numbers of samples were about 70%. The uniaxial Young's modulus of APA and D samples were about 65% - 75% of the reference values. In the triaxial test the corresponding rations are the same in the case of Eand APE marbles, but for APA and D it was about 90%. (Appendix 6.)

In triaxial tests the confinement of 5 MPa increases the Young's modulus. The Young's modulus in triaxial tests were between 107% and 154% of the corresponding uniaxial value. In most cases it was about 110% of the uniaxial value.

Table 26. Summary of the average values of the results and the differences between uniaxial and triaxial values.

Sample group		Uniaxial Young's modulus (GPa)	Triaxial Young's Modulus (GPa)	Difference tria./unia. (%)
E	**reference**	71.9	81.1	113%
	cycled	51.1	56.3	110%
	difference	71%	69%	
APA	**reference**	46.2	50.6	110%
	cycled	34.8	47.4	136%
	difference	75%	94%	
APE	**reference**	47.8	53.1	111%
	cycled	21.5	22.9	107%
	difference	45%	43%	
D	**reference**	45.7	50.1	110%
	cycled	29.8	45.9	154%
	difference	65%	92%	

3.6.5.4 Poisson's ratio

The uniaxial Poisson's ratio of the studied marble samples were between 0.15 and 0.45. The corresponding triaxial values were between 0.20 and 0.40. The difference between marble types were big, but the maximum standard deviation of one test group in both tests were only about 7% of the average value (Appendix 6).

According to the test results the thermal cycling has influence at least to the Poissons ratio of the APA and APE marbles (Table 27). The cycled uniaxial Poisson's ratio were about 55% - 65% and trixial about 80% - 90% of the reference value. The triaxial cycled Poisson's ratio of E samples were 78% of the reference value, but the differences between uniaxial values were insignificant. Both average Poisson's ratios of cycled D samples were nearly the same as the reference values.

The confinement of 5 MPa in triaxial tests lower slightly the Poisson's ratio. Exept for cycled APA and APE samples, the difference were in most cases about 10% - 20% (Table 27).

Table 27. Summary of Poisson's ratio.

Sample group		Uniaxial Poisson's ratio	Triaxial Poisson's ratio	Difference tria./unia. (%)
E	**reference**	0.37	0.34	91%
	cycled	0.36	0.26	74%
	difference	96%	78%	
APA	**reference**	0.41	0.39	94%
	cycled	0.26	0.31	116%
	difference	64%	79%	
APE	**reference**	0.32	0.29	93%
	cycled	0.17	0.26	148%
	difference	55%	88%	
D	**reference**	0.39	0.35	89%
	cycled	0.42	0.32	78%
	difference	106%	92%	

3.6.6 Critical stress states in compression,

3.6.6.1 Interpretation methods

A. Critical Stress States from Stress-Strain data

The critical stress states here refer to crack initiation stress (σ_{ci}), crack damage stress (σ_{cd}) and peak strength (σ_p) (Figure 120).

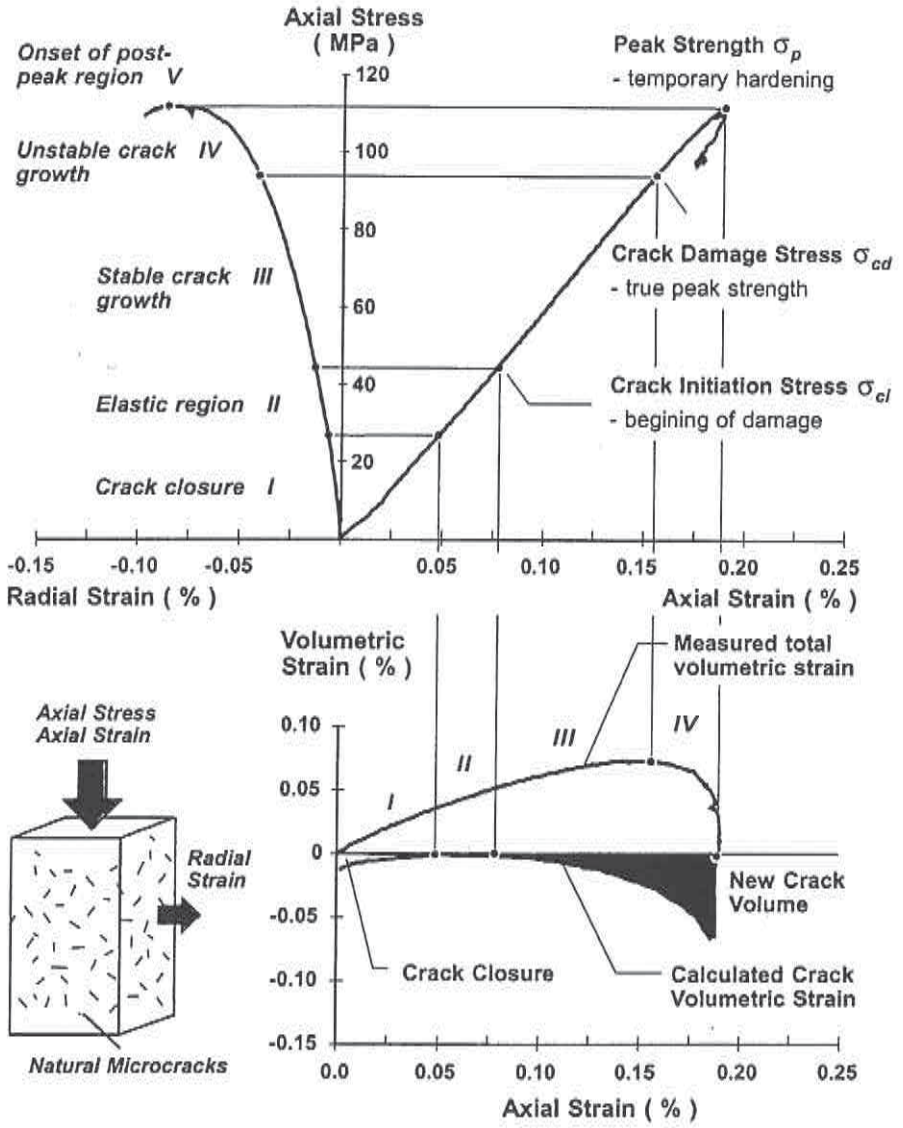

Figure 120. Determination of critical stress states σ_{ci}, σ_{cd} and σ_p (modified from Martin 1994).

The crack damage stress (σ_{cd}) is defined as the reversal of the volumetric strain (ε_v) curve. At this point the total volume of the specimen turns from compaction to dilation. The total volumetric strain (ε_v) is approximated from axial (ε_a) and radial strains (ε_r).

$$\varepsilon_v = \varepsilon_a + 2\varepsilon_r \tag{7}$$

The crack initiation stress is defined as a stress level where the crack volumetric strain ($\varepsilon_{v,cr}$) deviates from zero (Figure 120). The crack volumetric

strain ($\varepsilon_{v,cr}$) is calculated by subtracting the elastic deformations ($\varepsilon_{v,e}$) of the rock matrix from the total volumetric strain (ε_v). The elastic volumetric strain ($\varepsilon_{v,e}$) is defined by Young's modulus (E) and Poisson's ratio (ν) and current major (σ_1) and minor principal stresses (σ_3).

$$\varepsilon_{v,e} = \frac{1-2\nu}{E}(\sigma_1 - \sigma_3) \tag{8}$$

After subtracting the elastic volumetric strain ($\varepsilon_{v,e}$) from the total volumetric strain (ε_v), the crack volumetric strain curve is shifted so that the maximum value is zero (Figure 120).

The peak strength (σ_p) is defined as the highest observed axial stress.

B. Critical Stress States from Acoustic Emission data

Based on the knowledge of the former observations in the Laboratory of Rock Engineering (Hakala 1996) the use of acoustic emission measurements supports the analyse of the crack initiation (σ_{ci}) and crack damage (σ_{cd}) stresses. It seems to correspond well with the states of brittle failure, which are normally defined indirectly from stress-strain behaviour (Figure 121). The AE may give even more accurate results than the volumetric strain curves, because the measured fracturing is a direct observation of damage.

In this study the AE was measured during the compression and bending tests. For each event time, duration, sum of counts, energy, amplitude and rise time was recorded. The axial force from MTS was recorded as an external channel to syncronize the AE data with the stress-strain data.

The AE results are presented in the form of a cumulative number of counts as a function of axial stress. The results are divided to six different sub-groups according to the energy level. The dividing process have done so that the number of events is about the same in all six sub-groups.

The idea of defining the crack initiation (σ_{ci}) and crack damage (σ_{cd}) stresses from the cumulative amount of AE events - stress graph is shown in the Figure 122.

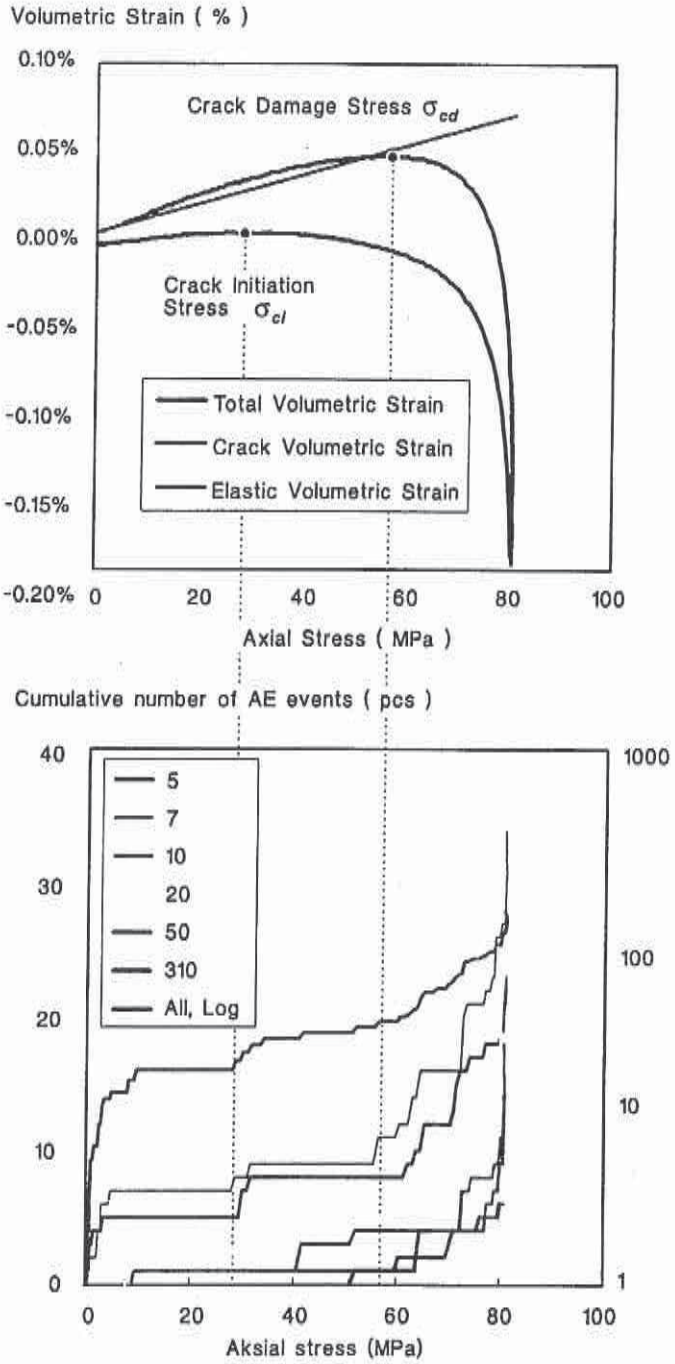

Figure 121. Comparison of typical strain and AE.

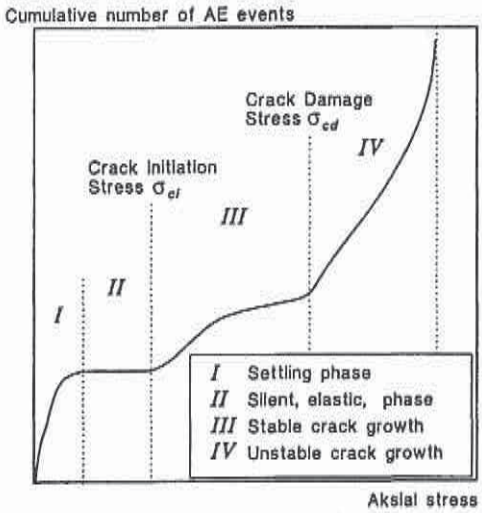

Figure 122. Definition of crack initiation stress and crack damage stress from typical design of AE data.

3.6.6.2 Peak strength

The measured uniaxial peak strength values varied from 141 MPa to 60 MPa. The corresponding triaxial values varied from 154 MPa to 84 MPa. From tested marble types E was clearly the strongest. The uniaxial peak strength was about 139 MPa ± 1.6 %. The average peak strength of the other marble types were between 73 MPa and 84 MPa. The maximum standard deviation was 3.7% of the corresponding average value (Appendix 6).

The triaxial peak strength of E marbles was about 152 MPa ± 0.9%. The average triaxial peak strength of the other marble types was between 86 MPa and 94 MPa and the standard deviations between 1.8% (1.5 MPa) and 5.6% (5.1 MPa).

According to the test results the thermal cycling has clear influence to the peak strengths of the tested marble types. The average peak strength of cycled samples were significantly lower than the corresponding reference values in every case (Table 28). The uniaxial peak strength of the cycled samples were between 84 - 96% of the reference values and the corresponding triaxial values were between 90% - 94%.

The confinement of 5 MPa in triaxial tests increases the measured peak strength of tested marble types. The triaxial values were 108% - 142% of the corresponding uniaxial values. If only deviatoric stress is considered the triaxial values were 104% - 134% of the uniaxial values.

Table 28. Summary of peak strength test results. The values in the

parentheses in the difference column are calculated reducing the confinement of 5 MPa from the triaxial value.

Sample		Uniaxial Peak strength (MPa)	Triaxial Peak strength (MPa)	Difference tria. / unia. (%)
E	**reference**	138.9	151.7	109% (106%)
	cycled	125.4	135.9	108% (104%)
	difference	90%	90%	
APA	**reference**	72.8	93.0	128% (121%)
	cycled	69.7	85.6	123% (116%)
	difference	96%	92%	
APE	**reference**	84.1	103.0	123% (117%)
	cycled	75.3	94.1	125% (118%)
	difference	90%	91%	
D	**reference**	75.7	97.0	128% (121%)
	cycled	63.7	90.7	142% (134%)
	difference	84%	94%	

3.6.6.3 Crack damage strength

The crack damage strength was definded in two different method. One method was based on the volumetric strain data by MTS and the other Acoustic Emission (AE) data.

The uniaxial crack damage values of tested four marble types according to the volumetric strain data varied from 121 MPa to 39 MPa. According to the AE data the uniaxial crack damage values were between 112 MPa and 21 MPa. The triaxial values varied from135 MPa to 53 MPa (Appendix 6).

The standard deviation of one test group in uniaxial test were between 1.6% (0.7 MPa) and 21.1% (13.2 MPa). In triaxial test the standard deviations varied from 1.6% (1.7 MPa) to 6.8% (4.7 MPa).

The tested E marble had clearly higher crack damage strength than the other marble types. In uniaxial tests the value was about 118 MPa ± 2.8 % and the triaxial value was about 133 MPa ± 1,6 %. The average uniaxial crack damage strength of the other marble types were between 43 MPa and 57 MPa and the triaxial values were between 54 MPa and 77 MPa (Table 29).

According to the test results the thermal cycling had clear influence only to the E and APE marble types. The cycled uniaxial crack damage value of D marble indicates also some reducing of the crack damage value during the

cycling, but the triaxial cycled value was even slightly higher than the reference value. The differences between reference and cycled values of triaxial APA and D and uniaxial APA values were all with in the standard deviations.

The confinement of 5 MPa in triaxial tests clearly increases the crack damage strength of tested marble types. The triaxial values were 112% - 239% of the corresponding uniaxial values. Without the confinement of 5 MPa in the triaxial values, the triaxial crack damage strength were still 106% - 222% of the uniaxial values. Generally in most of the cases the triaxial value were about 25% bigger.

The differences between the average values defined from MTS data to the values defined from AE data varied so, that the AE based values were between 79% to 106% of the MTS data based values. In general the AE based crack damage values were slightly lower, about 10%, than the MTS based values.

Table 29. Summary of the average crack damage values and the differences.

Sample group		Uniaxial			Triaxial	
		σ_{cd} (MPa)	σ_{cd} (AE) (MPa)	σ_{cd} (AE) / σ_{cd} (%)	σ_{cd} (MPa)	tri-x / uni-x (%)
E	**reference**	118.1	106.2	*90%*	132.7	112% (108%)
	cycled	93.6	87.4	*93%*	114.5	122% (117%)
	cycl./ref. (%)	*79%*	*82%*		*86%*	
APA	**reference**	45.0	44.8	*96%*	52.8	117% (106%)
	cycled	42.3	33.4	*79%*	58.2	137% (126%)
	cycl./ref. (%)	*94%*	*75%*		*110%*	
APE	**reference**	56.8	54.7	*96%*	77.3	136% (127%)
	cycled	50.7	40.0	*82%*	70.7	146% (135%)
	cycl./ref. (%)	*89%*	*73%*		*92%*	
D	**reference**	42.5	45.1	*106%*	68.5	161% (150%)
	cycled	29.0	29.2	*101%*	69.3	239% (222%)
	cycl./ref. (%)	*68%*	*65%*		*101%*	

The crack damage values of E samples were 69% - 87% of the corresponding peak strength valueas (Table 30). The other marble types had a little lower ratio, from 45% - 75%.

Table 30. Summary of crack damage values (σ_{cd}) as a function of peak strength (σ_p).

Sample group		$avg.\sigma_{cd}/\ avg.\sigma_p$		
		Uniaxial (%)	Uniaxial (AE) (%)	Triaxial (%)
E	reference	85%	76%	87%
	cycled	75%	69%	84%
APA	reference	62%	59%	58%
	cycled	61%	48%	68%
APE	reference	68%	65%	75%
	cycled	65%	53%	75%
D	reference	56%	60%	71%
	cycled	45%	47%	77%

3.6.6.4 Crack initiation strength

The defined uniaxial crack initiation values of four studied marble types varied according to MTS based volumetric strain data from 94 MPa to 10 MPa. The Acoustic Emission (AE) data based values varied between 86 MPa and 10 MPa. The triaxial crack initiation values varied from 123 MPa to 33 MPa (Appendix 6).

The standard deviations of one test group in uniaxial test were between 2.5% (0.6 MPa) and 35.5% (8.0 MPa). In triaxial test the standard deviations varied from 1.7% (0.6 MPa) to 21% (12 MPa).

The average crack initiation values of E samples were clearly higher than the other tested marble types had. The uniaxial values was about 87 ± 6 MPa and the triaxial value was about 106 ± 12 MPa. The average uniaxial crack initiation strength of the other marble types were between 35 MPa and 13 MPa. The triaxial values were between 54 MPa and 77 MPa.

According to the test results the thermal cycling had clear influence only to the E marble. The average crack initiation values of cycled E samples were 43% and 80% of the corresponding reference values. In triaxial tests the values and differerences of the other marble types were within the standard deviations. In uniaxial tests the average cycled crack initiation values of APA and APE were 54% - 85% of the reference values. The cycled values of D samples were even slightly higher or about the same as the reference values.

The confinement of 5 MPa in triaxial tests increases the crack initiation strength in most of the cases. Only the triaxial value of cycled E marble were clearly lower than the uniaxial value. Otherwise the triaxial values were 107% - 254% of the corresponding uniaxial values.

Without the confinement of 5 MPa the triaxial crack initiation values of APA reference samples and cycled E samples were lower than the uniaxial values. Otherwise the triaxial values without the confinement of 5 MPa were 14% - 122% higher than the corresponding uniaxial values.

The crack initiation values defined from AE data were in most cases lower than the values defined from MTS data based volumetric strain curves. Only the cycled APE samples had lower MTS based value. Otherwise the the AE data based values were between 49% to 95% of the MTS value.

Table 31. Summary of average crack Initiation values and the differences.

Sample group	Uniaxial			Triaxial	
	σ_{ci} (MPa)	σ_{ci} (AE) (MPa)	σ_{ci} (AE)/ σ_{cd} (%)	σ_{ci} (MPa)	tri-x / uni-x (%)
E reference	88.5	84.2	95%	105.9	120% (114%)
cycled	69.6	67.7	97%	46.0	66% (59%)
cycl./ref.(%)	79%	80%		43%	
APA reference	34.6	18.8	57%	37.0	107% (92%)
cycled	19.1	13.1	69%	33.8	177% (151%)
cycl./ref.(%)	55%	66%		91%	
APE reference	28.8	22.5	78%	44.4	154% (137%)
cycled	15.6	19.1	122%	39.7	254% (222%)
cycl./ref.(%)	54%	85%		89%	
D reference	23.5	13.4	57%	38.3	163% (142%)
cycled	24.2	11.9	49%	45.4	187% (167%)
cycl./ref.(%)	103%	89%		119%	

Table 32. Summary of crack initiation strengths (σ_{ci}) as a funktion of compresson strengths (σ_p).

Sample groups		avg.σ_{ci}/ avg.σ_p		
		Uniaxial (%)	**Uniaxial (AE)** (%)	**Triaxial** (%)
E	**reference**	*63.7*	*60.6*	*69.8*
	cycled	*55.5*	*53.8*	*33.8*
APA	**reference**	*47.5*	*27.2*	*39.6*
	cycled	*27.4*	*18.8*	*39.5*
APE	**reference**	*34.2*	*26.8*	*43.1*
	cycled	*20.5*	*25.5*	*42.5*
D	**reference**	*31.0*	*17.7*	*39.4*
	cycled	*37.7*	*18.8*	*50.1*

3.6.7 Bending test

3.6.7.1 Elastic parameters in bending

For all bending test samples the elastic parameter, Young's modulus *(E)* was defined. The loading method in the bending tests were three point loading (Figure 123). The Young's modulus *(E)* was defined by dividing the bending force *(F)* with the deflection at the center line *(y)* (Lama & Vutukuri 1978). The length of the beam *(L)* was needed, as well as the moment of inertia of the section (I_z) too.

$$E = \frac{F L^3}{48 y I_z} \tag{9}$$

The moment of inertia for rectangular samples is calculated from the width *(b)* and thickness *(h)* of the sample.

$$I_z = \frac{b h^3}{12} \tag{10}$$

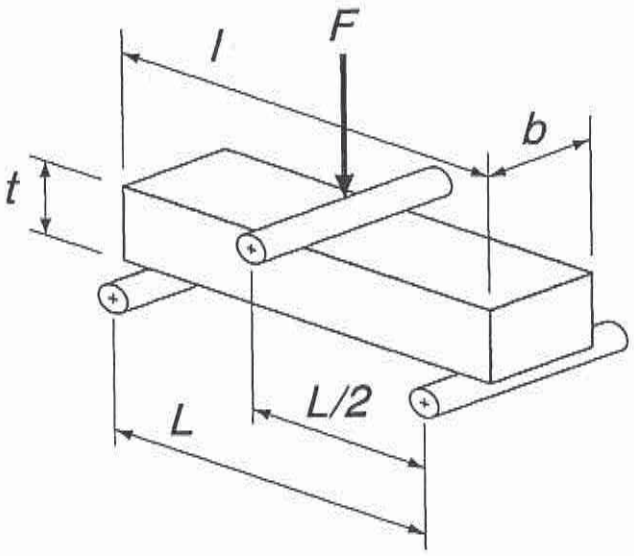

Figure 123. Three point loading of the bending test sample.

3.6.7.2 Bending strength

The measured bending strength values of four tested marble types varied from 25 MN/m^2 to 1.9 MN/m^2. The standard deviations of one test group were between 1% (0.1 MN/m^2) and 26% (2.2 MN/m^2) (Appendix 6).

From tested marble types E was clearly strongest. The average bending strength were about 24.3 MN/m^2± 2.2%. The bending strength of APA and APE marbles were about 15.2 MN/m^2± 15%.

The D marble were clearly the weekest of the tested marble types, 8.4 MN/m^2, and the standard deviation of the resutls (26%) were noticeably higher than the deviation of the other sample groups. One reason for that might be, that the samples looked visually different. The D18 sample looks quite a homogenous. There are only some gray spots. The D10 sample is not so homogenous and the D03 sample have a lot of gray spots. The gray material in the D samples may have an affect to the deviation of the measured bending strength of D marble.

According to the test results the thermal cycling has clear influence to the bending strength of the tested marble types (Table 33). The average bending strength of cycled samples were clearly lower than the corresponding bending strength of reference samples. The E marble had the smallest influence by the thermal cycling. The cycled bending strength were about 81% of the reference value. APE and APA marbles had the cycled value about 58% of the reference value. The D marble had biggest influence by the thermal cycling. The average cycled bending strength were only 23% of the reference value.

Table 33. Summary of the average bending strength values.

Sample group		Bending strength (MN/m^2)
E	**reference**	24.3
	cycled	19.8
	cycl./ref. (%)	*81%*
APA	**reference**	16.9
	cycled	10.1
	cycl./ref. (%)	*60%*
APE	**reference**	13.5
	cycled	7.6
	cycl./ref. (%)	57%
D	**reference**	8.4
	cycled	1.9
	cycl./ref. (%)	*23%*

3.6.7.3 Bending modulus

The defined bending modulus of four tested marble types varied from 46 GPa to 1.5 GPa. The standard deviations of test groups were between 17% (5.1 GPa) and 4% (0.1 GPa). From tested marble types E had clearly highest bending modulus, about 43.4 GPa ± 4.1%. The average bending modulus of APA and APE marbles were about 29.1 GPa ± 13%. The D marble had the lowest bending modulus, only 8.1 GPa ± 17% (Appendix 6).

Thermal cycling had clear influence to the bending modulus of the tested marble types. The average bending modulus of cycled samples were clearly lower than the corresponding modulus of reference samples.

The differences between the average bending modulus values of the reference samples to the cycled samples were between 20% and 68% (Table 34). The average values of the cycled samples were in every case significantly lower than the average values of reference samples. The cycled bending modulus of E samples were about 68% of the reference value. APE and APA marbles had the cycled value about 28% of the reference value. The D marble had the biggest influence by the thermal cycling. The average cycled bending modulus were about 20% of the reference value.

Table 34. Summary of the bending modulus.

Sample group		Bending Modulus (GPa)
E	**reference**	*43.4*
	cycled	*29.6*
	cycl./ref. (%)	68%
APA	**reference**	*30.4*
	cycled	*8.1*
	cycl./ref. (%)	27%
APE	**reference**	*26.4*
	cycled	*7.8*
	cycl./ref. (%)	29%
D	**reference**	*8.1*
	cycled	*1.6*
	cycl./ref. (%)	20%

3.6.8 The effect of number of cycles

The effect number of cycles were tested with APE and E samples and with the bending test configuration. The samples in this tests were cycled 1, 5, 10, 50 and 100 times. The measured bending strength values of APE samples varied from 12 MN/m^2 to 6.4 MN/m^2. The standard deviations of test groups were between 1.8 MN/m^2 and 0.1 MN/m^2. The maximum and minimum standard deviations of the average values were between 20% and 1.4% (Appendix 6).

The measured bending strength values of E samples varied from 24 MN/m^2 to 17 MN/m^2. The standard deviations of one test groups were between 2.3 MN/m^2 and 0.2 MN/m^2. The maximum and minimum standard deviations of the average values were between 10% and 0.9%.

The bending strength values of the reference and cycled samples measured in the bending tests were enclosed to the results of the this tests. They represent a non-cycled and 500 times cycled samples. All the average values and standard deviations for marble APE and E are presented in Appendix 6.

According to the test results presented in the chapter 3.7.7.2 (Bending strength) the thermal cycling at 500 times has clear influence to the bending strength. From the results of the APE samples in Table 35 it can be seen that the biggest difference in the bending strength is between the non-cycled and the one time cycled samples. That means that the major decrease in the bending strength of APE marble happens during the first cycle.

Taking into consideration the standard deviations it is clear that the differences between the different sample groups after five cycles are insignificant. The differences between the bending strength of 50, 100 and 500 times cycled samples are well within the deviation. So, most of the total decrease of the bending strength of APE marble seems to happen during the very first five cycles.

Table 35. The summary of the average bending strength values and the differences between the test groups for marble type APE.

Cycles (pcs)	Average Bending strength (MN/m2)	Difference (MN/m2)	Difference (%)
0	16.9		
1	11.2	-5.7	67%
5	10.1	-1.1	90%
10	9.8	-0.2	98%
50	8.9	-0.9	90%
100	10.5	1.6	118%
500	10.1	-0.4	96%

The results of the E marble are presented in Table 36. According to these test results the biggest difference in the bending strengths is between one time and five times cycled samples. The differences between the bending strength of sample groups after five cycles are insignificant. So, the biggest and main decrease of the bending strength of E marble happens during the very first five cycles too.

Table 36. The summary of the average bending strength values and the differences between the test groups for marble type E.

Cycles (pcs)	Average Bending strength (MN/m2)	Difference (MN/m^2)	Difference (%)
0	24.3		
1	22.7	-1.7	93%
5	18.6	-4.1	82%
10	19.6	1.0	105%
50	20.2	0.6	103%
100	19.1	-1.1	95%
500	19.8	0.7	104%

3.6.9 Discussion

3.6.9.1 Physical properties

This study reveals the clear effect of thermal cycling on the physical properties related to pore structure of marble at the temperature range simulating the Nordic climate. Pore structure is modified by introduction of thermal microfracturing, which results in the decohesion of the grain boundaries and cleavage fractures. Thermal cycling seems not to change mineralogy or density of marble types tested in this study.

Loosening of the grain structure leads to the increase of porosity and it speeds up the capillary water absorption remarkably. This means also a decay in the strength properties and may expose more pore surface to weathering and accelerated intrusion of external weathering agents. This may be also a partial reason for the bending of marble claddings.

Materials used in this study consisted of three marble types, which were expected to have different quality properties already before thermal cycling. Marble E with xenoblastic microstructure represents the good marble quality with low porosity and small coefficient of capillary water absorption. Type D, on the contrary, represents poor quality with higher porosity and big coefficient of capillary water absorption, whereas type A with intermediate microstructure represents also intermediate porosity and capillary water absorption characteristics.

This study indicates that the greatest reduction of the marble quality due to thermal cycling is directed to marble type E with the best original quality, so the thermal cycling seems to equalize the differences in pore characteristics between the marble types. The amount of quality reduction is in accordance with the results of earlier studies found in literature. Different structural orientation seems not to affect the behaviour of marble type A in thermal cycling.

The realized study with 500 cycles of treatment only, did not shed light on the changes of the physical properties of the marble types as a function of thermal cycles. According to the literature the greatest changes in the pore structure of marble are expected to be introduced during the first thermal cycles and only minor changes during repeated cycles. Obviously the majority of the changes in the physical properties revealed in this study occur already long before 500 cycles of treatment. Probably even the first drying of the untreated specimens to the temperature of +60°C modifies the pore structure of certain marbles so much, that "untreated" may not be a proper term in this study.

3.6.9.2 Mechanical properties

The testing program was very good and made clear the effect of thermal cycling. Taking into consideration that all the marble types were very homogenous and non-orientated massive rock, the amount of samples in same test group were enough. The deviations were very small .

Normally in uniaxial and triaxial tests the radial deformation is measured with roller chain extensometer. The roller chain couldn't be used because of the square cross-section of the samples. Instead of the chain extensometer the radial deformation was measured with two separately readen 30 mm long strain gages.

The test results presented in this report are fully comparable. There are no differences in handling of the samples and all the tests are made in the same manner. But, the method used in this study does not agree with the standards of ISRM. The cross-section of the samples were square instead of being circular. So, that may affect to the observed results and it is should be taken in to consideration if comparing to other test results.

The E marble is the strongest of all the studied four marble types. Both uniaxial (139 MPa) and triaxial (152 MPa) peak strengths and bending strength (24 MN/m^2) were significantly higher than the rest of the marble types had. The values were still high after the thermal cycling, which lowered the peak strengths only about 10% and bending strength about 20%. The Young's modulus (72 GPa) and bending modulus (43 GPa) of APA samples are considerably higer compared to the other marble types too. After the thermal cycling they were about 70% of the un-cycled reference values.

Type APA and APE have very same kind of strength parameters. The uniaxial (84 MPa) and <riaxial (103 MPa) peak strengths of APE seems to be a little higher than the uniaxial (73 MPa) and triaxial (93 MPa) values of APA. But, on the other hand, APA have a little higher bending strength (17 MN/m^2) than APE (14 MN/m^2). The Young's modulus (APA 46 GPa and APE 48 GPa) and the bending modulus (APA 30 GPa and APE 26 GPa) were at the same level. The effects of the thermal cycling were very equal too.

The cycled peak strengths were about 90% - 96% of the reference values. The bending strengths were about 60% after the cycling of the values they used to be before cycling. The bending modulus are correspondingly only about 30% after the cycling. The only exception seems to be the cycled Young's modulus. Both, uniaxial and triaxial, tests proves that the cycled Young's modulus of APE is only about 45% of the reference value. The difference between uncycled and cycled values of APA samples are clearly smaller. The cycled value was 75% of the reference value.

The D marble is the weakest of the studied marble types. The uniaxial (76 MPa) and the triaxial (97 MPa) peak strengths and the Young's mudulus (46 GPa) were at the same level with the values of APE and APA samples. But, the bending strength (8 MN/m^2) and modulus (8 GPa) were considerably lower. Thermal cycling seems to have enormous effect to the bending values of D marble. It is after the cycling process only about 20% of the already very low reference values.

The crack damage and crack initiation values were defined from uniaxial and triaxial tests. The uniaxial values were defined with two different method, using the volumetric strain data by MTS and the Acoustic Emission (AE) data. In general the uniaxial crack damage values were little over 60% and triaxial about 75% of the peak strength. Correspondingly the uniaxial crack initiation values were about 35% and triaxial about 45% of the peak strength. Thermal cycling didn't have any clear effect to the crack damage and initiation values. In most cases the values were lower after cycling, but in some cases they were even slightly higher after the cycling.

The determination of the crack initiation values of cycled samples may not be as straightforward. It is questionable if it is correct to define the crack initiation value for broken material from the volumetric strain data. There is not necessarily any more the elastic phase in the strain data, which is needed in the determination. The cycled samples were not possible unbroken, but it is not clear if they were too broken for the determination of crack initiation value.

The cycling test of APE and E samples proves that even the very first cycles can have the most significant influence. The numbers of the cycles does not have any major influence after the first five cycles. The differences after that in bending strengths are within the deviation.

3.7 DIRECT TENSILE STRENGTH TEST

3.7.1 Test results

Test results for each marble type before and after conditioning of the samples are presented in Figures 124-127. The diagrams represent the axial load as a function of the relative displacement measured across the specimen notch (50 mm gauge length). Each one of the pictures refers to the same material qualities. A softening branch appears for all type of materials, and the steepest slopes, as well as the highest peak loads, are showed, as a rule, by xenoblastic marbles (E and K types). We observe, in passing, that without a careful closed loop control, the post-critical branches would have not appeared. Complete results ar presented in Appendix 7.

From the test measurements it is also evident that the orientation of the rift plane may influence the material response. In general, we might expect that specimens loaded at right angle to rift plane show less resistance than when

the rift plane is parallel to the specimen axes. Possible differences are not very clear for E and even more so for K-type marbles (both are xenoblastic textures), but they become extremely clear for the other qualities. For D-marbles, in particular, the peak load for "pe-" type specimens (rift perpendicular to the specimen axis) may be less than half of "pa-" type specimens (rift parallel to the specimen axis) (Appendix 7).

We observe in passing that such order is in accord with a material classification based upon the granular texture, since E is the most xenoblastic marble, D the most homoblastic, while K and A are intermediate cases but K is more xenoblastic than A.

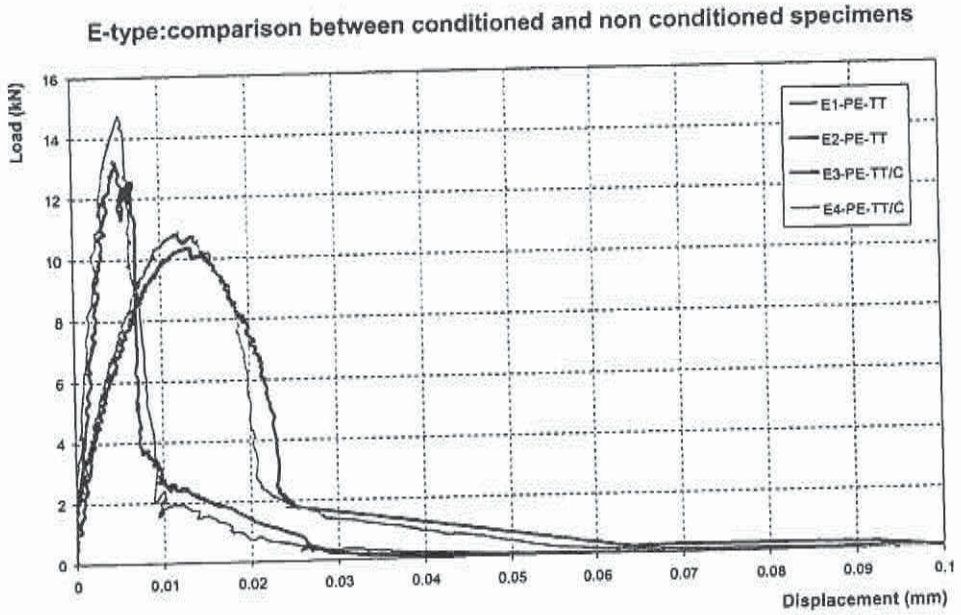

Figure 124. Comparison among non-conditioned and conditioned samples E-type marble. Specimens carved perpendicularly to rift plane.

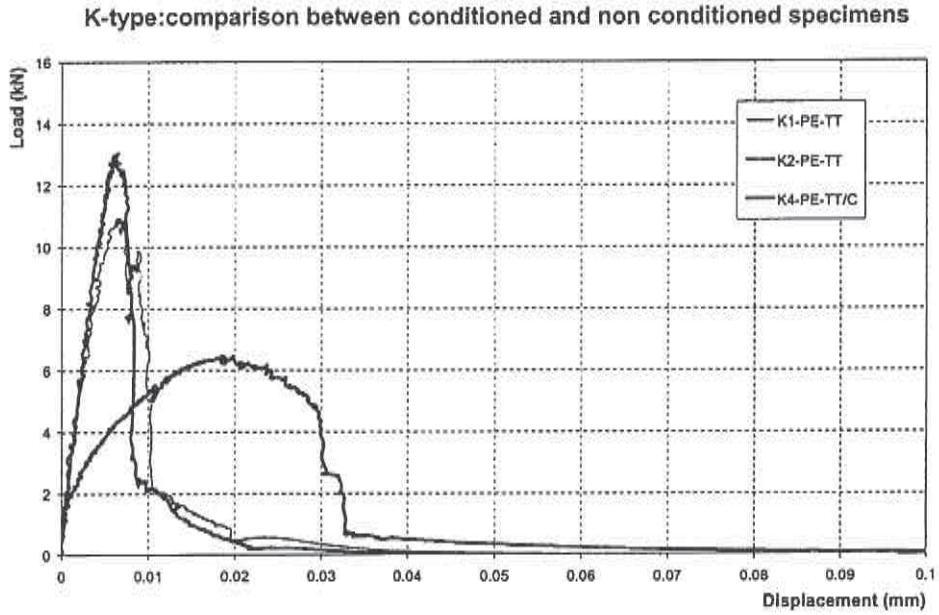

Figure 125. Comparison among non-conditioned and conditioned samples. K-type marble. Specimens carved perpendicularly to rift plane.

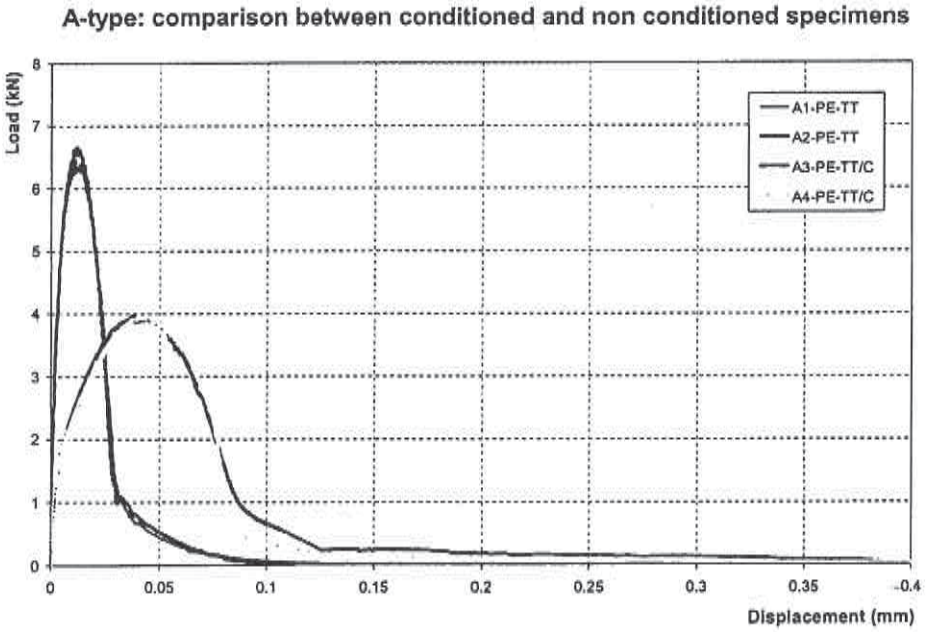

Figure 126. Comparison among non-conditioned and conditioned samples. A-type marble. Specimens carved perpendicularly to rift plane.

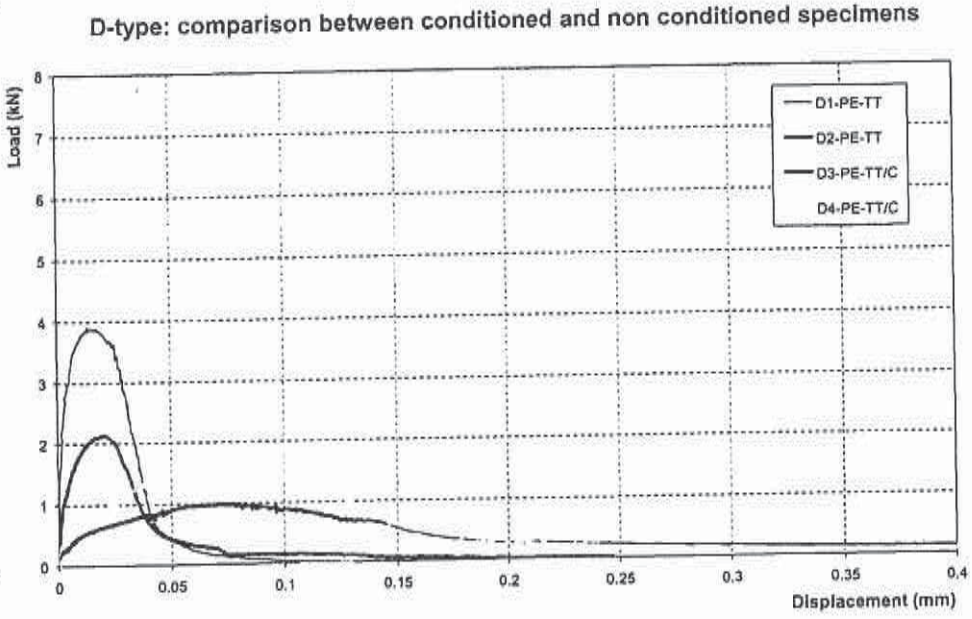

Figure 127. Comparison among non-conditioned and conditioned samples. D-type marble. Specimens carved perpendicularly to rift plane.

Different marble qualities show different attitudes towards thermal conditioning. The damaging effects for each marble type can be evaluated by examining the graphs represented in Figures 128-131, where for each material quality the responses of conditioned and unconditioned specimens are juxtaposed. In all cases, thermal treatments produce a generalized loosening of the rock: the peak load diminishes and the softening branches result less steep, while the area contained under the graph increases.

E type marble is the one for which the responses between conditioned and unconditioned sample differ the less. On the other hand, D type marbles show the greatest changes. Again, the microstructural texture seems to play a fundamental role. This is not surprising, since the greater inter-connection of xenoblastic granules with respect to the homoblastic ones, surely produces a greater resistance to the desegregation produced by thermal variations.

During the tests, the symmetric opening of the crack, controlled through the rotation of the specimens' heads, has been checked using laser Electronic Speckle Pattern Intorfermetry (ESPI). It has thus been possible to determine the exact instant of the crack nucleation, as well as the crack progression at the peak loads. Figure 128 refers to E-type unconditioned specimen with the rift plane parallel to the axes (ref. E1-PA-TT). Comprehensive measurement data is presented in Appendix 7.

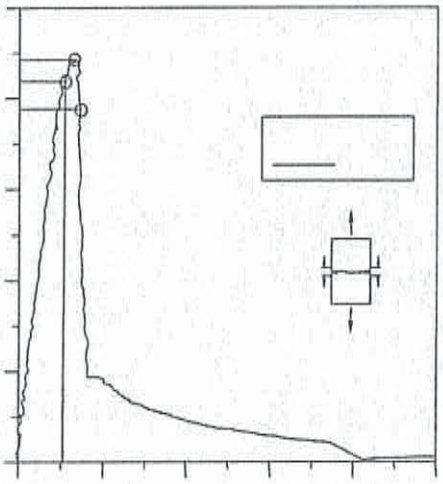

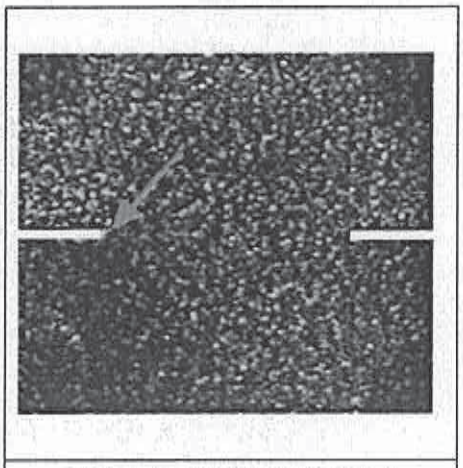

Crack nucleation. Point A

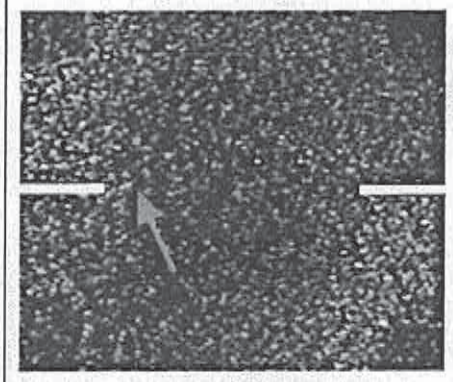

Crack at peak load. Point B

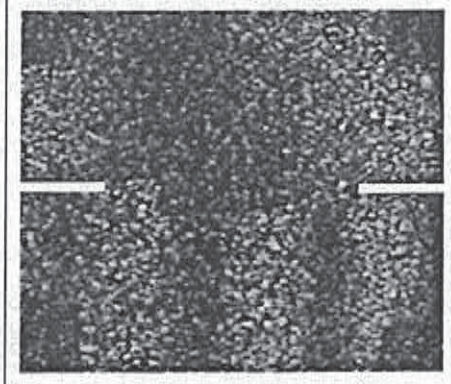

Crossing through crack. Point C

Figure 128. ESPI observation of the crack progression, with indication of crack nucleation (Point A in the graph), crack extension at peak load (point B) and crossing through crack (point C). Test # E1-PA-TT.

Processing the images obtained through the ESPI apparatus, it has also been possible to calculate the local strains in the specimen. Table 37 collects the data for six representative tests corresponding to the instant in which the crack nucleation occurs (points A in the previous graphs). The points where local strain has been calculated are in material portions in neighbourhoods of the borders and of the centre of the main initiating crack.

Comparing these data with the average strain also reported in the table, calculated by dividing the relative displacement recorder by transducers by the transducer length (50 mm), we notice that such values are of the same order of magnitude of the local measurements at the borders of the initiating crack. This is a confirmation that the crack has not opened yet, otherwise the relative displacement of the crack surfaces would have affected the average strain. In other words, if a main crack had opened, the average strain would have resulted greater than the local strain (Figure 129).

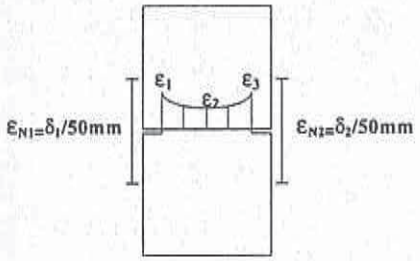

Figure 129. The three different location at which local strain has been calculated from ESPI data.

Table 37. Local strain (at 3 different location, Figure129) obtain from ESPI measurements and corresponding average strain obtain from transducers (50 mm gauge length). Crack initiation (points A in the graphs).

	Strain				
	From ESPI			from transducers	
Test	ε_1	ε_2	ε_3	ε_{N1}	ε_{N2}
E1-PE-TT	0.000107	0.0000628	0.0000877	0.0000852	0.0000828
E3-PE-TT/C	0.0000747	0.0000482	0.0000715	0.0000798	0.0000772
K1-PE-TT/C	0.0000612	0.0000531	0.0000935	0.0000802	0.000143
K4-PE-TT/C	0.000116	0.0000506	0.000104	0.000124	0.000123
D1-PE-TT	0.0000925	0.0000547	0.0000826	0.0000912	0.0000788
D3-PE-TT/C	0.000305	0.000158	0.000253	0.000342	0.000369

The values of the peak stress, peak strain, tangent elastic modulus both in the hardening and in the softening branches (calculated at 50% of peak load) are summarized for the all the 23 tests in Table 38. An indication of the material fracture energy can also be obtained, albeit roughly, by calculated the area under the load vs. displacement graphs.

Table 38. Summary matrix for direct tensile tests.

Specimen	Peak stress	Ultimate strain	Young's Modulus (50% peak load)	Young's Modulus in softening (50% peak load)	Material fracture energy
	(MPa)	(με)	(GPa)	(GPa)	(Joule/m^3)
E1-PA-TT	8.89	745.10	65.97	-83.01	65.48
E2-PA-TT	8.80	1966.40	58.93	-80.27	63.75
E1-PE-TT	8.95	2483.70	90.83	-107.15	70.76
E2-PE-TT	8.06	1807.95	56.41	-102.80	65.70
E3-PE-TT/C	6.12	38757.20	29.88	-39.92	157.73
E4-PE-TT/C	6.41	32556.70	31.34	-89.30	141.85
K1-PA-TT	6.13	514.70	37.46	-91.97	72.51
K2-PA-TT	8.21	18799.15	61.13	-167.38	65.15
K1-PE-TT	7.07	1928.70	37.65	-56.99	64.25
K2-PE-TT	8.30	3001.80	64.23	-55.26	55.55
K3-PE-TT/C	Failed	-	-	-	-
K4-PE-TT/C	3.86	21586.30	11.09	-46.09	110.29
A1-PA-TT	5.76	20906.45	41.11	-15.67	156.35
A1-PE-TT	4.18	3324.65	30.20	-15.13	107.06
A2-PE-TT	4.62	36115.95	33.09	-14.64	118.40
A2-PE-TT/C	2.32	12131.95	3.56	-2.98	185.42
A1-PE-TT/C	2.33	15478.85	3.08	-3.97	167.01
D1-PA-TT	3.21	4016.10	26.07	-3.29	152.84
D2-PA-TT	2.73	8234.45	14.07	-2.07	202.17
D1-PE-TT	2.21	2576.30	14.84	-5.04	74.88
D2-PE-TT	1.38	4942.50	4.94	-2.97	93.95
D3-PE-TT/C	0.54	11830.20	0.49	-0.22	94.35
D4-PE-TT/C	0.56	11681.75	0.55	-0.46	79.37

3.7.2 Discussion

It is interesting to notice that the local strain measured in unconditioned sample (no thermal treatment) is of the same order of magnitude for the all materials. This means that in the pre-critical regime, before a main crack is developed, the tensile response is the same for all material types, independently of the microstructure. This is not surprising, since in the pre-critical stage no possibly grain sliding occurs.

Thermal treatments do not influence considerably the response of material E in the pre-critical stage. However, the conditioning increasing the strain level in material K and even more son in material D. For the latter, the strain becomes three times that calculated in the unconditioned samples. This is a clear effect of the microstructural loosening produced by thermal changes, which is of course more effective in the homoblastic than in the xenoblastic materials.

An interesting finding from the exam of this table is that, apparently, the fracture energy of xenoblastic marbles is less than that of homoblastic marbles. This is an immediate consequence of the greater apparent ductility of the homoblastic with respect to the xenoblastic qualities. In fact, the peak load decreases is somewhat compensated by the increased ductility, so that the underlying area increases as a whole.

Analogously, we notice that for the same material the fracture energy may be enhanced by thermal treatments. This is again to be attributed to a ductility increase, caused this time by a generalized loosening of the granular microstructure, which accompanies the thermal treatment. Also in this case, the energy increase is percentile more evident in homoblastic than in xenoblastic marbles. In other words, we find that thermal treatment apparently increases the material toughness. We anticipate that tests with the pre-cracked beam technique show, on the contrary, the opposite trend: thermal treatment diminishes the marble toughness.

A possible explanation for this somehow paradoxical result may be the following. In a direct tensile tests a "cloud" of microcracks is usually produced around a dominant crack. Such irregularity is usually referred to a s the process zone. The value of the fracture energy calculated by evaluating the area under the graphs represents an indication not only of the fracture energy spent when opening a dominant crack, but also of the energy dissipated in the process zone.

Evaluating the local strains be means of laser interferometry, it has been possible to estimate the extension of the process zone. The conclusion is that the process zone is much larger in the homoblastic than in the xenoblastic marbles. This is essentially due to the geometry of the grains: homoblastic textures may allow consistent grain sliding before failure.

Consequently, the energy necessary to produce the specimen rupture, which is equal to the product between the specific fracture energy and the total area of all the fractures produces, may results greater in the homoblastic than in the xenoblastic marbles. In fact, despite the specific fracture energy since in the former the number of fractures produced is much larger than in the latter.

The same argument can also explain the apparent energy increase due to thermal treatments. We anticipate that when a dominant crack is introduced *a priori*, likewise in the case of pre-cracked beams (Section 3.9), the nucleation of a dominant crack is driven by the introduced discontinuity. In other words, the formation of a process zone is restricted by the presence of a sharp notch. This is way the results obtainable with pre-cracked bending may be qualitatively opposite.

3.8 PRE-CRACKED BENDING TEST

3.8.1 Test results

For the two-step procedure previously outlined, i.e. *i*) insertion of a natural crack *ii*) fracture toughness tests under 3-Point-Bending, a high-capacity servo-hydraulic MTS testing machine and an electro-mechanical MTS testing machine were used, respectively. To determine crack length, a visuali-

zation technique using a mix of magic blue and acetone was adopted (Appendix 7).

Normalized pre-crack lengths could be obtained in the different marbles with the two techniques. The load at which propagation from the notch occurred could not be determined accurately, as, differently from ceramics (Nicoletto & Esposito, 1991-1996), a distinct "click" sound could not be heard. This appears to be a peculiarity of marbles, confirmed by the unsuccessful use of acoustic emission techniques on this material. It can be noted that the two marbles responded differently to the pre-cracking techniques.

The B method did not generally give acceptable performance due to the highly localized stresses that develop in the specimen at the bridge corner. This stress concentration generally caused the marble to crush (especially D-type) before the stress intensity for cracking initiation was attained at the machined notch. On the other hand, both marbles could be confidently pre-cracked with the SB method. Suitable values of the $(EI)_b/ (EI)_s$ ratio where 4.83 for E-marbles and 1.82 for D-marbles, respectively.

The total number of tests performed has been collected in Table 35. The natural precracking bridge-method was abandoned after a few preliminary tests. Thus, evaluation of the material fracture toughness was limited to sandwich-beam pre-cracked specimens and to specimens containing natural pre-cracks 150-μm-wide, obtained though a precision diamond saw.

Each test is referred to with simple initials. The first two letters indicate the material (E, K, A, D) and the test number; the second two letters give the position of the marble rift plane with respect to the specimen axis (-pe=perpendicular; -pa=parallel); the letters –BE stand for Bending-Test. For what the precracking method is concerned, the initials B or SB indicate natural pre-cracking obtained through either the bridge method (B) or the sandwich beam method (SB), whereas N is used in the case of notched specimens (the notch obtained with a diamond saw).

Finally, possible thermal treatments are mentioned through C1 and C2. Each initial refers to a different conditioning: C1 indicates 60 thermal cycles from –10°C to +30°C, whereas C2 indicates 60 thermal cycles from 5°C to +45 °C (notice that the thermal interval is the same, but in C2 the 0°C point is not comprised). Thus, for example, E3-PE-BE-N/C1, indicates the third bending test on E-type marble, with rift plane perpendicular to specimen axis, pre-cracked with a notch and subjected to C1-type thermal conditioning (–10°C to +30°C).

Table 39. Test summary for pre-cracked beam bending tests

Bending tests								
N°	Spec. name	Marble-type	test nr.	termal conditioning	Dim (cm)	Angle to rift	Technique	Fracture toughness ($MPam^{0.5}$)
1	E1-PE-BE-N	E	N1	NO	1x2x10	90	notch	1.08
2	E1-PA-BE-N/C1	E	N1	60 cyc.-10°C to+30°C	1x2x10	0	notch	1.05
3	E2-PA-BE-N/C2	E	N2	60 cyc.+5°C to+45°C	1x2x10	0	notch	1.03
4	E1-PE-BE-N/C1	E	N1	60 cyc.-10°C to+30°C	1x2x10	90	notch	1.04
5	E2-PE-BE-N/C1	E	N2	60 cyc.-10°C to+30°C	1x2x10	90	notch	1.06
6	E3-PE-BE-N/C1	E	N3	60 cyc.-10°C to+30°C	1x2x10	90	notch	1.05
7	E4-PE-BE-N/C2	E	N4	60 cyc.+5°C to+45°C	1x2x10	90	notch	1.19
8	E5-PE-BE-N/C2	E	N5	60 cyc.+5°C to+45°C	1x2x10	90	notch	1.19
9	E6-PE-BE-N/C2	E	N6	60 cyc.+5°C to+45°C	1x2x10	90	notch	1.04
10	K1-PA-BE-SB	K	N1	NO	1x2x10	0	sand.beam	1.34
11	K2-PA-BE-N	K	N2	NO	1x2x10	0	notch	0.93
12	K1-PE-BE-SB	K	N1	NO	1x2x10	90	sand.beam	1.25
13	K2-PE-BE-N	K	N2	NO	1x2x10	90	notch	0.78
14	K3-PE-BE-N	K	N3	NO	1x2x10	90	notch	0.79
15	K4-PE-BE-N	K	N4	NO	1x2x10	90	notch	0.72
16	K1-PA-BE-N/C1	K	N1	60 cyc.-10°C to+30°C	1x2x10	0	notch	0.78
17	K2-PA-BE-N/C2	K	N2	60 cyc.+5°C to+45°C	1x2x10	0	notch	0.86
18	K1-PE-BE-N/C1	K	N1	60 cyc.-10°C to+30°C	1x2x10	90	notch	0.74
19	K2-PE-BE-N/C1	K	N2	60 cyc.-10°C to+30°C	1x2x10	90	notch	0.72
20	K3-PE-BE-N/C1	K	N3	60 cyc.-10°C to+30°C	1x2x10	90	notch	0.73
21	K4-PE-BE-N/C2	K	N4	60 cyc.+5°C to+45°C	1x2x10	90	notch	0.74
22	K5-PE-BE-N/C2	K	N5	60 cyc.+5°C to+45°C	1x2x10	90	notch	0.71
23	K6-PE-BE-N/C2	K	N6	60 cyc.+5°C to+45°C	1x2x10	90	notch	0.62
24	A1-PA-BE-SB	A	N1	NO	1x2x10	0	sand.beam	1.14
25	A2-PA-BE-N	A	N2	NO	1x2x10	0	notch	0.69
26	A1-PE-BE-SB	A	N1	NO	1x2x10	90	sand.beam	0.9
27	A2-PE-BE-N	A	N2	NO	1x2x10	90	notch	0.6
28	A3-PE-BE-N	A	N3	NO	1x2x10	90	notch	0.89
29	A4-PE-BE-N	A	N4	NO	1x2x10	90	notch	0.86
30	A1-PA-BE-N/C1	A	N1	60 cyc.-10°C to+30°C	1x2x10	0	notch	0.69
31	A2-PA-BE-N/C2	A	N2	60 cyc.+5°C to+45°C	1x2x10	0	notch	0.55
32	A1-PE-BE-N/C1	A	N1	60 cyc.-10°C to+30°C	1x2x10	90	notch	0.51
33	A2-PE-BE-N/C1	A	N2	60 cyc.-10°C to+30°C	1x2x10	90	notch	0.77
34	A3-PE-BE-N/C1	A	N3	60 cyc.-10°C to+30°C	1x2x10	90	notch	0.77
35	A4-PE-BE-N/C2	A	N4	60 cyc.+5°C to+45°C	1x2x10	90	notch	0.48
36	A5-PE-BE-N/C2	A	N5	60 cyc+5°C to+45°C	1x2x10	90	notch	0.83
37	A6-PE-BE-N/C2	A	N6	60 cyc.+5°C to+45°C	1x2x10	90	notch	0.62
38	D1-PA-BE-SB	D	N1	NO	1x2x10	0	sand.beam	-
39	D2-PA-BE-N	D	N2	NO	1x2x10	0	notch	-
40	D1-PE-BE-SB	D	N1	NO	1x2x10	90	sand.beam	-
41	D2-PE-BE-N	D	N2	NO	1x2x10	90	notch	-
42	D3-PE-BE-N	D	N3	NO	1x2x10	90	notch	0.34
43	D4-PE-BE-N	D	N4	NO	1x2x10	90	notch	0.3
44	D1-PA-BE-N/C1	D	N1	60 cyc.-10°C to+30°C	1x2x10	0	notch	0.19
45	D2-PA-BE-N/C2	D	N2	60 cyc.+5°C to+45°C	1x2x10	0	notch	0.18
46	D1-PE-BE-N/C1	D	N1	60 cyc.-10°C to+30°C	1x2x10	90	notch	0.17
47	D2-PE-BE-N/C1	D	N2	60 cyc.-10°C to+30°C	1x2x10	90	notch	0.2
48	D3-PE-BE-N/C1	D	N3	60 cyc.-10°C to+30°C	1x2x10	90	notch	0.24
49	D4-PE-BE-N/C2	D	N4	60 cyc.+5°C to+45°C	1x2x10	90	notch	0.08
50	D5-PE-BE-N/C2	D	N5	60 cyc.+5°C to+45°C	1x2x10	90	notch	0.1

E/K/A/D= Marble type
PA/PE= Parallel or perpendicular to plane rift
BE=3 point Bending test
N= Notch Technique
P= Sandwich beam precracking technique
C1=termal cycle 1 (from -10 °C to +30°, 4 cycles a day for 15 days)
C2=termal cycle 2 (from +5 °C to +45°, 4 cycles a day for 15 days)

3.8.2 Discussion

Examining the data in Table 39, it is evident that E-type marble (xenoblastic texture) is much tougher than the D-type marble (homoblastic texture). Intermediate cases are represented by K and A type, the former being tougher than the latter. As a general conclusions, the xenoblastic marbles are tougher than the homoblastic varieties. This finding can be explained from the different microstructural texture arrangements.

Another noteworthy remark is that the notch values are always lower than the natural crack data, essentially for two reasons:

- elimination of a toughening effect in the crack wake,
- reduced mixed mode effect at the crack tip.

On the other hand, the notch width, when lower than the average grain size, is expected to act as a wake-free natural crack. The fracture toughness data of the E-type marble are in line with the data of (Sglavo, 1999).

Passing to discuss the thermally treated marbles, we notice again that the conditioning, as a rule, lowers the fracture toughness. The most remarkable differences are, again, in the homoblastic texture marbles, in the A type and even more so in the D type, for which the fracture toughness may become even less than one half of the original value. No sensible differences can be noticed between the two types of thermal conditioning, which give similar results.

The bending response of E-type marbles is represented in Figure 130. From this picture, it is evident that the orientation of rift plane and the thermal conditioning can only have a limited influence on the response. E-type marbles result tougher and rather resistant to thermal damage.

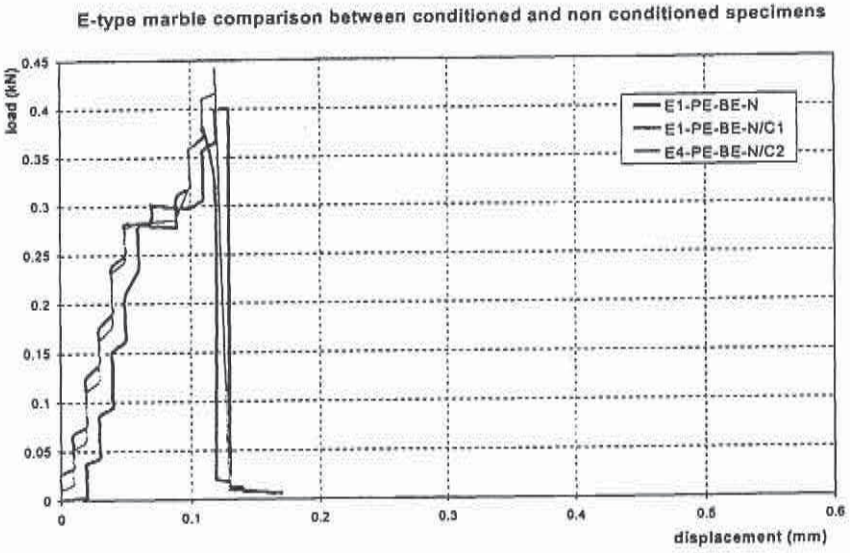

Figure 130. Comparison between condition and unconditioned E-type marbles. Rift plane perpendicular to specimen axis.

Completely different is the behavior of D-type marbles, reported in detail in Appendix 7. For such a material, both the orientations of the rift plane, as well as the thermal conditioning, play a decisive role in the response. Among the thermal treatments, the one referred to as C2, as results clear from Figure 131, seems to produce the most remarkable degradation.

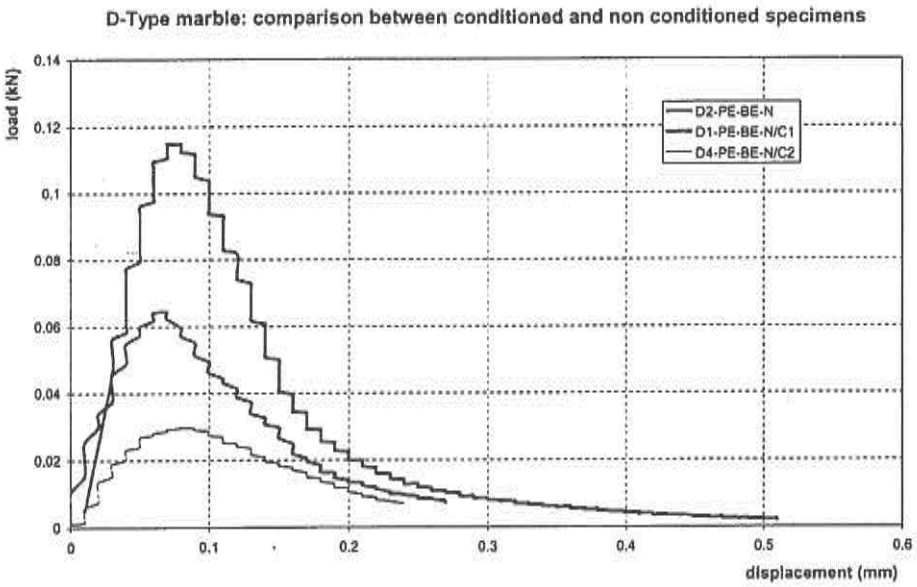

Figure 131. Comparison among the bending response of unconditioned (D2-PE-BE-N) and two differently conditioned (D1-PE-BE-N/C1 and D4-PE-BE-N/C2) D-type marbles (Table 39).

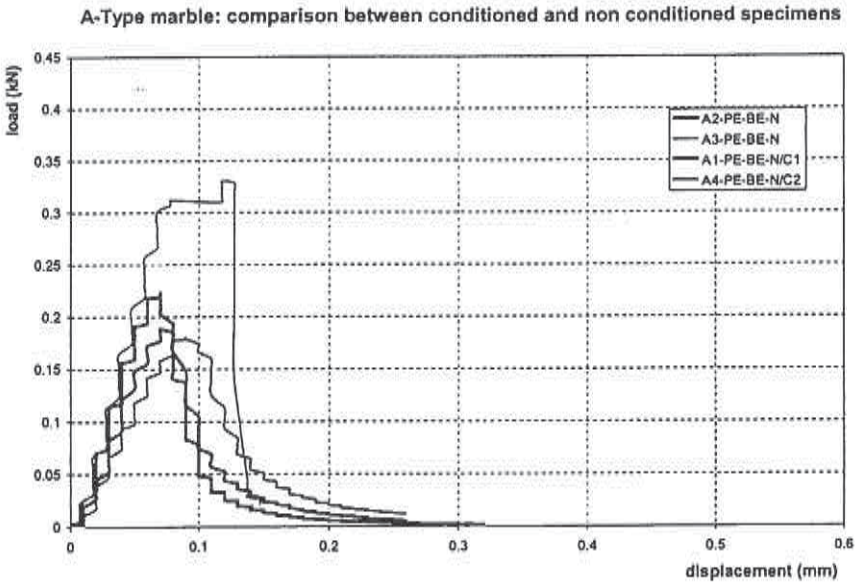

Figure 132. Comparison among the bending response of A-type marbles for unconditioned and two differently-conditioned specimens.

The behavior of A-type marbles is represented in Figure 133. The difference in the material response between naturally pre-cracked (with sandwich beam tecnique) and notched specimens as well as the difference in the rift plane orientation is evidenced according to the test data. We have already noticed that naturally precracked beams are more resistant than notched specimens, and of course, -pe samples are weaker than –pa samples. The thermal conditioning, as reported before, has a remarkable effect on toughness.

Similar graph is reported in Figure 133 for K-type marble. This case can be considered intermediate between E and A marbles. The effects of thermal conditioning are in any case very limited.

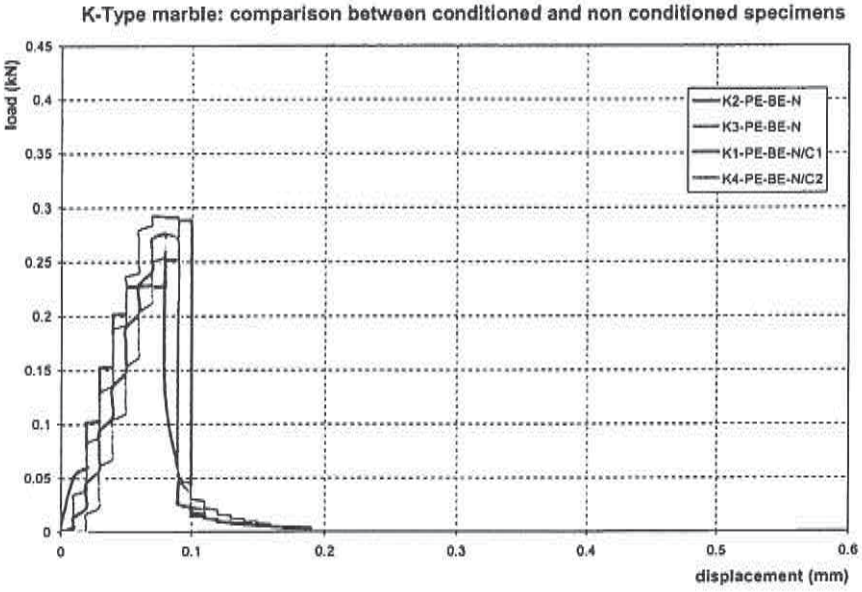

Figure 133. Comparison among the bending response of unconditioned and two differently-conditioned K-type marbles. Rift plane orthogonal to specimen axes.

What should be noticed, apart the aforementioned considerations, is that the apparent ductility of the four materials is comparable, whereas the main difference are in the peak load. We recall, in passing, that in linear elastic fracture mechanics the peak load is the parameter that determine the material toughness. The fact the final sag is comparable for the various materials is another indication that, due to the high discontinuity produced by the precracking, the extension of the process zone results very limited. To this respect, this kind of tests seems to be more accurate in directly describing fracture toughness than tensile tests.

3.9 PERMANENT DILATATION TESTS

3.9.1 Two-sided treatment

Specimens were subjected to quasi-static thermal cycles varying from approximately $-50°C$ to $+55°C$ (such values are not too far from the temperature excursion measured at the top of the roof of Finland all, during seasonal changes) and their dilatation continuously recorded by the experimental apparatus. Figure 134 shows the results for an A-type marble.

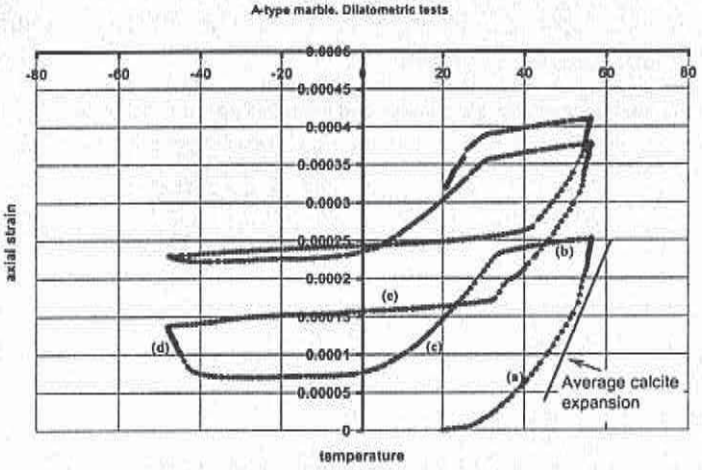

Figure 134. Average strain as a function of temperature for A-type Marble. First and second cycle.

Five different phases can be recognised in the material response. The first one, referred to as (a), corresponds to the first temperature increment, from $t=+20°C$ (room temperature) to $t=+55°C$. What should be noticed is the superlinear growth of thermal strain, which should be compared with the slope of the straight line also drawn in Figure 134, corresponding to the theoretical average dilation of pure calcite ($\alpha=12\cdot10^{-6}\ °C^{-1}$). The greater expansion of the composite with respect to the component can be attributed to the development of cracks. SEM investigations show that these are transgranular in type. Moreover, the analysis of the simple model discussed in (Giacomini *et al.*, 2001), shows that the transgranular cracking is very likely to be accompanied by the relative sliding of the grain borders, in order to accommodates the incongruent deformation of the grains themselves.

The cooling stage can be conveniently distinguished into three branches: phase (b), from $t=+55°C$ to $t=+30°C$; phase (c), from $t=+30°C$ to $t=-40°C$; phase (d), from $t=-40°C$ to $t=-50°C$. The main difference between (b) and (c) is that the graph in (b) is pseudo-horizontal, whereas the beginning of (c) is indicated by a sudden change in the slope. This can be explained assuming that the frictional contact among the grains prevents an instantaneous recovery of the strain. Reverse sliding starts only at the beginning of phase (c)

and then gradually slows down, as logically expected, when the temperature is further decreased. This may be a confirmation that the dilatation accumulated during phase (a) should be, at least partially, attributed to sliding of the grains. The distinguishing character of phase (d) consists in the fact that, lowering the temperature beyond a certain limit, the material expands rather than further contracting.

This phase can be correlated with the breaking of intergranular bonds subsequent to the incongruent granular contraction at low temperatures. We observe in passing that the aforementioned model (Giacomini *et al.*, 2001) suggests that *tensile* stresses at the grain borders are greater for negative (temperature decrease) rather than for positive temperature variations, for the same temperature interval. This may explain why marble deterioration is more pronounced in cold rather than warm climates.

Finally, if at this point temperature is increased again, the material starts to expand once more, entering phase (e). The distinguishing character of (e) is that the slope of the corresponding graph is almost parallel to that of phase (b), an evident sign, in our interpretation, of the significant role played by friction. Phase (e) ends at $t \cong +30°C$. It is important to notice that if the cycle had stopped t room temperature ($t=+20°C$), marble would have shown a significant permanent dilatation.

In further cycles the strain follows a similar characteristic trend, where all the five aforementioned phases can again be recognized. A few comments are however necessary. First of all, the slope of the graphs referring to phases (b) and (e) goes slowly increasing, an indication that the friction coefficient diminishes with ongoing cycles, probably do to the smoothening out of the contact surfaces. Secondly, the beginning of phases (a), characterized by superlinear growth of strain with temperature, is shifted rightwards with ongoing cycles. For example, it was around $33°C$ in the 2^{nd} cycle; it becomes around $42°C$ at the 9^{th} cycle.

What is even more important is that, the volume increase occurring in phases (d) diminishes with cycling. This is a characteristic of ongoing damage. The higher is the number of thermal cycles the specimen has undergone, the lower is the number of bonds that can be broken if a new cycle is performed. In fact, roughly speaking, if the weakest bonds have already been broken in the previous history, the strongest bonds are the ones that remain active.

3.9.2 One-sided treatment

One-sided thermal variations may as well produce a permanent dilatation. Figure 135 represents, for example, the response of the same A-type marble when its temperature is varied from $+20°C$ to $-35°C$ (the two pictures refer to cycles 1-2 and 4-5 respectively). Again, similarly to phase (d) in Figure 135, we notice a characteristic expansion when the temperature is decreased

beyond a certain limit. However, such contribution decreases very quickly at each cycle, as Figure 135b confirms. These experiments show that, in general, two-sided thermal conditioning may be more dangerous than one-sided variations.

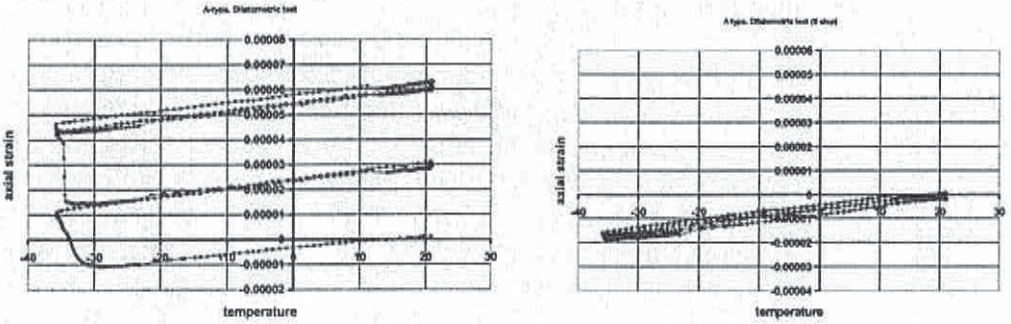

a b

Figure 135. Average strain as a function of temperature for marble A. Thermal cycles between t=+20°C and t=–35°C. Cycles **a**)1-3 and **b**) 4-6.

3.9.3 Anisotropic impact

It is also important to mention that the marble response may show remarkable anisotropy. Figure 136 shows, for example, the behavior of the same quality of marble when the average strain is measured in a direction at right angle with respect to the one considered before. Despite there are similarities with Fig 134, now the distinction among the aforementioned five phases (a)-(e) is less clear than before. Such a noteworthy difference is due to the fact that, in general, there are directions where the orientation of the grains is statistically more pronounced so that also the marble response is influenced at the macroscopic level

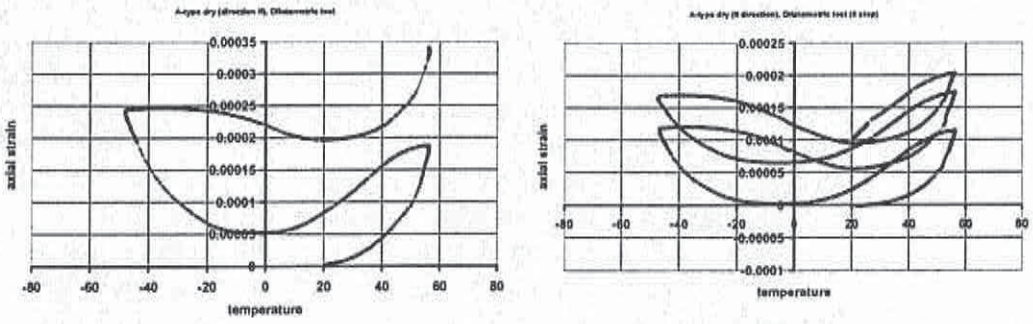

a b

Figure 136. Average strain vs. temperature for A-type Marble. Same material as in Figure 135, but specimens rotated 90°. Thermal cycles between t=+55°C and t=–50°C. Cycles n. 1-2 **a** and n. 4-5 **b**.

3.9.4 Affect of moisture

In order to investigate the influence of moisture, wet sample were also tested. The diagrams for the same A-type marble, with specimens cut in the very same direction as in Figure 134 and 135, are reported in Figure 137. What should be noticed here is the first phase, again referred to as phase (a), which produces a much larger dilatation than for the dry sample in Figure 134. Correspondingly, also the dilatation at very low temperatures, called again phase (d), is much less than in Figure 134. This is an evidence that the effect of humidity is that of facilitating the relative sliding of the grains. In rough words, we may say that humidity acts as a lubricant.

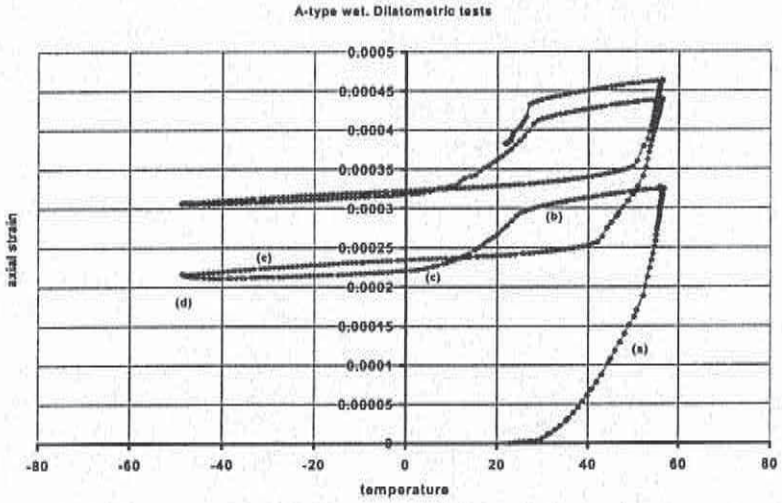

Figure 137. Average strain vs. temperature. A-type Marble in wet conditions. First and second cycle.

These considerations, especially those concerning humidity, may only be considered conjectural at this time. It is however expected that at least some of the questions mentioned will be clarified by further studies.

3.[illegible] Permanent dilatation by number of cycles

Measuring the permanent dilatation produced by thermal cycling may also be a an appropriate test to assess the vulnerability of different marble qualities. Figure 138 represents, in semi logarithmic scale, the measured permanent dilatation as a function of the number of thermal cycles from $-50°C$ to $+55°C$ performed on three different marble types. It is noteworthy that such graphs are, approximately, represented by straight lines. The slope of each graph may thus be an index of the material attitude to damage: smaller slopes correspond to more durable materials.

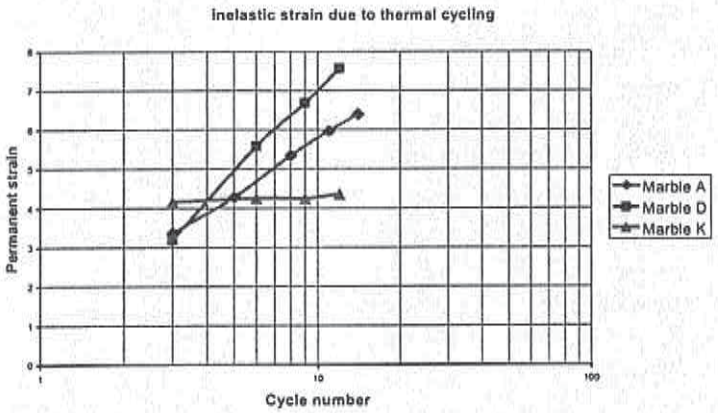

Figure 138. Permanent dilatation vs. number of cycles (log-log scale) for three marble qualities. Cycles performed between $-50°C$ and $+55°C$.

Figure 138 represents, in semi logarithmic scale, the measured permanent dilatation as a function of the number of thermal cycles from $-50°C$ to $+55°C$ performed on three different marble types. It is noteworthy that such graphs are, approximately, represented by straight lines. The slope of each graph may thus be an index of the material attitude to damage: smaller slopes correspond to more durable materials. Measuring the permanent dilatation produced by thermal cycling may also be a an appropriate test to assess the vulnerability of different marble qualities.

3.9.6 Summary

In summary, we can affirm that thermal variations can produce granular decohesion similar to that observed in Finland Hall façade and produce, at the macroscopic level, the permanent dilatation of marble. In this study, we have evidenced the anisotropy of marble response and we have discovered the effects of humidity, which acts as a lubricant and may accelerate the accumulation of permanent strain. It is very probable that differences in the thermo-hygrometric conditions between the inner and the outer surface of the façade may be responsible of a different dilatation of the inner and outer material fibers. This would explain the bowing of the facade panels.

The reason why marble qualities behave differently is to be found, once again, in the microscopic arrangement of the crystals. Any marble is composed for more than 99% of pure calcite, whereas the other accessory components have practical no influence on the mechanical properties even if they are responsible for chromatic effects, likewise the veining. Due to the higher imbrications, granular decohesion is certainly more favored in homoblastic than in xenoblastic marbles. Indeed, the curve with lowest slope in Figure 135 corresponds to xenoblastic marbles. Therefore, this study suggests that the grain texture may be a major qualifying characteristic for selecting marbles able to endure over the years.

3.10 MODELLING OF GRANULAR DECOHESION

3.10.1 Microstructurally motivated models

3.10.1.1 Theoretical evaluation

We will now focus our attention on the effects of thermal variations and propose a simple micro-mechanically motivated model, which can provide an explanation of the degradation process in marbles subjected to thermal changes (Appendix 7).

In our interpretation, the causes of decohesion are attributed to the anisotropy of the thermal expansion of calcite. Calcite crystallizes in the rhombohedric form and, as a result of this asymmetry, its coefficient of thermal expansion is greater in the direction of the optic axes than at right angle to that. Consequently, since the grains of marble are usually randomly oriented, any temperature increase, even if uniform, may produce the springing apart of continuous grains, resulting in a self-equilibrated state of stress.

In order to present a qualitative model, which without redundant hypotheses reproduces all but the basic features of the phenomenon, we consider a marble portion composed of a certain number of identical calcite grains in plane stress or plane strain. Rigorously speaking, 21 elastic constants are necessary to represent the elasticity of calcite, but here we will assume, at least as a first order approximation, that the material is elastically homogeneous and orthotropic. Analogously, we will assume thermal orthotropy with respect to the same directions of elastic symmetry. Therefore, referring to a particular orthogonal system of axes (x_1,x_2), the constitutive relations for the material here considered can be written in the form

$$\begin{pmatrix} \varepsilon_{11} \\ \varepsilon_{22} \\ \varepsilon_{12} \end{pmatrix} = \begin{bmatrix} \frac{1}{E_1} & -\frac{\nu_1}{E_1} & 0 \\ -\frac{\nu_2}{E_2} & \frac{1}{E_2} & 0 \\ 0 & 0 & \frac{1}{2G} \end{bmatrix} \begin{pmatrix} \sigma_{11} \\ \sigma_{22} \\ \sigma_{12} \end{pmatrix} + \begin{pmatrix} \alpha_{11} \\ \alpha_{22} \\ \alpha_{12} \end{pmatrix} \Delta t \,, \tag{11}$$

where σ_{ij} and ε_{ij} $(i,j=1\text{-}2)$ represent the components of stress and strain respectively, whereas Δt denotes the temperature increase. For what the elastic moduli and coefficients of thermal expansion is concerned, if x_2 is oriented in the direction of the optic axis of calcite, we assume from the Literature (Winkler 1994) the values reported in Table 40.

Table 40. Values of the elastic parameters and coefficients of thermal expansions for modelling the calcite response

Elastic moduli	*GPa*	Coefficient of expansion	$°C^{-1}$
E_1	94.5	α_{11}	$-4.3 \cdot 10^{-6}$
E_2	140	α_{22}	$2.6 \cdot 10^{-5}$
$E_1/\nu_1 = E_2/\nu_2$	1400	α_{12}	0
G	42.9		

The simplest assemblage of crystal granules that can conveniently represent the phenomenon is presented in Figure 139. Here, the constituent square-shaped grains are identical, but are differently oriented. In particular, the local x_1 axis of those grains labelled with an A letter is horizontal, whereas the B grains are rotated of 90 degrees.

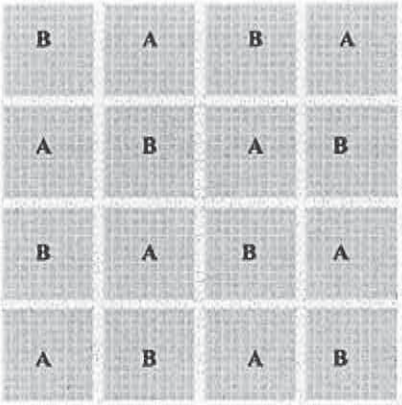

Figure 139. The assemblage of calcite grains in the FEM model.

The deformation of the assemblage consequent to a temperature variation, in particular for a temperature decrease, is qualitatively of the type represented in Figure 140. The resulting grain shapes are the consequence of the anisotropic thermal expansion of calcite which, because of the particular orientation of the orthotropy axes, produces the springing apart of contiguous grains and the nucleation of an internal stress state.

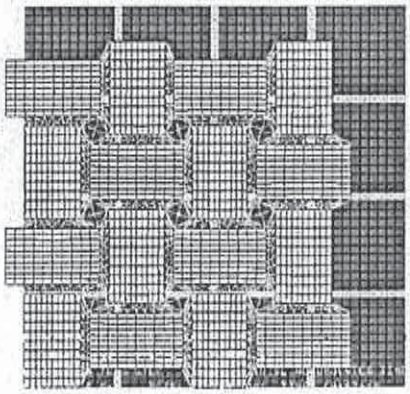

Figure 140. Thermal strains in chessboard-oriented calcite grains.

For quantitative prediction, it is fundamental to model the interface cohesive forces between any two contiguous grains. The interface contact forces are simulated by truss elements, much shorter than the grain diameter, obeying to an elastic, non-linear, softening constitute relation. The bars are of two different types and, for convenience, will be referred to using the labels *s* and *n*. Elements *n* are placed at right angle to the grain boundaries, whereas the *s* elements are at 45° with respect to them, forming the diagonal of an ideal truss. It is clear that, to the first order, the *s*-elements model the contact layer response to shear actions.

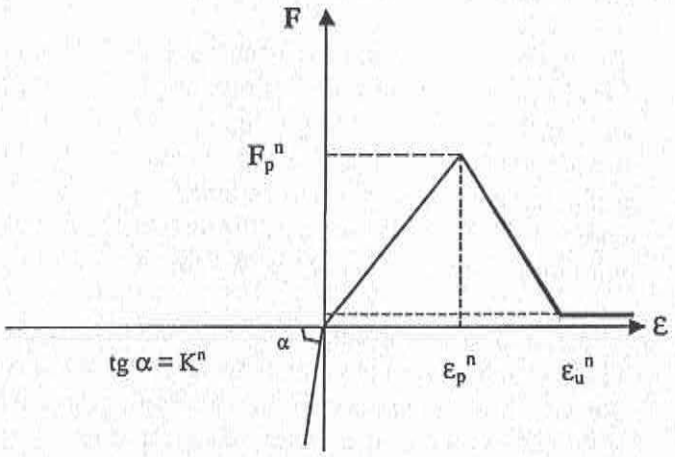

Figure 141. Constitutive relationship for the *n*-type elements.

The constitutive relationship for the *n*-type bars is represented in Figure 141. The slope of the compression branch, indicated with K^n has been calculated to be comparable to the elasticity of calcite itself, in order to reproduce the contact forces when grains are pressed together. Representative parameters for what the tensile response is concerned are represented by the peak load and peak strain F_p^n and ε_p^n and by the ultimate strain ε_u^n. These

parameters have been calculated from the direct tensile tests described in Section 3.8.

The constitutive relationship for the *s*-type elements is instead represented in Figure 142. This is an odd function in the strain and the corresponding parameters ε_p^s and ε_u^s have been taken, as a first order approximation, equal to ε_p^n and ε_u^n. Besides, we have taken $F_p^s = F_p^n$.

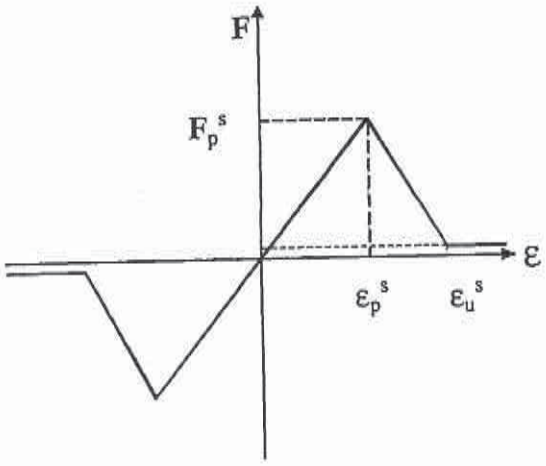

Figure 142. Constitutive relationship for the *s*-type elements.

The grains themselves have been modelled using standard isoparametric linear elastic elements in plane stress or plain strain, both thermally and elastically orthotropic according to the constitute law. The numerical solution of the proposed model has been obtained using the ABAQUS FEM code. Each grain has been set, for convenience, $1cm$ wide and $0.1cm$ thick and it is composed of 100 orthotropic linear elastic finite elements in plane stress, with mechanical properties as in Table 40.

The parameters representative of the constitutive laws (Figures 141 and 142) for the truss elements composing the interface layer are summarized in Table 41. These numbers refer to a particular material type, but experiments on different qualities of Carrara white marbles, apparently very similar, have provided values that differ from these even of an order of magnitude. It is likely that these parameters, which characterize the cohesive properties of the interface layer between any two grains, give an indication the marble attitude towards granular decohesion.

Table 41. Considered values of the representative parameters for the constitutive relationships in Figures 141 and 142.

F_p^n	3.52 N	F_p^s	3.52 N
ε_p^n	815 με	ε_p^s	815 με
ε_u^n	$1.6 \cdot 10^4$ με	ε_u^s	$1.6 \cdot 10^4$ με
K^n	$0.5 \cdot 10^{-10}$ N/με		

3.10.1.2 Practical application

For this assembly, we are interested in calculating the state of stress in the elements when subjected to a (negative) temperature variation Δt=–60°C. Such a value has been suggested by the measured temperature on the façade of the Finland Hall in Helsinki. The resulting deformed shape is represented in Figure 143 where, for convenience, the undistorted mesh is also drawn in the back. Observing the elongation of the bars composing the interface layer, we have an indication of the interface forces exchanged between the grains.

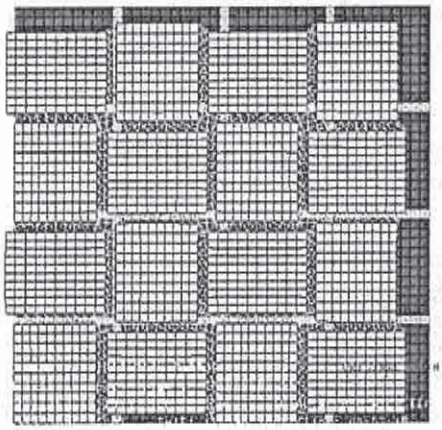

Figure 143. Deformation of the grain assemblage for Δt=–60°C. Displacements 100 x magnified.

It is interesting to notice that the most dangerous states of stress are usually located at the grain interfaces. This result is in agreement with the conclusions obtained in closed form in (Royer-Carfagni 1999), through an approximate model.

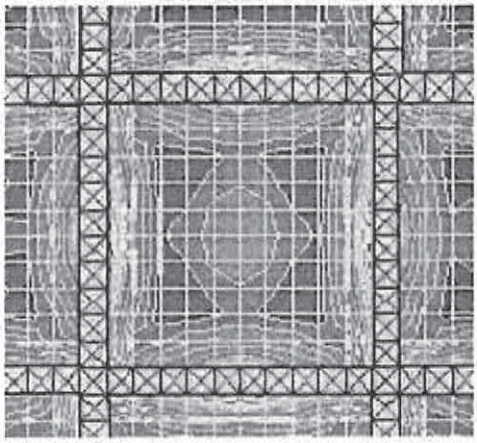

Figure 144. Von-Mises stress state in a neighborhood of a representative grain.

For the same grain, Figures 145a and 145b represent the normal and tangential components of the contact stress. Such values have been calculated assuming that the axial load in the truss elements is uniformly distributed upon an appropriate portion of the grain boundary. In general, since we assume that both strains and local rotations are small, the *s*-type members are responsible of the shear stress, whereas both *s* and *n*-type members contribute to the normal component. However, at the grain corners, where five bars converge, we have conventionally calculated the stress acting on each one of the two sides of the corner in the following way.

Commenting first Figure 145a, we notice that the resultant of the normal stress acting on each one of the sides of the grain is practically zeroed. We also observe that, in general, the central portions on each side is compressed whereas tensile stresses act in proximity of the grain corners, particularly in the direction where the material shrinks the most.

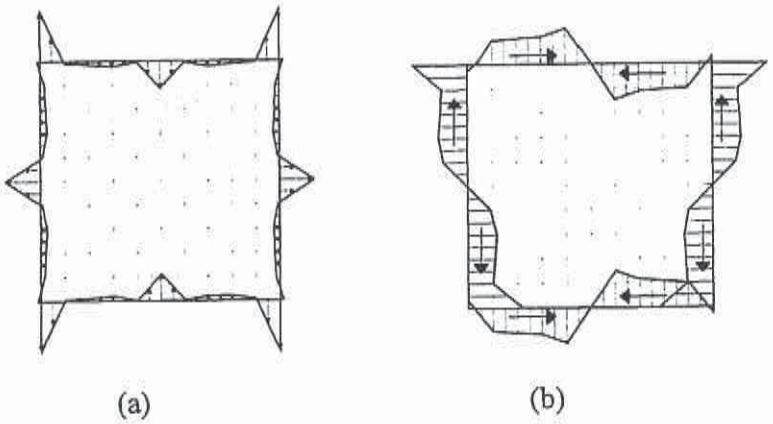

Figure 145. Normal (a) and shear (b) components of stress corresponding to Δt=–60°C.

The shear stress diagram, reported in Figure 145b, is, by symmetry, represented by odd functions. It is interesting to notice that, apart from a small central portion, important shear stresses are present on the whole grain boundary. This is not surprising since it is clear, observing also Figure 143, that the anisotropic thermal expansion induces the relative "sliding" of continuous grains, which is opposed by the shear resistance of the interface layer. The decay of the shear stress on the horizontal sides of the grain, in proximity of the grain corners, is due to the yielding of some of the *s*-elements there located, which enter the softening branch (Figure 142). In particular, yielding is in general achieved in the diagonal truss members connecting the corners of the grains at a texture node. Such point, as results clear also from Figure 143, is usually the "critical" point of the assembly.

Evidently, in our model, yielding of the truss members indicates granular decohesion damage. In order to further discuss such an effect, it may be interesting to compare these results with those obtained from a slightly different model. In particular, we consider the case in which the truss interface members remain indefinitely elastic, i.e. the linear branches departing from the origin in the constitute laws of Figures 141 and 142 are indefinitely extended beyond the peak load, so that softening is eliminated. The diagrams of the normal and shear stresses, previously reported in Figure 145, now become as represented in Figure 146.

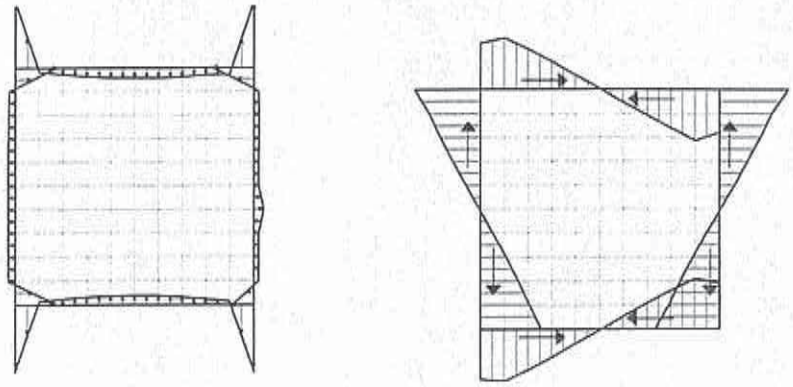

(a) (b)

Figure 146. Normal (a) and shear (b) components of stress corresponding to Δt=–60°C for indefinitely elastic truss members.

3.10.1.3 Discussion

What is clear from the comparisons of Figures 145 and 146 is that now the normal stress presents very high peaks in correspondence of the grain boundaries, whereas the diagram of the shear stress is almost triangular in shape. The analysis of the stress state in each grain confirms that the most dangerous state of stress are exactly at the grain corners, in complete agreement with the results of the approximate analysis contained in (Royer-Carfagni 1999). Yielding of the truss members, when they present a softening regime, smoothens out these peak loads, as indicated by Figure 145.

In conclusion, despite all the approximations introduced, which render any consideration valid only at the qualitative level, the model appears capable of reproducing the basic features of the granular decohesion damage due to thermal actions. The numerical simulation shows that, in agreement with an approximate analytical solution discussed elsewhere (Royer-Carfagni, 1999), the stress state is the most critical at the grain borders, thus justifying the intergranular, rather than transgranular, nature of fractures.

Moreover, stress concentrations appear at the grain corners, in proximity of the texture nodes. Such concentrations produce the yielding of the neighbouring truss elements (modelling the interface layer), an indication of ongoing damage in the cohesive bonding between the grains. In particular, we can infer that the collapse mechanics is due to shear stresses, which similarly to mode II fracture, produce the relative sliding of the grain boundaries.

As a final remark, the model indicates that, as a consequence of plausible constitutive laws for the cohesive interface layer, negative temperature variations are more dangerous than positive variations. This finding provides a possible explanation of why, as confirmed by experience, marble

deterioration is more pronounced in monuments exposed to cold rather than warm climates.

3.10.2 A phenomenological model in statistical mechanics.

Measuring the permanent dilatation produced by thermal cycling may also be a an appropriate test to assess the vulnerability of different marble qualities. The experiments referred to in Section 3.10 have in fact shown a correlation between the microstructural damage (granular decohesion) and the macrostructural permanent expansion of marbles.

Figure 147 has been already in Section 3.10. and represents, in semilogarithmic scale, the measured permanent dilatation as a function of the number of thermal cycles from $-50°C$ to $+55°C$ performed on three different marble types. It is noteworthy that such graphs are, approximately, represented by straight lines. This observation, if confirmed by the experience, could allow to represent the marble behavior at very high cycle number just performing a limited series of experiments. In fact, the long-term behavior could be obtained just extrapolating the data from the interpolation line.

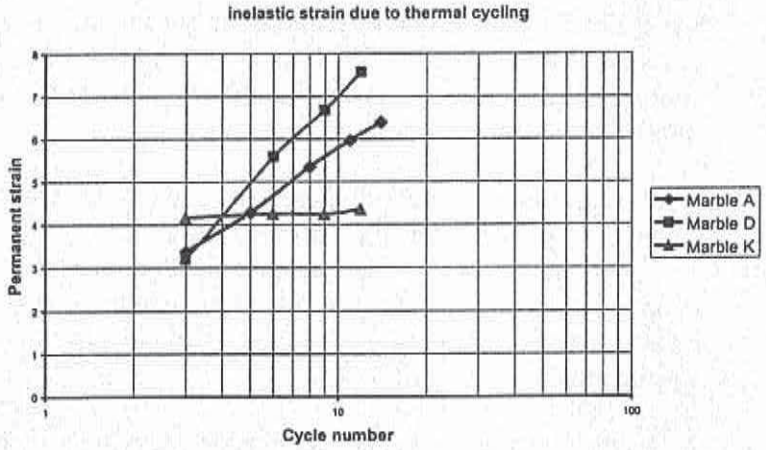

Figure 147. Permanent dilatation vs. number of cycles (semilogaritmic scale) for three different qualities of marble. Cycles performed between $-50°C$ and $+55°C$.

The aim of this Section is to present a simple, phenomenological model, able to interpret this intriguing behavior, in particular the pseudo-linear dependence of permanent strain on the logarithm of the number of thermal cycles n, as shown in Figure 147.

One of the principal hypotheses consists in assuming that the increment in inelastic deformation is produced by a series of events that are *independent* one from the other. In other words, the occurrence of a process in a certain

particle does not influence the behavior of the neighboring constituent elements. One argument, in particular, uphold such a hypothesis. At the microscopic level, SEM observations have shown that the degradation mechanism is essentially due to decohesion of the constituent grains. Hardly any transgranular cracking at all can be found, so the process can be considered to occur at a length scale of the same order of magnitude as the diameter of a unit grain.

Therefore, by our way of thinking, the basic process producing inelastic deformation consists in the braking of the granular bonding at some place. In particular, we may suppose that breaking occurs when the average stress in the considered point, say τ, equals a certain activation stress τ_a. We further assume that braking of one bonding produces a relative displacement of the specimen's ends by a certain quantity v_p so that, if h denotes the height of the sample,

$$\varepsilon_p = \frac{v_p}{h} \tag{12}$$

represents the plastic contribution to the specimen's overall axial strain due to the yielding of *one* bond. Of course, each bond can yield only once. We may model this that by saying that its activation stress becomes very large (practically infinite) after it has flowed.

Now, taking into account all these assumptions, we want to characterize the material response when the specimen is cyclically thermally loaded. The key-point in the analysis is recognizing that in real materials, especially rocks, various circumstances, such as micro-inhomogeneous, micro-cracks, micro-inclusions, produce a system of self-balanced micro-stresses when the specimen is uniformly heated.

As a result of the theoretical conclusion (Appendix 7) the following equation (13) has been formed for anticipated logarithmic dependence:

$$\varepsilon(n) = \varepsilon_p \frac{\Theta\ \Pi_0}{\gamma^{[T_u]}}\ \ln(n) + A\ , \tag{13}$$

Formula (4.2.18) expresses the macroscopic material's behavior when subjected to cyclic thermal loading. The quantities ε_p and Π_0 appearing therein are clearly material parameters, unlinked to the testing conditions. On the other hand, constant A is representative of the strain increase consequent to the initial settling of the specimen, occurring as a rule in the very first cycle. This parameter may depend upon the most disparate causes (i.e. bedding errors, micro-inhomogeneities, etc.) and should consequently be considered a random variable. The results of the tests performed do in fact exhibit wide

scattering as far as this parameter is concerned, confirming a non-continuous dependence on the macroscopic testing conditions.

Consequently, increasingly heterogeneous materials (but this parameter may depend also on the microstructure, i.e. xenoblastic vs. homoblastic textures) are characterized by increasingly large values of the function $P^{[T_n]}(\tau')$, corresponding to great Θs and small γs. Moreover, it is clear that

$$T_1 < T_2 \Rightarrow \gamma^{[T_1]} > \gamma^{[T_2]} . \tag{14}$$

In fact, the higher the applied temperature variation is, the greater the probability that granular bonds be subjected to high stresses.

As a final remark, it is worth stressing once again that the central assumption underlying all the above considerations is that of the *statistical independence* of the events causing the effect as observed at the macroscopic level.

3.11 MICROSTRUCTURAL CHARACTERIZATION OF MARBLES.

3.11.1 Skeleton method

Observation of material thin sections has suggested the following empirical observations. Homoblastic textures contain convex grains of various dimensions closely packed together, whereas grains of almost the same dimensions, mainly concave shaped, form xenoblastic textures. Therefore, it is natural to consider as representative parameters, able to describe the shape of the grains, the area A and the perimeter P. In fact, for the same value of P, the area is smaller for concave than for convex grains. Therefore, A/P^2 has been the first parameter to be considered (Appendix 7).

We have also addressed the question whether, in order to differentiate the two texture types, another parameter connected to the waves of the contour could be useful. We have thus referred to shape indexes usually employed in Computer Vision (CV) (Gonzalez & Woods, 1991), developed in particular for the automatic recognition of text characters. Among the various indices used in this field, we indeed find A/P^2, now referred to as compactness, and the convexity, defined as the ration between A and the figure convex hull. A third parameter able to define the contour roughness is the skeleton S (Jain, *et al.*, 1995, Parker, 1997).

The numerical algorithm used in this research finds the skeleton in the following manner: for each point internal to the figure, the distance from points of the border is calculated. If the resulting function has more than one absolute minimum, in other words if at least two points of the border presents

the same minimal distance, then the points belongs to S. For figures defined by polylines, S is composed (Figure 148) by three different kinds of lines:

i) bisectors of acute angles,
ii) segments which are equidistant from two non-adjacent sides and
iii) parabola sectors (equidistant from one vertex and one side, when a concave angle is present).

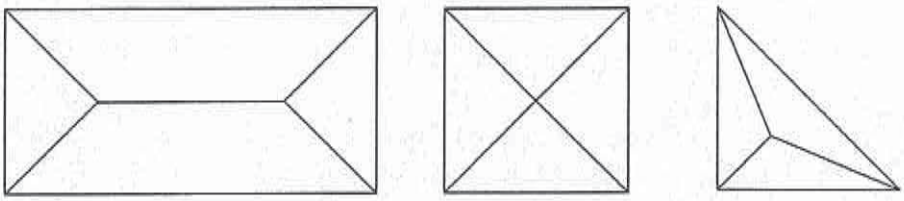

Figure 148. Polygons and corresponding skeleton.

The skeleton is usually used in CV for *thinning* the object contours. However here it is used to characterize the grain shape. In fact the number and length of the various branches composing the skeleton are influenced by the contour protuberances. To illustrate, we consider in Figure 149 the skeletons of the represented polygon. Perturbing with a little asperity one of the sides of the polygon, significantly modifies the skeleton, suggesting that wiggly contours have are characterized by high values of S.

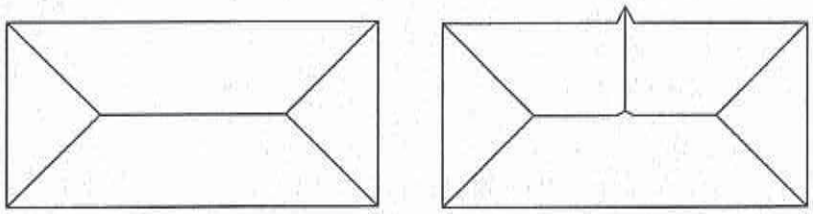

Figure 149. Influence of the contour roughness on the skeleton S.

Four distinct parameters have been considered for shape characterization: A/P^2, A/S^2, $A/(P*S)$) and P/S. The first should be indicative of the figure compactness, the second is influenced by the contour roughness, while the third is intermediate between the two. The last parameter (P/S) is perhaps the less discriminating, since for the same value of P, very similar figures may present very different S.

We have first tested the method with simple geometrical figures and, successively, we have passes to the analysis of the grain shapes microscopically observed through thin material sections. The shape indexes have been calculated using the Image Processing function available in MATLAB. In order to obtain digital images, we proceeded as follows. For polygons, it is

sufficient to draw them with a standard graphic software, which indeed use the matrix binary representation. Digitalizing the grain shapes is more complicated.

Testing the image processing procedure with simple polygons, we have noticed that the skeleton shape appears different from what expect on the base of the definition. Most likely, this is due to the algorithm from which S is defined: the software extract the skeleton using a modified thinning, using an iterative procedure. Computing time is reduced, but the skeleton is only approximated. In particular, very little protuberances are neglected by the algorithm.

Once the procedure has been set, we have applied our method to 20 different qualities of marble. Of course, the procedure is not completely automatic, since it is the operator who defines, using the computer mouse, the grain contours. In order to evaluate how the selection of the vertexes in the approximating polyline and their location influences the shape parameters, we made different tests. For example, for the xenoblastic grain represented in Figure 150, we have repeated the data acquisition procedures 10 times, maintaining fixed the number of vertexes of the approximating polyline and, more or less, their position. In this way, our intention was to evaluate the influence of the operator. The results are reported in Table 42.

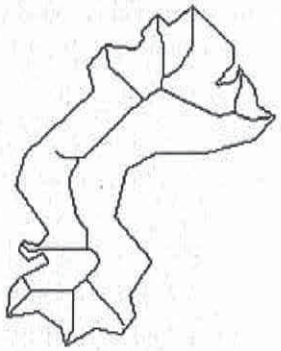

Figure 150. The xenoblastic grain considered in the repeatability tests for the contour acquisition.

Table 42. Tolerances in the shape parameters in the repeatability tests.

Variation	ΔA)	ΔP)	ΔS)	$\Delta A/P^2$)	$\Delta A/S^2$)	ΔA/(P*S))
Absolute	586	22,6	154,1	0,001486	0,018185	0,008421
% of the average	5,5 %	3,47 %	8,27 %	6 %	18,57 %	10,23 %

It is clear that the parameter which shows the highest deviation is S. However the approximation is, in general, acceptable. As a second repeatability

test, we have considered possible changes when the number of vertexes in the approximating polyline is gradually varied. This has caused a progressive smoothening out of the grain contours because possible irregularities are neglected. In other words, the grain gradually becomes homoblastic.

3.11.2 Marble classification

In order to evaluate the efficiency of the classification obtained through the parameters A/P^2, A/S^2, $A/(P*S)$ e P/S, we have considered 20 marble qualities, differing not only for their mechanical properties, but also for the microstructural layout. In particular, we have selected 7 xenoblastic, 6 intermediate and 7 homoblastic marbles, referred to in Table 43. The corresponding properties have been derived from (Gattiglio et al., 1980) and the number in parentheses refer to the reference number therein reported.

Table 43. The 20 considered marble qualities, with indication of the originating quarry.

Xenoblastic texture	**Intermediate texture**	**Homoblastic texture**
Bianco Fondone (1)	Statuario Fossa del Donato (6)	Arabescato Boccanaglia (3)
Arabescato Cervaiole (2)	Nuvolato Fantiscritti (11)	Calacatta Boccanaglia (4)
Bianco Ravaccione (8)	Arabescato Gioia (13)	Venato Crestola (5)
Statuario Ravaccione (9)	Bianco Costa (15)	Bianco Lorano (7)
Bardiglio Costa (16)	Venato Carpano (17)	Zebrino Ponti di Vara (10)
Venato Madielle (19)	Bianco Valsora (18)	Venato Cima di Gioia (12)
Bianco Trambiserra (20)		Venato La Piana (14)

For each marble, the data in (Gattiglio et al., 1980) furnish the main mechanical properties and micrographs of three thin sections, cut parallelly to rift, head grain or grain plane. Despite grains are, as a matter of fact, 3D objects, we surmise that their shapes can be conveniently characterized through a 2D analysis, by means of three thin sections at right angle one another. For each marble type, we have considered 15 different grains, 5 for each thin sections. For each of the 15 images, the area (A), the perimeter (P) and the skeleton (S) have been calculated.

The classification obtained by considering the average values of the shape parameters are reported in table 40, where each material is identified by the same number reported in Table 44. It should be noticed that the classification derived from A/P^2, A/S^2 e $A/(P*S)$ are comparable, and are in agreement with the empirical classifications reported in the Literature: xenoblastic (homoblastic) textures are characterized by the lower (higher) values of

the cofficients A/P^2, A/S^2 e $A/(P*S)$, whereas the qualities classified as intermediate occupy the central positions.

Table 44. Classification obtained through parameters A/P^2, A/S^2, $A/(P*S)$ e P/S.

Marble n.	A/P^2*10^{-2}	Marble n.	A/S^2*10^{-2}	Marble n.	$A/(PS)*10^{-2}$	Marble n.	P/S
2 (X)	1,480	2 (X)	1,949	2 (X)	1,694	2 (X)	1,135
20 (X)	1,530	20 (X)	2,077	20 (X)	1,776	1 (X)	1,140
9 (X)	1,753	1 (X)	2,776	9 (X)	2,203	20 (X)	1,154
19 (X)	1,954	9 (X)	2,806	19 (X)	2,333	16 (X)	1,185
1 (X)	2,098	19 (X)	2,807	1 (X)	2,402	19 (X)	1,199
8 (X)	2,229	8 (X)	3,650	8 (X)	2,835	15 (I)	1,210
16 (X)	2,721	16 (X)	3,849	16 (X)	3,204	6 (I)	1,231
15 (I)	3,085	15 (I)	4,586	15 (I)	3,715	9 (X)	1,238
17 (I)	3,267	17 (I)	5,510	17 (I)	4,194	17 (I)	1,273
13 (I)	3,726	6 (I)	5,848	6 (I)	4,657	8 (X)	1,278
6 (I)	3,761	13 (I)	6,318	13 (I)	4,822	5 (H)	1,283
11 (I)	3,857	11 (I)	6,597	11 (I)	5,034	4 (H)	1,290
18 (I)	3,940	18 (I)	6,964	18 (I)	5,203	3 (H)	1,292
7 (H)	5,113	5 (H)	8,836	5 (H)	6,769	13 (I)	1,295
5 (H)	5,263	7 (H)	9,358	7 (H)	6,865	12 (H)	1,298
4 (H)	5,369	4 (H)	9,363	4 (H)	7,004	11 (I)	1,300
10 (H)	5,490	12 (H)	9,642	12 (H)	7,332	18 (I)	1,314
12 (H)	5,633	3 (H)	9,871	3 (H)	7,395	7 (H)	1,327
14 (H)	5,670	14 (H)	11,253	14 (H)	7,896	14 (H)	1,393
3 (H)	5,684	10 (H)	13,590	10 (H)	8,573	10 (H)	1,548

On the other hand, the classification obtained through P/S is not in agreement with our expectation. This result is not surprising because of the reasons mentioned above. The coefficient P/S does not represent a reliable parameter for the texture classification. It is then possible to provide a first quantitative classification of the marble textures based on the shape parameters. Such classification is reported in Table 45.

Table 45. Shape-parameter range for xenoblastic, intermediate and homoblastic textures.

Xenoblastic	$A/P^2<0,03$	$A/S^2<0,04$	$A/(P*S)<0,035$
Intermediate	$0,03<A/P^2<0,045$	$0,04<A/S^2<0,08$	$0,035<A/(P*S)<0,06$
Homoblastic	$A/P^2>0,045$	$A/S^2>0,08$	$A/(P*S)>0,06$

From an intuitive point of view, it is logical that the greater interlocking of xenoblastic textures with respect to the homoblastic textures may influence the mechanical material properties. We have thus tried to examine a possible correlation between the shape parameters and the the mechanical characteristics of marbles. The corresponding values have been also found in the literature (Gattiglio, et al., 1980).

In general, based on the available test data, xenoblastic marbles present greater flexural strength, smaller water absorption, smaller coefficient of thermal dilatation, higher elastic modulus, than the homoblastic qualities. Other mechanical properties, likewise the compression strength (even after freezing and thawing cycles) or the impact-test resistance, which mainly depend on the development of transgranular microfractures, are not correlated with the shape parameters. However, a very good correlation has been noticed for the coefficient of water absorption, which increases almost linearly with the values of any of the shape-parameters A/P^2, A/S^2 and $A/(P*S)$. This finding is justified by the referring to a microstructural motivated model, highlighting in particular some inconsistency in the standards according to which the water absorbtion is calculated. More detailed presentation of the subject is available in Appendix 7.

3.12 RESEARCH AT CEVALOR

3.12.1 Marble type A

Table 46. Initial characterisation of sample A (cut against)

Initial Characterisation	Sample A (Cut against)	
	Average	Standard deviation
Resist. to Compression (Mpa)	83,0	5,0
Water Absorption at PtN (%)	0,12	0,01
Open Porosity (%)	0,4	0,1
Volumetric Mass (Kg/m^3)	2707	1,2
Microscopic Observation	See report in annex	
Resistance to Flexural Strength under conc. Load (Mpa)	13,0	1,0

Table 47. Initial characterisation of sample A (cut in favour)

Initial Characterisation	Sample A (Cut in favour)	
	Average	Standard deviation
Resist. to Compression (Mpa)	95,5	12,9
Water Absorption at PtN (%)	0,12	0,01
Open Porosity (%)	0,4	0,0
Volumetric Mass (Kg/m^3)	2693	18
Resonance Frequency (HZ)	2188	-
Ultrasonic Propagation Speed (m/s)	6,4x10^{-2}	-
Thermal Shock	No visual remark	-
Crystallisation Test	being done	-
Dynamic Modulus of Elasticity (x10^9 N/mm^2)	4,6x10^9	-
Microscopic Observation	See report in annex	-
Resistance to Flexural Strength under conc. Load (Mpa)	16,3	0,7

Table 48. Characterisation of the sample A marble resistance, each 25 cycles of freeze/thaw

Resistance characterisation	Each 25 cycles of the freeze/thaw								
	26	53	81	101	143	167	191	216	232
Resist. to Compression (Mpa)	89,0	83,6	84,8	85,1	90,9	86,0	89,6	78,9	84,7
Water Absorption at PtN (%)	0,17	0,18	0,19	0,17	0,18	0,20	0,20	0,19	0,26
Open Porosity (%)	0,5	0,6	0,5	0,6	0,6	0,6	0,6	0,5	0,7
Volumetric Mass (Kg/m^3)	2711	2698	2699	2698	2697	2699	2695	2701	2699
Resonance Frequency (HZ)	2243	2243	2313	2282	2352	2452	2138	2020	1980
Ultrasonic Propagation Speed (x10^{-2} m/s)	6,1	6,0	6,0	6,1	6,1	6,1	6,0	6,4	6,4
Thermal Shock	No visual remark								
Dynamic Modulus of Elasticity (x10^9 N/mm^2)	4,9	4,9	5,2	5,1	5,4	5,8	4,4	4,0	3,8
Microscopic Observation	See report in annex								
Resistance to Flexural Strength under conc. Load (Mpa)	12,7	11,3	11,8	10,1	10,0	11,6	8,8	8,4	8,1

The crystallisation tests were made in the beginning and at the end of 232 cycles of freeze/thaw. The results were generally; loss mass and tarnished appearance. The loss of material, during the initial characterisation test was of 1,5% and after the 232 cycles, was of 3,18%, this may be a consequence of the increase on the porosity and consequently of the water absorption.
It's possible to conclude that marble, when submitted to thermal variations, and in presence of salt mist, shows alterations.

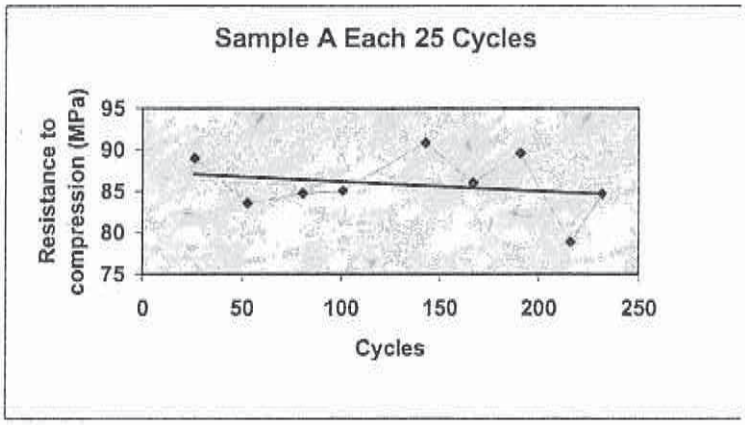

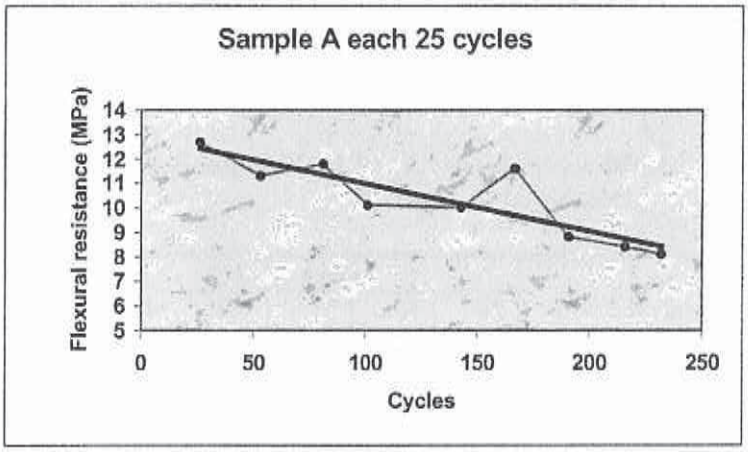

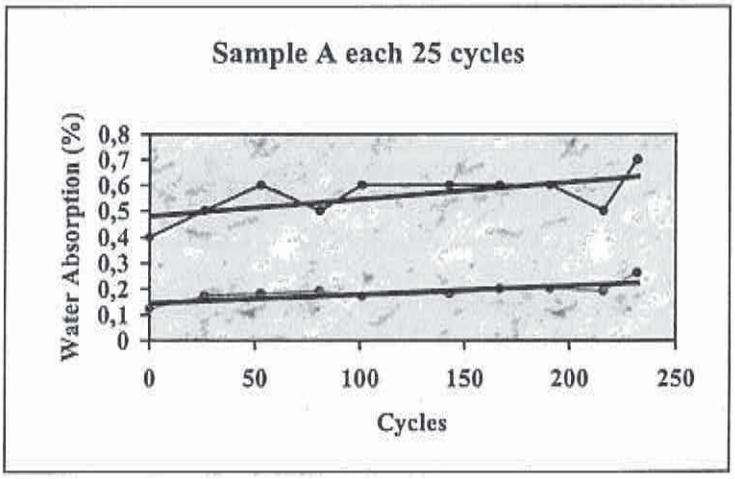

Figure 151. Interpretation of marble A test results.

It's a marble who appears to have a lower mechanical resistance specially when submitted to flexural tests. It can easily occur modifications in the structure, with the appearance of elastic proprieties, which leads to reductions on the resistance to flexural strength. After 232 cycles of freeze/thaw, a high increase in the porosity was noted, and consequently the water absorption became higher, specially when compared with the initial characterisation (porosity 0,4% and water absorption 0,12%).

3.12.2 Marble type D

Table 49. Initial characterisation of sample D (cut in favour)

Initial Characterisation	Sample D (Cut in favour)	
	Average	Standard deviation
Resist. to Compression (Mpa)	73,6	8,2
Water Absorption at PtN (%)	0,16	0,03
Open Porosity (%)	0,4	0,0
Volumetric Mass (Kg/m^3)	2703	10,8
Microscopic Observation	See report in annex	
Resistance to Flexural Strength under conc. Load (Mpa)	4,6	0,6

Table 50. Initial characterisation of sample D (cut against)

Initial Characterisation	Sample D (Cut against)	
	Average	Standard deviation
Resist. to Compression (Mpa)	92,5	7,6
Water Absorption at PtN (%)	0,15	0,01
Open Porosity (%)	0,5	0,1
Volumetric Mass (Kg/m^3)	2702	1
Resonance Frequency (HZ)	1993	-
Ultrasonic Propagation Speed (m/s)	$4,4x10^{-2}$	-
Thermal Shock	No remark	
Crystallisation Test	Loss mass (92,43 %)	
Dynamic Modulus of Elasticity (N/mm^2)	$3,9x10^9$	-
Microscopic Observation	See report in annex	
Resistance to Flexural Strength under conc. Load (Mpa)	4,2	0,3

Table 51 Characterisation of the sample D marble resistance, each 25 cycles of freeze/thaw

Resistance characterisation	Each 25 cycles of the freeze/thaw							
	28	**62**	**86**	**116**	**142**	**170**	**198**	**245**
Resist. to Compression (Mpa)	71.3	86.9	72.4	87.6	86.6	86.7	86.0	82.0
Water Absorption at PtN (%)	0.18	0.18	0.18	0.21	0.19	0.18	0.18	0.19
Open Porosity (%)	0.42	0.39	0.50	0.53	0.48	0.49	0.50	0.47
Volumetric Mass (Kg/m^3)	2629	2654	2681	2645	2685	2641	2669	2682
Resonance Frequency (HZ)	1808	2168	1872	2150	1493	1580	1538	2133
Ultrasonic Propagation Speed ($x10^{-2}$ m/s)	4.2	4.3	4.1	4.1	4.0	4.1	3.9	4.0
Thermal Shock	No visual remark							
Dynamic Modulus of Elasticity ($x10^9$ N/mm^2)	3.1	4.5	3.4	4.4	2.2	2.4	2.5	4.4
Microscopic Observation	See report in annex							
Resistance to Flexural Strength under conc. Load (Mpa)	4.3	3.5	2.9	2.7	3.8	3.3	3.5	3.3

The crystallisation tests were made in the beginning and at the end of 245 cycles of freeze/thaw. The results were the degradation of the specimens The loss of material, during the initial characterisation test was of 49,36 % and after the 245 cycles, was of 92,43%, this may be a consequence of the increase on the porosity and consequently of the water absorption.

It's possible to conclude that marble, when submitted to thermal variations, and in presence of salt mist, show alterations.

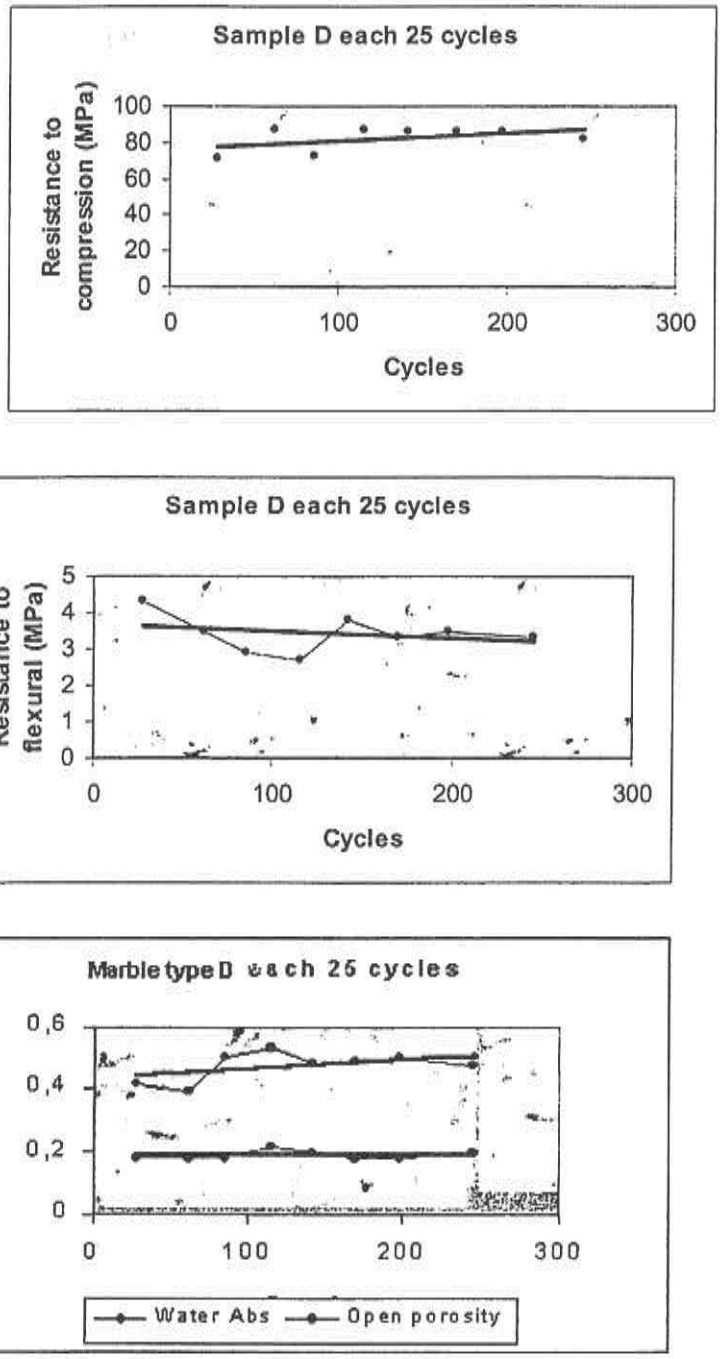

Figure 152. Interpretation of marble D test results.

It's a marble who appears to have a lower mechanical resistance specially when submitted to flexural tests. It can easily occur modifications in the structure, with the appearance of elastic proprieties, which leads to reductions on the resistance to flexural strength.

After 116 cycles of freeze/thaw, a high increase in the porosity was noted, and consequently the water absorption became higher, specially when compared with the initial characterisation (porosity 0,4% and water absorption 0,15%). After that become constant, maybe because the degradation of the grains were given fine material to fulfil the porous. That can be confirm with the microscopy report (see in annex).

3.12.3 Marble type E

Table 52 - Initial characterisation of Sample E (cut against)

Initial Characterisation	Sample E (Cut against)	
	Average	Standard deviation
Resist. to Compression (Mpa)	102,8	7,5
Water Absorption at PtN (%)	0,11	0,01
Open Porosity (%)	0,4	0,0
Volumetric Mass (Kg/m^3)	2705	2
Microscopic Observation	See report in annex	
Resistance to Flexural Strength under conc. Load (Mpa)	21,8	1,7

Table 53. Initial characterisation of sample E (cut in favour)

Initial Characterisation	Sample E (Cut in favour)	
	Average	Standard deviation
Resist. to Compression (Mpa)	103,5	10,7
Water Absorption at PtN (%)	0,11	0,01
Open Porosity (%)	0,3	0,03
Volumetric Mass (Kg/m^3)	2714	3
Microscopic Observation	See report in annex	
Resistance to Flexural Strength under conc. Load (Mpa)	18,1	2,4

Table 54. Characterisation of the sample E marble resistance, each 25 cycles of freeze/thaw

Resistance characterisation	Each 25 cycles of the freeze/thaw							
	28	**46**	**74**	**102**	**150**	**174**	**202**	**216**
Resist. to Compression (Mpa)	104.7	112.5	116.9	106.9	112.5	118.6	120.2	120.3
Water Absorption at PtN (%)	0.13	0.16	0.16	0.16	0.17	0.17	0.16	0.17
Open Porosity (%)	0.30	0.40	0.29	0.29	0.37	0.43	0.44	0.40
Volumetric Mass (Kg/m^3)	2656	2601	2656	2648	2650	2682	2676	2675
Resonance Frequency (HZ)	2127	1887	1717	1848	1980	2225	2283	2647
Ultrasonic Propagation Speed ($x10^{-2}$ m/s)	6.1	6.1	6.0	6.0	6.0	6.0	6.1	5.9
Thermal Shock	No visual remark							
Dynamic Modulus of Elasticity ($x10^9$ N/mm^2)	4.3	3.3	2.8	3.3	3.7	4.8	5.0	6.7
Microscopic Observation	See report in annex							
Resistance to Flexural Strength under conc. Load (Mpa)	14.8	16.4	13.2	13.4	11.7	13.9	13.0	12.3

The Crystallisation tests were made in the beginning and after 216 cycles of freeze/thaw. The results obtained were the same, just tarnished appearance. But no colour or structural changes on the samples were noticed (see photo 1 and 2)

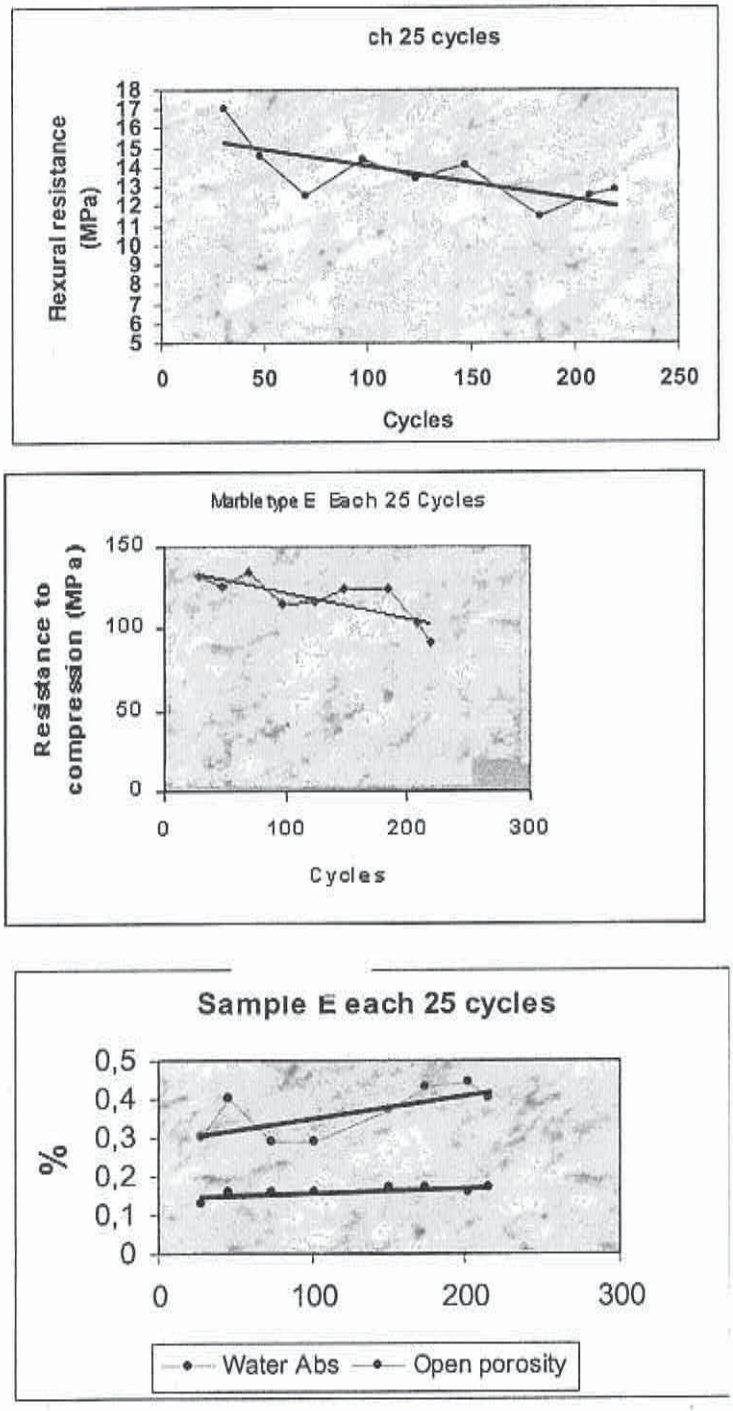

Figure 153. Interpretation of marble E test results.

It's a marble with highest mechanical resistance, to flexural and compression, and to freeze/thaw environments.

After 240 cycles of freeze/thaw, no visual alteration appeared, nor loss mass. The physical tests have given basically constant results, so it is possible to conclude that no alteration in the structure occurred, this is supported by the results obtained by microscopy (see report in annex).

3.12.4 Marble type K

Table 55. Initial characterisation of sample K (cut against)

Initial Characterisation	Sample K (cut against)	
	Average	Standard deviation
Resist. to Compression (Mpa)	79,6	7
Water Absorption at PtN (%)	0,05	0,01
Open Porosity (%)	0,15	0,00
Volumetric Mass (Kg/m^3)	2715	2
Resonance Frequency (HZ)	1748	-
Ultrasonic Propagation Speed (m/s)	$6{,}5\times10^{-2}$	-
Thermal Shock	No visual remark	-
Crystallisation Test	No alteration	
Dynamic Modulus of Elasticity ($\times10^9$ N/mm^2)	$3{,}0\times10^9$	-
Microscopic Observation	See report in annex	
Resistance to Flexural Strength under conc. Load (Mpa)	23,1	2,1

Table 56. Initial characterisation of sample K (cut in favour)

Initial Characterisation	Sample K (cut in favour)	
	Average	Standard deviation
Resist. to Compression (Mpa)	111,5	3,4
Water Absorption at PtN (%)	0,05	0,01
Open Porosity (%)	0,15	0,00
Volumetric Mass (Kg/m^3)	2715	2
Microscopic Observation	See report in annex	
Resistance to Flexural Strength under conc. Load (Mpa)	21,4	0,6

Table 57. Characterisation of the sample K marble resistance, each 25 cycles of freeze/thaw

Resistance characterisation	Each 25 cycles of the freeze/thaw								
	30	48	70	98	124	148	184	208	220
Resist. to Compression (Mpa)	132,2	125,1	134,6	114,3	115,6	123,0	123,9	102,6	92,0
Water Absorption at PtN (%)	0,10	0,11	0,13	0,12	0,13	0,13	0,13	0,15	0,13
Open Porosity (%)	0,25	0,30	0,35	0,26	0,33	0,31	0,28	0,25	0,31
Volumetric Mass (Kg/m^3)	2737	2716	2717	2709	2693	2711	2689	2689	2684
Resonance Frequency (HZ)	1920	2000	1974	1607	1712	1917	1942	1582	1712
Ultrasonic Propagation Speed ($x10^{-2}$ m/s)	6,2	6,3	6,2	6,2	6,2	6,2	6,2	6,2	6,1
Thermal Shock	No visual remark								
Dynamic Modulus of Elasticity ($x10^9$ N/mm^2)	3,6	3,9	3,8	2,5	2,8	3,6	3,7	2,4	2,8
Microscopic Observation	See report in annex								
Resistance to Flexural Strength under conc. Load (Mpa)	17,0	14,6	12,5	14,4	13,4	14,1	11,5	12,5	12.8

The crystallisation tests were made in the beginning and at the end of 220 cycles of freeze/thaw. The results were generally, tarnished appearance and no loss mass.

The loss of material, during the initial characterisation test was of 0,25% and after the 220 cycles, was of 0%, this may be a consequence of no significant increase on the porosity and consequently of the water absorption.

It's possible to conclude that marble, when submitted to thermal variations, and in presence of salt mist, wasn't shown alterations.

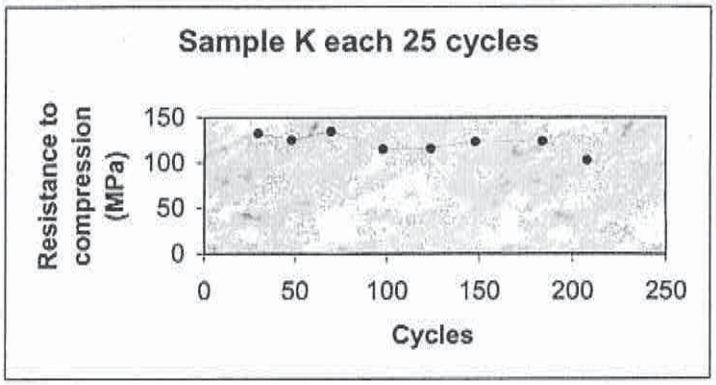

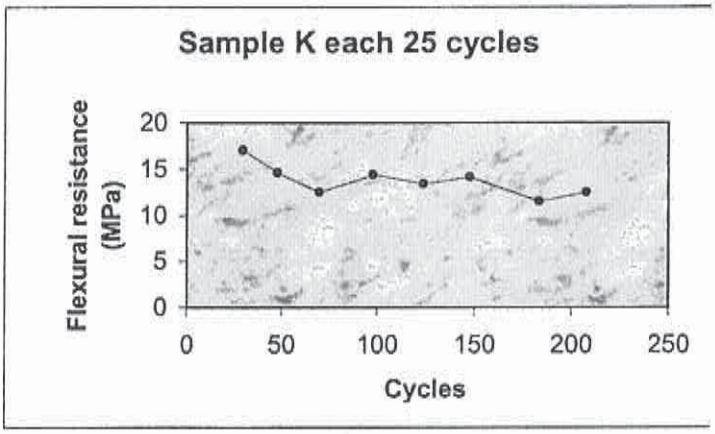

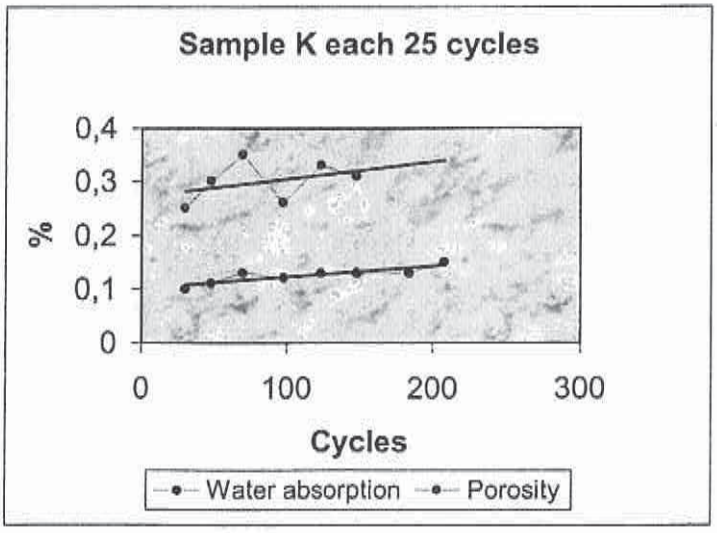

Figure 154. Interpretation of marble K test results.

According to the graphics, it's possible to conclude that the Italian marble sample K, is the most resistant sample of all the tested proposed samples for this project.

Thus, it can be said that in terms of physical and mechanical characterisation this marble presents a good behaviour when submitted to the temperature of freeze/thaw cycles, used in this project.

The interpretation of the compression and flexural resistance results, show that this marble doesn't present relevant alterations showing a slight decrease of resistance, although no conclusive.

Relatively to the absorption of water and open porosity the results also showed a certain tendency for the increase of the porosity, although not significant.

3.12.5 Case studies

3.12.5.1 The use of marble in facades in the North of Portugal.

Buildings
Being the north of Portugal, a region rich in granite, it is normal that the buildings are mainly built in this material. However during the 60's it was very common to have concrete buildings with the facade of the lower floor in marble.

Today these buildings are not in very good conditions, many slabs have fallen down and they need urgent renovation. In the modern buildings the architects are using more and more Portuguese limestone.

Gravestones
During the times stone has always been used for the building of graves. In Portugal marble, granite and limestone are very much applied in the tombs and mausoleums. In this field we can find some applications of Carrara Marble. The use of this material was always a sign of richness. It was used not only in graves on the ground and mausoleums but also in graves on the walls.

3.12.5.2 Stone companies

Company A
This is an importer of Carrara marble but never applied in outside facades.

The types that are usually imported are Gioia, Didora, CD, Semap and Statuario. In interior walls, the only problem are yellow stains that can appear. To avoid this problem they use a special kind of glue.

This company once applied a Green greek marble with white veins that also started to bow. This material had to be substituted by other material.
For exterior they always use Portuguese marble.

Company B
This company uses Carrara Marble but never applies it in outside facades
In the inside works they never had problems. Is not a direct importer, buys the marble from other Portuguese importers.

Company C
Never applied **Carrara Marble** in outside facades, but 20 years ago this company was responsible for the building of a **Carrara Marble** grave in a graveyard near Porto. Our days this grave is completely bowed.

Company D
Being located in the south of Portugal, this company is used to build facades in marble and limestones. Never had any problems with the facades built until now. Uses **Carrara Marble** in interiors

Compagny E
Is a company specialist in gravestones (graves and mausoleums).
These graves are built either in granite or marble. Never used Carrara Marble. The mausoleums are general built by one single wall, with 8 cm of thickness and 280 cm length and 60 cm.

3.12.5.3 Architects

The architects contacted never used **Carrara Marble** for outside facades. The reason it is the high price and not the problems related with the application of this material. In most of the cases they never had heard about the problems related with bowing, and some knew the Finland Hall case.
In this moment, most of the architects are using for outside facades of important buildings Portuguese limestones.

In the 19th century, in the graveyards Portuguese marble was not applied for the graves. The most common marble was **Carrara Marble.**
The restoring that she usually does to grave stones is gluing small pieces and cleaning but in Braga graveyard there are some graves on the walls that show bowing as we can see in the pictures (Figure 155).

3.12.5.4 Examples of objects

ATRIUM SALDANHA

- **Location** - Lisbon
- **Outside Facade** – Estremoz Marble
- Ventilated facade with mechanic fixation
- Bushammered
- 3 cm
- 80 cm/ 120 cm
- 12 000 m2
- Protected with Grafitix
- The outside facade was meant to be built in Giallo Dorato.
- **Inside** – Greek marble

The only problem with façade is the dirty, and never appear bowing problems. This building company never applied Carrara in outside facades

OPORTO BUILDING

- **Location** – Porto
- **Outside Facade** –Estremoz Marble
- Bush hammered
- Halfen fixings
- Stone thickness 3 cm
- Granite Yellow Boticas Polished

No problems with this façade (Figure 156).

3.12.5.5 Centro tecnológico da piedra

To complete our research we contacted other Technological Centres in other countries. We contacted a Technological Centre in Spain (Macael) region . In this spanish area there are many buildings with outside facades in Macael marble, and even the Technological Centre building is in Macael marble. Never bowing problems in this buildings, only problems with some braked? stones in facades with mechanical fixation. In this centre there is an investigation going on to try to find the reason of the breaking stones on floors built with rectangular tiles (2m x 1 m). These tiles appear broken in the middle 2m x 1m. When they are square that doesn't happen. Until now they think that this phenomena is due the calcite orientation .

Figure 155. A gravestone in Braga (North Portugal) showing clear warping.

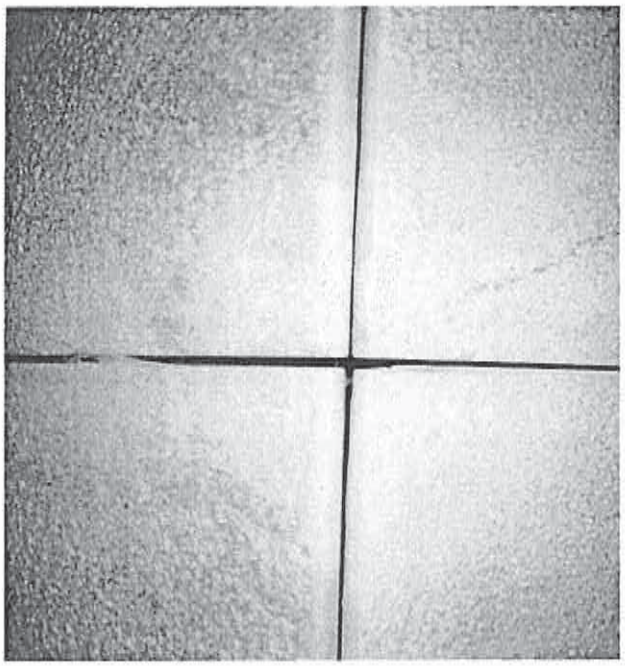

4 PRACTICAL APPLICATIONS

4.1 Instructions for constructing a durable marble façade

4.1.1 General

This research has indicated quite clearly that deterioration of marble panels is due to the granular decohesion of calcite grains. According to Royer (see annex 7) thermal variations are causing granular decohesion even when uniformly distributed throughout the specimen. Very low temperatures (-20°..-30°C) seem to be more damaging, even without frost effect. But also temperatures from +30°C to +50°C are causing permanent changes in the microstructure of some marbles. This kind of surface temperatures can be quite easily measured also in Nordic climates as Koskinen has showed. Weathering agents i.e. humidity and acid rain, are accelerating, rather than starting the degradation process.

Deterioration can be divided in two main categories; physical and esthetical. The latter can be very easily seen as bowing and changes in colour. This phenomena changes the appearance of the façade to somewhat different from architect's original idea. The former is more difficult to see and also more dangerous. The material is, as discussed in previous chapters, gradually losing it's strength, which may cause a considerable safety risk if not recognised early enough.

4.1.2 Selection of marble

Marble is nowadays used in the façades for esthetical reasons. Therefore, the selection of material should start from selecting a few (5..10) possible qualities for further studies according to the desired appearance; colour, veining etc.

These selected marbles shall then be examined more carefully under microscope. Recent studies have shown clearly that many material properties are influenced by the microstructure. Therefor the texture of each marble should be defined comprehensively and only those of xenoblastic or intermediate microstructures are qualified for further studies. Texture of each marble is defined by indicators A/P^2 and A/S^2 (see Royer, annex 3).

In this stage also the flexural strength for virgin specimen is tested and those below 12 MPa are rejected. Bending should be done according to EN12372 with the modification of drying temperature, which should not exceed +40 degrees centigrade. This modification is essential since higher temperatures may cause serious damage for the studied material and thus distort the results.

Those qualities passed these preliminary tests shall proceed to further examinations which include testing certain physical properties for virgin, un-

conditioned samples and thermally treated samples. Thermal treatment is done for dry samples as thermal cycles from -25°C to +50°C. Control of the weathering chamber should be done by measuring the actual temperature inside a few samples being located in the chamber so that they give representative picture of the temperature of all of the samples. This is a very easy and reliable way to ensure that samples are actually induced to the desired thermal stress.

Dry samples can be used because driving force for deterioration seems to be thermal changes and humidity is "only" accelerating the process. Using dry samples gives us more certainty that all different qualities are in exactly the same conditions, which is vitally important when comparing materials. Marble classification form can be summarised as below (modified from Royer, annex 3):

Marble type: ..... Texture: (xenoblastic or homoblastic) A/P^2=...., A/S^2=.....		
Test	Unconditioned samples	After 20 cycles from –25°C / +50°C
Bending strength	*12 MPa*	*10 MPa*
Water absorption	*0,12*	*0,2*

Values filled in the form represent the requirements for material to be used in the case of Finlandia Hall. For other cases these threshold values must be reconsidered according to the conditions the façade must tolerate.

4.2 Technical specifications for a stone cladding

4.2.1 Functional considerations

Apart from the right choice of stone material it is essential for the desired function of a natural stone cladding to use the correct solutions for structural implementation of the object. A modern stone facade is many ways quite different from the historical buildings. Throughout the history of architecture stone has been used as a massive, load-bearing structure. In the modern facade construction, however, stone has typically the role of giving the building its final appearance and a shelter against weathering agents. Stone is in the modern applications cut in thin panels and fixed in the building with mechanical anchors.

Change from massive structures to thin veneers has brought along many new technical and functional requirements. With respect to the stone itself it is evident that used as a thin veneer the importance of weather resistance properties is emphasized because of the slenderness of the stone panels. This is in fact one of the reasons giving rise to the severe nature of the

problems with marble facades. On the other hand technical solutions for fixing the stone to the building must be designed taking into account both the requirements coming from the modern building technology as well as the aspects related to the stone cladding itself. In modern construction stone cladding is normally built with thin stone panels of 30-50 mm thickness.

Important design consideration is the physical functionality of the stone veneer. This is especially important in northern climate areas where the temperature gradient between inside and outside of the building is greater than in the southern areas. Main aspects to be taken into account in the physical design of the facade cladding are the thermal and humidity conditions and the expected deformations in materials and structures.

In order to secure the desired quality of the stone material and the installation work a specific quality control system for the building project is needed. Quality control measures are to be taken

- at the quarry
- at the processing plant
- at building site

Controlling laboratory testing of the material properties shall be carried out according to the quality assurance plan of the project.

4.2.2 Structural design principals

The approach was divided into design and dimensioning aspects in the following four areas:

- connection between panel and fixing
- fixing anchor / secondary frame structure
- connection between fixing anchor and a secondary frame structure
- connections into the concrete/steel frame of the building

As a conclusion following structural principals are recommended to be applied for a natural stone cladding:

- panels are fixed independently to the frame of the building using load bearing and restraint anchors of stainless steel or aluminium (figure T1)
- anchors are placed in the joints between stone panels and fixed to the edges of the stone panel with stainless steel pins (figure T2)
- load bearing anchors, placed in the lower part of each panel, carry the weight of the stone panels and part of the wind forces;
- restraint anchors, placed in the upper part of each panel, take only wind forces

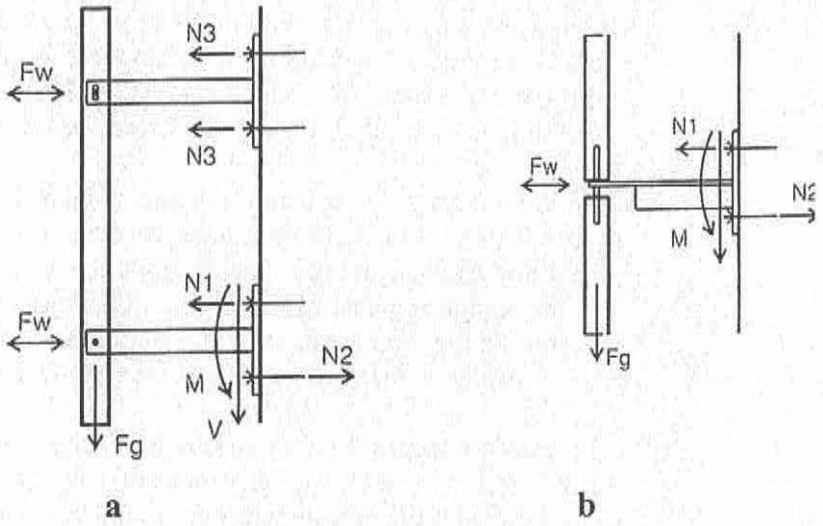

Figure T1. Static principals of a natural stone cladding. Vertical fixing (a), horizontal fixing (b).

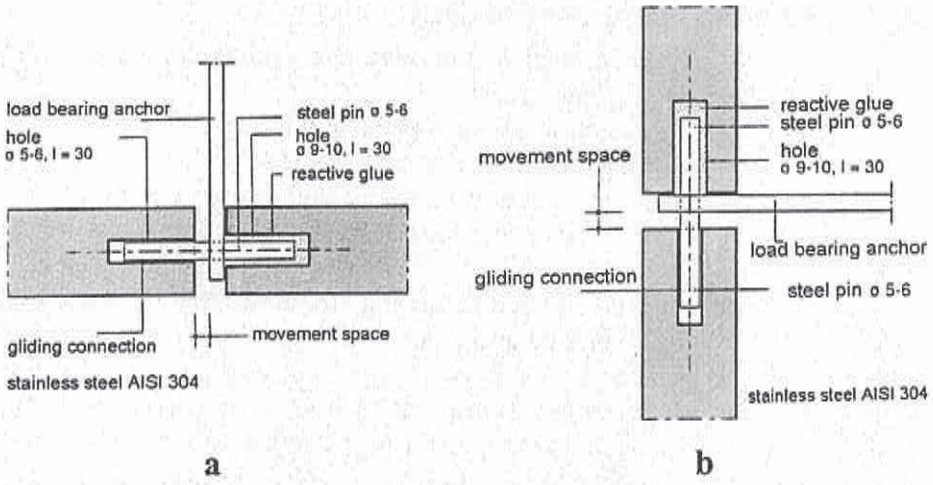

Figure T2. Connection between stone panel and the fixing anchor. Vertical fixing (a), horizontal fixing (b).

4.2.3 Building physical design principals

The approach was divided into design and dimensioning aspects in the following four areas:

- water permeability/tightness
- jointing method
- ventilation of the facade structure

- deformations due to temperature, humidity and movements
- protective impregnating treatments

As a conclusion following physical design principals shall be applied for a natural stone cladding:

- stone cladding shall be jointed by elastic mass to prevent rain penetration and to allow small deformations of structural elements without a risk for internal strains
- humidity in the wall structure shall be led out using a ventilation gap placed behind the stone cladding; proper function of the ventilation gap is arranged by using sufficient openings for both air going in and coming out
- connections between panels are designed elastic to allow deformations due to thermal expansion
- internal stresses, due to fixings and deformations between structural elements, are eliminated by proper design of the fixings
- protective agents shall be considered if there is a need to protect the cladding against environmental impurities

4.3 Monitoring the physical state of an existing façade

4.3.1 General

Monitoring of the physical state of façades should be included in every real estate's maintenance program. Considering marble façades, designing of the monitoring program starts from recognising the most critical part of the façade where the climatical stresses are the most severe. Typically the highest temperatures can be measured in the façades facing south, south-west and west. In Nordic climates these are also the compass directions where temperature changes are the strongest. The focus of monitoring should be on these parts of a façade, but of course also other parts of façade must be monitored, possibly less intensively.

The first and easiest inspection should be visual inspections. Changes in colour and appearance should be followed carefully.

4.3.2 Bowing measurements

A practical way of monitoring the process of granular decohesion is to measure the bowing of panels. As Royer explains in his report (annex 3), bowing is caused by differences in the level of granular decohesion through the thickness of a marble panel. By measuring the bowing we can thus notice the starting decohesion and later follow the progress of deterioration.

Measuring can be done with different types of "rulers", but essential is that bowing in both directions, concave and convex, can be measured with the same apparatus. According to our experiences from measurements, an accuracy of 0,1 mm is enough for following the development of bowing and also

practically reasonable. Bowing measurements are recommended to be done in the first stage in every six months; time period can later be adjusted if needed.

4.3.3 SEM -analyses

In addition to bowing measurements also more accurate methods are needed. These methods include SEM –analyses and testing the flexural strength of the panels on the façade continuously during the lifetime of the façade. Samples for the former should be taken from the previously defined most critical part of the façade. These samples can be very small and so the traces of sampling are easily hidden from spoiling the view. The amount of the samples must be considered regarding the façade in question, but for Finlandia Hall –case two samples every second year should be enough. The idea of these samples is to actually peek inside the panels and to verify the condition of them. Also the openings between the calcite grains can be measured and their importance can be interpreted.

4.3.4 Flexural strength testing

Sampling for the flexural testing is more difficult, but this testing is considered to be essential. The only possible way of sampling- due to the amount needed for statistically reliable results- is to release complete panels from the façade. This requires a bit of arrangements since estate owner should stock spare panels for the ones decided to be tested and also since the initial strength of the panels tested must be known in order to define the decrease of the strength. Practical solutions for the latter are numerous, but one recommendation is to select one block for the monitoring, test the strength of it and then install the rest of the panels made of it. These panels should be marked clearly for later identification. Samples are then taken (and tested) from these panels once every five years.

4.3.5 Criteria for façade renovation

From the above described method can be derived very easily otherwise very difficult decision to be made: when to renovate the façade. One must set, when designing the façade, certain threshold values allowed for bowing and loss of strength. When monitoring is giving values close to these values, planning of the renovation should be started and when those values are exceeded, renovation works should be started.

4.4 Recommended actions for façade maintenance

Because of the nature of the deterioration process, even the most careful maintenance cannot prevent the panels from bowing and loosing their strength. Therefore, the effort should be put on upholding the outlook of the façade as long as possible. This is done by cleaning the panels with suitable method according to the amount of dirt accumulating on them. When cleaning the panels also the state of the joint sealings can be easily checked and fixed if needed. This is essential to prevent the frost damage the water leaks into the façade could otherwise produce.

The physical state of fixings should be checked every once and a while. Even stainless steel can be subjected to corrosion in some conditions, which may lead to serious accidents if not recognised early enough.

APPENDIXES

1. VTT Building and Transport, Environmental conditions
2. VTT Building and Transport, Test wall
3. VTT Building and Transport, One-sided weather resistance test
4. VTT Building and Transport, Protective agent
5. Helsinki University of Technology, Laboratory of Engineering Geology and Geophysics
6. Helsinki University of Technology, Laboratory of Rock Engineering
7. University of Parma
8. Cevalor
9. Bowing measurements
10. Financial report